12-2015

Sequence Stratigraphic Framework of Carbonate Diagenesis within Neogene Glaciomarine Sandstones of the Victoria Land Basin, Antarctica: Insights into Reservoir Quality in Polar Settings

Daniel P. Dunham
University of Nebraska-Lincoln, ddunham2@huskers.unl.edu

Sequence Stratigraphic Framework of Carbonate Diagenesis within Neogene Glaciomarine Sandstones of the Victoria Land Basin, Antarctica: Insights into Reservoir Quality in Polar Settings

By

Daniel P. Dunham

A Thesis

Presented to the faculty of

The Graduate College at the University of Nebraska

In Partial Fulfillment of Requirements

For the Degree of Master of Science

Major: Earth and Atmospheric Sciences

Under the Supervision of Professors Tracy D. Frank and Christopher R. Fielding

Lincoln, Nebraska

December, 2015

Sequence Stratigraphic Framework of Carbonate Diagenesis within Neogene Glaciomarine Sandstones of the Victoria Land Basin, Antarctica: Insights into Reservoir Quality in Polar Settings

Daniel P. Dunham, M.S.

University of Nebraska, 2015

Advisor: Tracy D. Frank and Christopher R. Fielding

The controls on reservoir quality of most clastic sedimentary deposits are well-documented and understood. However, comparatively little is known about the reservoir potential of glaciogenic and glaciomarine deposits. This study investigates the Neogene strata of the AND-2A core recovered by the ANDRILL-Southern McMurdo Sound Project in the Victoria Land Basin, Antarctica, as an analog for assessing controls on reservoir quality in glaciomarine deposits. A petrographic analysis was conducted on 60 sandstone samples from various depths throughout the core, and carbonate diagenetic phases and morphologies were documented. Four sequences were examined in detail. Point counting on all samples was done to determine percentages of cement, porosity, detrital mud, and framework grains. Results show that reservoir quality in glaciomarine sandstone is dramatically affected by the presence of diagenetic carbonate and strong correlations exist between carbonate cement abundance, paleoclimate, and sequence stratigraphic systems tract. Sandstones that formed during the coldest (polar and subpolar) climate regimes have relatively low porosities (<15%) due to occlusion of pore space by carbonate cement.

Decreased input of fine-grained sediments during colder climate regimes resulted in higher permeability deposits that were prone to infiltration by brine upon burial. By contrast, many texturally mature sandstones deposited in highstand deltaic settings during more temperate climate regimes preserve higher porosities (25 – 45%) and lack significant cementation. Sequence stratigraphic relationships indicate that these porous sandstones are best developed in highstand delta systems that formed during ice minima, when substantial volumes of meltwater were released from glacier termini. Individual sandstone bodies, which likely extend laterally over several kms, tend to be enclosed by muddy lithologies. Porosity in these sandstones was retained due to discharge of dilute meltwater during deposition and subsequent isolation of sands between impermeable barriers. Patterns identified in this study may prove useful in predicting and locating target reservoirs in other glaciogenic and glaciomarine settings worldwide.

Acknowledgements

I would like to thank my advisers; Dr. Tracy Frank and Dr. Christopher Fielding for allowing me to work under them while completing this project. Your expertise and guidance is something I will always be grateful for and allowed me to become the true scientists I always wanted to be. This work is supported by the National Science Foundation Grant #PLR-1341390, awarded to T. Frank and C. Fielding. We would like to thank the ANDRILL-SMS drillsite science team for their efforts in collecting and characterizing the AND-2A core. Additional thanks to Charlotte Sjunneskog and the staff at the Antarctic Research Facility for allowing access to the core and their help in sample collection. Lastly, I would like to thank my lab mates and numerous officemates over the past two years for their valuable insight and friendship: Sebastein Blanchard, Andrew Hutsky, Bobbi Brace, Zack Kita, Shamar Chin, Kat Chen, Matt Peppers, and Tom Baldvins.

TABLE OF CONTENTS

LIST OF FIGURES

LIST OF TABLES

APPENDICES

INTRODUCTION

The roles of paleoclimate, tectonic history, depositional environment, and diagenetic history and their influence on reservoir quality are well studied and understood in most clastic sedimentary reservoirs. The reservoir potential of glaciomarine deposits has, however, received little attention in the research literature. Although glacial and glaciomarine deposits are not as abundant as other clastic facies, there are still many that serve as hydrocarbon reservoirs worldwide, notably the Ordovician Illizi Basin, Algeria (Hirst et al., 2002), the Ordovician System in the Sbaa Basin, Algeria (Tournier et al., 2010), Permo-Carboniferous strata in the Parana Basin, Brazil (Franca and Potter, 1991), the Permo-Carboniferous Al Khlata Formation, Oman (Levell et al., 1988), the Permo-Carboniferous Unayzah Formation, Saudi Arabia (Melvin et al., 2010), and the Permo-Carboniferous Juwayl Member of the Wajid Formation, Saudi Arabia (Melvin and Norton, 2013). Like most clastic deposits, sandstones are the principal lithology acting as reservoirs in glacial and glaciomarine deposits (onshore Bolivia (Bache et al., 2012), onshore Jordan (Douillet et al., 2012), Tassili N' Ajjer in Algeria and Libya (Girard et al., 2012), Illizi basin in Algeria (Hirst. 2012 and Lang et al., 2012), Norwegian Sea (Ottesen et al., 2012)).

Most studies involving glaciogenic reservoirs have focused on the development of facies models and sequence stratigraphy. The diagenetic history of these settings is understudied and poorly understood, and therefore, very little literature documenting the distribution of porosity and cement in these settings is available.

The current study addresses this issue and provides insights into the controls on cement abundance and the distribution of cement and porosity within glaciogenic reservoirs.

Neogene strata of the Victoria Land Basin (VLB), Antarctica, comprising diamictites, conglomerates, sandstones, muddy sandstones, sandy mudstones, and mudstones, provide an ideal reservoir analog for more ancient deposits from high-latitude settings that have undergone complex burial and tectonic histories. The AND-2A core also proves to be an ideal analog due to the rich database of information that accompanies it, including detailed studies on: chronology (Acton et al., 2008), depositional environments (Fielding et al., 2008; Fielding et al., 2011; Passchier et al., 2012), sequence stratigraphy (Fielding et al., 2008; Fielding et al., 2011), petrography (Panter et al. 2008), and geochemistry (Panter et al. 2008; Frank et al., 2010; Fielding et al., 2012).

The Neogene strata investigated herein are from the AND-2A core recovered in the Southern McMurdo Sound region of the Ross Sea during the ANDRILL-SMS project. The VLB preserves 3-4 km (Cooper et al., 1987) of Cenozoic strata. This area is in a key location for studying the Antarctic paleoenvironmental history through the Cenozoic because of its proximity to three major ice centers, the West Antarctic Ice Sheet, the East Antarctic Ice Sheet, and the Ross Ice Shelf. The focus herein is on sandstones from the AND-2A core, a continuous, 1138.54 m long drillcore recovered by the ANDRILL-Southern McMurdo Sound (SMS) project.

This paper aims to 1) identify diagenetic controls on porosity distribution in glaciogenic sandstones of Neogene age that were formed in broadly glaciomarine settings and have been buried to hundreds of meters below the sediment-water interface, 2) understand relationships among reservoir quality, paleoclimate, and sequence stratigraphy, and 3) develop a model for predicting controls on reservoir quality in glaciogenic deposits. Assuming the analog used here is applicable elsewhere, our results will aid in future exploration of glaciogenic hydrocarbon basins worldwide, and furthermore, could be used to optimize development of established resources in actively producing basins with a glaciogenic origin.

GEOLOGICAL SETTING

The VLB is part of the West Antarctic Rift system, a Cenozoic failed rift complex that covers a 750-1000 km wide area- extending from Marie Byrd Land to the East Antarctic Craton (Tessensohn and Wörner, 1991; Behrendt et al., 1991; Cooper et al., 1987; Henrys et al., 2007) (Fig. 1). The VLB is one of several graben and half-graben systems that formed adjacent to the Transantarctic Mountains (Cooper et al., 1987). A combination of high sedimentation rates and accommodation from rifting and thermal subsidence has preserved a high resolution, ice-proximal, relatively stratigraphically complete succession (Florindo et al., 2008).

Due to a lack of surface exposure in the Southern McMurdo Sound region, all information regarding the stratigraphic record is derived from seismic reflection surveys and various stratigraphic drillcores recovered in the VLB. Seismic reflection surveys from the area are documented by Cooper et al. (1987), Brancolini et al. (1995a, b), Bartek et al. (1996), and Hamilton et al. (2001). Drilling programs in the VLB and Southern McMurdo Sound have been ongoing since the early 1980's, drilling programs include: the Dry Valley Drilling Project (McGinnis, 1981), CIROS-1 and 2 (Barrett 1989; Barrett and Hambrey 1992), Cape Roberts Project (Cape Roberts Project Science Team, 1998, 1999, 2000), and the ANDRILL Program (Naish et al., 2007; Harwood et al., 2008). Integration of drilling data and seismic surveys allow for the reconstruction of the VLB's history.

Fielding et al. (2006, 2008b) identified five main phases of basin formation in the VLB. (1) Regional uplift and erosion of the Transantarctic Mountains during the Early Cenozoic (pre-34 Ma), (2) Early rifting (34-29 Ma) of the basin is recorded by wedges of strata that are confined by early extensional faults, (3) Main rifting (29-23 Ma) is characterized by lenses of strata that thicken symmetrically from the basin margins into a central depocenter, and by the continuity of stratal events over the top of Early Rift extensional topography. Main rifting was followed by (4) a period of passive thermal subsidence (23-13 Ma) which is recognized by an evenly distributed sheet of strata that thicken into the depocenter but are continuous over the earlier rift strata to the margins of the basin. (5) Lastly, renewed rifting occurred from ~7.6 Ma-present and was responsible for the formation of the Terror Rift and extensive volcanic activity (Cooper et al., 1987; Henrys et al., 2007).

Sedimentology and Stratigraphy of the AND-2A Core:

The AND-2A core records the Miocene and Pliocene Stages of the VLB. The AND-2A core was divided into seventy-four sequences by Fielding et al. (2011). Each sequence preserves evidence for ice proximal conditions (coarse grained base) and ice distal conditions (overlying fine-grained lithology). Geochronological data (Acton et al., 2008) indicates that the seventy-four sequences were likely formed over timeframes corresponding with the Milankovitch band and can be considered high-frequency (fourth and fifth order) (Vail et al., 1991; Catuneanu, 2006) sequences. The recovered section was subdivided into fourteen lithostratigraphic units based on the abundance of diamictite, sandstone, mudstone, volcanogenic component, biogenic silica, and conglomerate (Fielding et al., 2008a). Furthermore, thirteen lithofacies were recognized that record a range of depositional environments, including subglacial, ice contact pro-glacial and glaciomarine, and open shallow marine environments with minimal influence from ice sheets (Fielding et al., 2008a). The Neogene succession of the Victoria Land Basin is dominated by diamictites formed in glacial and ice-proximal proglacial marine settings. Typically, diamictite fines upwards into conglomerate, sandstone, and muddy sandstone and is interpreted to record glacial retreat. As ice dissipated and led to a relative rise of sea level, muds became the dominant lithology. The mudstone-dominated section then coarsened upwards into sandy mudstone and sandstone. In this way, stratal cycles were formed by repeated advance and retreat of glacial ice into the basin.

Depositional cycles on the order of tens of meters thick separated by erosional surfaces, interpreted as sequence boundaries, comprise the basis of a sequence stratigraphic framework for the cored succession. Interpretations of the depositional sequences for the AND-2A core are based on the original sequence stratigraphic model proposed by Fielding et al. (1998, 2000) and modified by Dunbar et al. (2008b) for the Cape Roberts Project cores recovered from the northern VLB. The idealized sequence for AND-2A (Fig. 2), developed by Fielding et al. (2011), is marked by an erosional surface caused by glacial advance at the base (sequence boundary). Sequence boundaries are interpreted as recording relative sea-level minimums and glacial advances that cause substantial erosion of previously deposited sediment. In ice-proximal settings the erosional surface (sequence boundary) marking glacial advance is labeled the "Glacial Surface of Erosion". In ice-distal settings, away from glacial influence, the glacial surface of erosion may not exist, but instead, sequence boundaries will be developed as sharp, planar, or gradational coarsening upward contacts between ice-proximal and ice-distal facies (Fielding et al., 2011). Within these sequences, sequence boundaries are overlain by diamictite and conglomerate deposited in ice-proximal glaciomarine settings (Fielding et al., 1997) (lowstand systems tract). The diamictite and conglomerate fine upwards into sandstone, sandy mudstone, and muddy sandstone (transgressive systems tract). The fining upward sequence records a progressive increase in paleo-water depth and an increased influence from hemipelagic fallout, and shows less influence from transport of sediment along the seabed (Fielding et al., 2011). Fining upward sequences are interpreted to represent deposition in glaciomarine shelf or ramp settings (Fielding et al., 1997).

The end of the fining upward sequence is marked by a very fine grained, commonly fossiliferous, mudstone (maximum flooding interval). Mudstone then coarsens upwards into muddy sandstone, sandy mudstone, and sandstone (highstand systems tract). The coarsening upward sequence started to form when sea-level had reached a relative maximum and began to drop as the next glacial advance began. During this time, sedimentation rates exceeded the rate of accommodation and seabed transport by waves and currents expedited the accumulation of fine-grained, texturally mature sands in deltas and other prograding, nearshore systems (Fielding et al., 2011). Mudstone, muddy sandstone, sandy mudstone, and very-fine sandstone are representative of shallow marine environments deposition (Fielding et al., 1997). The sequence is then truncated by the next sequence boundary.

Fluctuations in paleoclimate regime, dominantly controlled by obliquity (41 ka) (Dunbar et al., 2008), are believed to have caused variations from the idealized sequence that include changes in sequence thickness, variety and range of facies within sequences, changes in the completeness of sequences in terms of systems tracts, and changes in the proportion and character of diamictites (Fielding et al., 2011). Fielding et al. (2011) recognized six recurring stratigraphic "motifs" in the AND-2A core that record paleoclimatic-mode shifts. Climate regimes represented by the motifs are: 1) cold polar-subpolar glacial regimes, 2) subpolar glacial regimes, 3) high-latitude temperate glacial regimes, 4a/4b) high-latitude glacial regimes with distant glaciers, and 5) regimes minimally influenced by distal glaciers (Table 1). Motif 1 is recorded by diamictite-dominated cycles with minor proportions of other lithologies.

Motif 1 diamictites are interpreted as recording ice-proximal, marine proglacial or subglacial deposits that were formed under a dynamic climate regime with repeated glacial advances. Motif 1 sequences are often thin and incomplete due to the interpreted frequent advances of grounded tidewater glaciers. Motif 2 is diamictite dominated with a slightly larger proportion of other lithologies. Motif 2 is still representative of ice-proximal conditions with repeated tidewater glacial advances, and represents occasional grounding of the advancing glaciers with a more significant influence from meltwater. Motif 3 preserves a variety of lithologies. Diamictites are much thinner than in motifs 1 and 2, and sandstones are more abundant. Motif 3 is interpreted as recording tidewater or floating tongue glaciers that periodically advanced into the basin but not to the same extent as those in motifs 1 and 2. Motif 4 contains higher abundances of sandstones and/or mudstones and is subdivided into two sub-motifs. Motif 4a is only present within one sequence and contains a 20 m thick succession of stratified sandstone between two intervals of diamictite dominated strata (motif 1). Flat and low angle lamination and local cross-bedding indicate that motif 4a was likely deposited in an open, nearshore marine environment, with minimal glacial influence. Motif 4b is characterized by higher abundances of mudrock. Motif 4b includes dispersed gravel and bioturbation, indicating deposition in an offshore marine shelf setting with distant glacial activity. Motif 5 is mudrock-dominated with indications of diverse and intense bioturbation. Motif 5 is interpreted as recording a distal glaciomarine setting during periods of ice advance and open marine conditions. Stratigraphic motif stacking patterns were used to develop a climate record for the AND-2A core (Fig. 3).

There is a wide range of environments recorded, but, polar/sub-polar, heavily glaciated regimes are the dominant motif in the core.

Pore Water Geochemistry of the AND-2A Core:

Analysis of pore water recovered during the drilling of AND-2A (Panter et al., 2008) revealed the presence of a brine (six times seawater salinity) at depths below 200 mbsf in the basin. Relationships between concentrations of Na-Br-Cl and SO_4-Br-Cl indicated that the brine was the product of seawater freezing along the margins of advancing ice sheets (Frank et al., 2010), with numerous advance-retreat cycles producing the body of brine that now resides in the subsurface. The brine is depleted in $\delta^{18}O$ relative to seawater due to precipitation of mirabilite ($Na_2SO_4 \bullet 10H_2O$) during the seawater freezing process and subsequent zeolitization and devitrification of volcanic glass during burial (Frank et al., 2010). Fielding et al. (2012) integrated $\delta^{18}O$ values with bore hole temperature data to predict the composition of cement that should precipitate from the brine. Modeling results, when compared with oxygen isotopic data from cements, indicated that the brine is the most likely cementing agent.

METHODS

The AND-2A core reached a depth of 1138.54 meters below sea floor (mbsf), recovering strata that range from Lower Miocene to Pliocene in age (Harwood et al., 2008).

Sixty sandstone samples from the AND-2A core were selected for this study. Samples were selected to include sandstones representing all of the interpreted stratigraphic motifs, various systems tracts, and a wide range of depths. Samples collected range in core depth from 37.04 mbsf to 1093.61 mbsf. Sandstones from twenty-seven individual sequences were sampled across a wide range of depths in the AND-2A core in order to encompass a variety of depositional settings, paleoenvironments, and sequence stratigraphic systems tracts. Four sequences were chosen for in depth analysis. These four sequences include two sequences representing polar-subpolar climate regimes and two sequences representing temperate climate regimes. They were selected based on their completeness and close resemblance to the idealized sequence.

Thin sections were impregnated with blue-dyed epoxy to aid in determination of micro- and macro-porosity. In order to distinguish between different carbonate phases, samples were stained using a solution of Alizarin red-S and potassium ferricyanide, using methods similar to those described by Miller (1988). Point counting was conducted on the 60 samples using a standard petrographic microscope following methods outlined by Harwood (1988). Counts were taken at 20x magnification for 300 points per sample using a grid spacing that encompassed the entire thin section.

Due to an abundance of lithic fragments and a desire to determine modal grain composition, rather than modal mineralogy, traditional QFR point counting methods were used. Quartz, feldspar, and lithic grain abundances were determined, as well as the volumes of cement, detrital mud, and porosity. Results were plotted on ternary diagrams (Fig. 4) to determine sandstone type (Folk, 1980) and provenance (Dickinson, 1985).

RESULTS

Sandstone Framework Grains and Matrix:

Sandstones are litharenites, sublitharenites, lithic wackes, and sublithic wackes derived from a recycled orogenic source, namely crystalline basement and the Transantarctic Mountains, with additional input from the nearby Erebus Volcanic Province and some older volcanic centers below the Ross Ice Shelf (Talarico and Sandroni, 2011). Labile framework grains are very well preserved and tend to display little to no alteration (Fig. 5a), although igneous rock fragments in samples from deeper portions of the core display evidence of alteration in the form of sericitization of feldspars. There is also evidence of zeolitization and/or devitrification in volcanic glass in deeper portions of the core. There does not appear to be any strong correlation between sandstone type and sequence stratigraphy, paleoclimate regime, or depth in the core (Table 2; Fig. 6).

Detrital mud content is highly variable (Fig. 6; Fig. 7), but in general is more abundant in the transgressive systems tract sandstones and less so in the lowstand systems tract sandstones (Table 2). Due to this variability in detrital mud content, sorting ranges from poorly sorted to well-sorted and sandstones range from very-fine grained to coarse grained.

Cement Distribution:

The abundance of secondary carbonate (cement) is highly variable, ranging from less than 1% to nearly 40% (Table 2; Fig. 6). In some cases, however, very-fine carbonate is found associated with the detrital mud fraction of sandstones and it is difficult to differentiate between the detrital carbonate component and carbonate cement. Cement is composed almost entirely of carbonate minerals, including Fe-poor calcite, Fe-rich calcite, and dolomite. There are three morphologies of calcite cement present, (1) microcrystalline (Fig. 5b), (2) blocky (Fig. 5c), and (3) poikilotopic (Fig. 5d). The dominant carbonate phase is Fe-poor calcite (Fig. 5e), although, Fe-rich calcite is present in a few samples. Late stage, coarse, saddle dolomite is also present, dominantly where filling secondary pore space, and is often associated with cross-cutting fractures (Fig. 5f). Microcrystalline and blocky morphologies of dolomite are also present, but are rarer.

Overall, cement volume increases with depth in the AND-2A core (Table 2; Fig. 6). Below 700 mbsf the abundances of cement are consistently greater than 12%, whereas, above 700 mbsf cement abundances above 12% are recorded but intermittently distributed. Poikilotopic cement is most common below 800 mbsf, and those samples contain correspondingly low abundances of detrital mud and low porosity values. Blocky morphologies are rarer than other morphologies. Where present, blocky morphologies often occur in conjunction with microcrystalline and poikilotopic morphologies, and also coincide with low porosity values. Microcrystalline morphologies are most common and are readily distributed throughout the core.

Although microcrystalline morphologies are readily distributed, there does not appear to be any strong correlations between the microcrystalline morphology and detrital mud or porosity values.

Low porosity values (5-15%) due to cement occlusion occur in samples recording cold climate regimes (stratigraphic motifs 1-3). Sandstone samples representative of colder periods contain cement volumes up to 28% and generally minimal volumes of detrital mud. Some samples from warmer periods also contain higher abundances of cement but in many cases cement volumes are less than 5% (Table 2; Fig. 6; Fig. 7).

Porosity Distribution:

Porosity values are largely dependent on the presence or absence of detrital mud and cement, which occlude pore space (Fig. 6). There is a significant decrease in porosity below 700 mbsf, which coincides with an increase in cement volume below this point. On top of this general trend, data show that porosity is also lower in samples representative of cold climate regimes, with sandstones within stratigraphic motif's 1, 2, and 3 (cold subpolar/polar glacial regime, subpolar glacial regime, high-latitude glacial regime with proximal wet-based glaciers) characterized by low (<10%) porosities. The lowest values (0-5%) correspond to the Upper and Lower Miocene sections when polar-subpolar conditions prevailed. Low porosity values also coincide with increased fine-grained matrix in the sequences that reflect high-latitude temperate glacial regimes (Motif 4a/4b).

High porosity (15-44%) sandstones are associated with stratigraphic motif's 4b and 5 (Fig. 7) (high-latitude temperate glacial regime with distant wet-based glaciers and minimally influenced glacial regimes) with the highest (25-44%) values in samples deposited during the warmest periods of the Miocene, in particular, the Mid-Miocene Climatic Optimum.

Sequence Stratigraphic Relationships:

Sandstones from different systems tracts show considerable variation in the abundance and distribution of porosity, cement, and detrital mud (Fig. 7). Lowstand systems tract sandstones tend to have very low porosities, often less than 5%. The lowstand systems tract sandstones also contain higher abundances of cement in general (10-30%), and poikilotopic cement is more common in the lowstand samples than the transgressive and highstand systems tract samples (Table 2).

Porosity is highest in highstand systems tract sandstones, including deltaic sandstones that formed in high-latitude temperate glacial regimes with distant wet-based glaciers (Motifs 4a and 4b). Porosity is in many cases greater than 20%, although some highstand samples are muddy, with detrital material greatly reducing primary porosity. Cement volumes are also reduced in many samples of the highstand systems tract sandstones. Samples from the transgressive systems tract sandstones have a wide variety of cement, detrital mud, and porosity values and no trends are recognized.

Trends within Sequences:

Analysis of sandstones within four sequences shows that the broad patterns described above are also evident within high-frequency fourth and fifth order sequences. Two sequences representing polar-subpolar glacial regimes and two sequences representing temperate glacial regimes were selected for in-depth analysis due to their completeness and close resemblance to the idealized sequence. The polar-subpolar (stratigraphic motif 2) sequences selected span depths of 340-355 mbsf (mid-Miocene) and 726-744 mbsf (early Miocene). The temperate (stratigraphic motif 4b) sequences selected depths between 450-471 (early Miocene) mbsf and 726-744 mbsf (early Miocene).

The two polar-subpolar sequences are the most complete in terms of the preservation of systems tracts. Within each sequence, sandstones from the lowstand, transgressive, and highstand systems tracts were selected and analyzed. Both sequences show trends in porosity and cement distribution that are consistent with those found at the broad scale of the AND-2A core. Lowstand systems tract sandstones from both sequences representing polar-subpolar glacial regimes have lower porosity values of 22% (340-355 mbsf) and 14% (726-744 mbsf) and higher cement volumes of 16% (340-355 mbsf) and 21% (726-744mbsf) relative to volumes observed in sandstone samples from the highstand systems tract. The highstand systems tract sandstones from these sequences have higher porosities: 31% in the 340-355 mbsf sequence and 24% in the 726-744 mbsf sequence.

Higher porosity in the highstand systems tract samples from sequences deposited during polar-subpolar conditions coincides with lower abundances of cement in the highstand samples, 12% in the 340-355 mbsf sequence and 18% in the 726-744 mbsf sequence

The two sequences representing temperate glacial regimes do not contain representative samples from all systems tracts due to a lack of clean sandstones, but nonetheless provide valuable insight into the stronger influence of muddy lithologies associated with warmer climate conditions. Overall, porosity in the highstand systems tract sandstones of these sequences is up to 12% higher than the highstand sandstones deposited under polar-subpolar glacial regimes. Likewise, cement abundances are significantly less (typically 5-10%) in the sandstone samples representing warmer time periods. The sequence that lies 608-638 mbsf contains a greater abundance of muddy lithologies than the sequence between depths of 450-471 mbsf. The influence of muddy lithologies on porosity is evident when these two sequences, deposited under similar conditions, are compared. Sandstones from the muddier sequence (608-638 mbsf) have porosity values up to 43% and sandstones from the temperate sequence containing lower abundances of muddy lithologies have a maximum porosity value of 23%. Further evidence of the relationship between the presence of muddy lithologies and porosity is seen in sandstones encased by muddy lithologies such as mudstones and sandy mudstones. The highest porosity values (18-43%), due to a lack of cementation, in samples (462.33, 465.53, 609.03, 611.62, 621.69 mbsf) from temperate sequences come from these sandstones.

DISCUSSION

Results reveal that key reservoir properties of glaciomarine sandstones in the AND-2A core vary with stratigraphic motif (climate regime) and sequence stratigraphic position. Sandstones deposited in cold climate regimes (motifs 1-3) are relatively clean (Fig. 5g; Fig. 6), but they have low porosities because they are heavily cemented (Fig. 8a). Lowstand systems tract sandstones, which represent times when glacial ice extended furthest into the basin, are also characterized by heavy cementation and low porosity. The lowstand systems tract is dominated by diamictite and conglomerate, and sandstones are often thin and discontinuous. The extreme grain-size range that typically constitutes diamictites allows for mixing of the fine-grained sediment of diamictites with sandstones of the lowstand systems tract to further occlude porosity.

Given that previous work has identified cryogenic brine formed via seawater freezing as the fluid responsible for precipitating these cements (Frank et al., 2010; Fielding et al., 2012), heavy cementation of sandstones that formed during the coldest periods implied a relationship between climate regime and reduced reservoir properties. Upon burial, these sandstones were infiltrated by brine and pore space was occluded by cement. A lack of muddy lithologies to act as a seal in the deposits of lowstand and cold climate regimes facilitated infiltration of brine into sand bodies during burial in these settings. In summary, the propensity for cementation due to high permeability, the thin nature, and overall paucity of sand bodies within the lowstand sequences of cold climate regimes suggests that these sandstones do not display characteristics likely to generate prospective reservoirs (Fig. 9).

Deposition during temperate climate conditions (motifs 4a-5) was dominated by sandstones and mudstones that formed in a coastal (likely deltaic) or nearshore marine (Delta front or shoreface) environment with significant meltwater influx (Fielding et al., 2008a; Passchier et al., 2012). Highstand systems tract sandstones from these intervals are often very clean and porous, with little to no cement occlusion (Fig. 5f; Fig. 6, Fig. 7; Fig. 8b). Those that do have low porosities tend to be muddy (matrix-rich). Higher sea levels and increased erosion during warmer times allowed for deposition of fine-grained material and increased mixing of sand with clay and silt. Even in these low muddy sands, however, secondary cement is rare.

The lack of cementation in these sandstones is attributed to the presence of interfingering mudstones that accumulate via hemipelagic fallout during deglaciation and sea level rise. In the highstand systems tract, muddy seals form that encase sand bodies to prevent infiltration of brines upon burial, which allows for preservation of porosity. Predictions by Fielding et al. (2012), based on basinal geometry, suggest that highstand systems tract sand bodies enclosed by muddy lithologies will pinch out up dip into these fine-grained muddy seals and create a stratigraphic trap. As previously mentioned, formation of encasing muddy lithologies in the highstand systems tract provided barriers to the infiltration of brine into porosity networks upon burial. In addition, an influx of glacial meltwater, during times of minimal influence from glacial ice, displaces diagenetic fluids and is buried along with the sand, decreasing the potential for cementation. The combination of encasing muddy lithologies and an increase of glacial meltwater allows for preservation of highly porous, clean sandstones (Fig 7).

Clean sands are a minor proportion (approximately 8%) of the total stratigraphic thickness of the AND-2A core. However, many highstand deltaic sandstone bodies deposited during warmer climate regimes are laterally extensive, and therefore, can be considered viable reservoirs (Fielding et al., 2012).

In summary, the propensity for cementation is significantly lower in the highstand sequences of warmer climate regimes due to the sealing capabilities of encasing muddy lithologies and a greater influx of dilute meltwater that is buried along with the sands. The clean, highly porous, laterally extensive nature of these sand bodies, along with the ability to form stratigraphic traps, suggests that these sandstones display characteristics likely to generate prospective reservoirs (Fig. 9).

The previously mentioned trends identified in whole core analysis are also evident when examining individual sequences. High-resolution trends indicate that porosity is much greater in sequences that contain high abundances of muddy lithologies to act as seals to sand bodies. A direct comparison of four individual sequences identify the sands encased by muddy lithologies as the best potential reservoirs, regardless of climatic regime, although warmer regimes still display higher average porosities than the cold regimes. Individual sequences also display sequence stratigraphic trends of high porosity values in the highstand systems tract and low porosity values in the lowstand systems tract. The continuity of patterns seen on both the broad scale and in high frequency samples indicates that results identified in this study should be evident and widely applicable across a broad spectrum of scales

Previous work by Blackstone (2009) examined the reservoir potential of sandstones deposited during the Mid-Miocene Climatic Optimum (MMCO). A grain size analysis and a petrographic analysis were conducted on the section 605-662 mbsf of the AND-2A core. Results from this study indicate that reservoir quality sands are most dominant in the deltaic highstand and transgressive systems tracts. Transgressive systems tract sands in this section average 24% porosity, and deltaic highstand systems tract sands average 32% porosity during the MMCO.

A lower average porosity in the transgressive systems tract is attributed to poor overall sorting and a higher abundance of mud. The higher values in the highstand systems tract are due to poor lithification and very low abundances of carbonate cement. Overall, the porosity during this warmer climate regime is higher than the 19% whole core porosity documented by Dunbar et al. (2008a), and is well within porosity ranges documented elsewhere in the VLB (13-46% in CIROS-1 (Barrett, 1989)).

Below c. 700 mbsf, most porosity is occluded by cement, with poikilotopic cement prominent. This pattern indicates that there are additional processes associated with burial diagenesis that must also be taken into consideration. With increasing time and depth, most lithologies are eventually infiltrated by brine, increasing the likelihood for cement precipitation. These relationships suggest that trends associated with sequence stratigraphy and paleoclimate found throughout the core may become less important with increasing burial depth.

Implications for Assessment of Reservoir Quality in Glacially Influenced Systems:

Similarities between the results found in the VLB and those of producing glaciogenic systems indicates that the VLB is a viable analog for glaciogenic reservoirs worldwide. The highest quality reservoirs (17% porosity) in the Parana Basin are in the highstand systems tract of the Permo-Carboniferous Itarare Group. These highstand sands are interpreted to have been deposited by prograding deltas with a fluvial influence (Vesely et al., 2007). Sedimentation of the Itarare Group was predominantly in a glaciomarine environment (Rocha-Campos, 1967), particularly, shallow marine settings (Vesely et al., 2006). The Itarare Group deposits are very similar to the deposits found in AND-2A. Itarare Group sequences are dominated by diamictite, massive sandstone, and siltstone (Franca and Potter, 1991). In both AND-2A and the Itarare Group, high porosity reservoirs are most prominent in the highstand systems tracts of deltas. Similar to the VLB, in the Parana Basin, there are large, laterally extensive sand units that can be mapped across the entire basin (Franca and Potter, 1991). Vesely et al. (2007) recognized the sealing capabilities of muddy lithologies that occur in conjunction with sands that display the best potential for high reservoir performance. Vesely et al. (2007) also found that ice-proximal (lowstand systems tract) sands display poor porosity and low reservoir potential, although, the low porosity in this case is attributed to heterogeneity of sandstones, rather than an increase in cementation. Although carbonate cements are abundant (siderite, Fe-rich dolomite, Fe-rich calcite, calcite) in Itarare sandstones, anhydrite is the most common cement (Franca and Potter, 1991).

Trends documented in AND-2A are consistent throughout the core and similar trends are also apparent in the Parana Basin. The similarities in porosity distribution, lateral extent, and influence of muddy lithologies between the two locations, each with similar depositional histories, indicates that the results from this study can potentially be applicable worldwide.

The Plio-Pleistocene glacially derived Naust Formation, Norwegian Sea is documented by Ottesen et al. (2012) as a potential unconventional target in The Peon gas field. Naust Formation deposits are composed of prograding glaciogenic debris flows, glaciomarine, and glaciofluvial sediments. The target reservoirs in this setting are poorly documented, but consist of laterally extensive glaciofluvial sands deposited during deglaciation. Estimated recoverable reserves from the Peon gas field are 15-30 billion Sm^3 (oil-gas). Most of the higher quality reservoirs in AND-2A occur in sands representative of deposition during deglaciation. The most common reservoirs that record this in AND-2A are the deltaic sands, but, the fact that other deposits in analogous settings occur suggests that the potential exists for conventional and unconventional (lower porosity debris flows and heterolithic lithologies) reservoirs throughout glaciogenic systems.

CONCLUSIONS

Observations from the AND-2A core reveal that reservoir quality in the deposits of polar shelves is determined by factors that are absent or of reduced significance in lower latitude systems. For example, cold temperatures, which limit the rate of chemical reactions, are maintained to significant burial depth. Another key factor relates to climate change, the effects of which are amplified in polar settings. As glacial severity increases, so does the propensity for the formation of cryogenic brine in glaciomarine systems. The presence of such brines may impact reservoir quality by driving cementation that occludes primary pore space prior to significant burial. On the other hand, primary porosity can be maintained in deposits formed during warmer climate intervals, especially those formed when meltwater flux is high.

A strong correlation between reservoir quality and variations in paleoclimate and sea level was identified both in general and within individual sequences in the Neogene succession of the AND-2A core. The main influence on porosity in sandstones that formed during the coldest climate regimes is cementation by cryogenic brine, which leads to occlusion of most primary porosity. Cementation is more prominent in deposits of colder settings due to a lack of enclosing muddy lithologies that could prevent infiltration of the brine body. The main control on porosity in sandstones formed during the warmest climate regimes is the detrital mud content, and there is little drive for cementation. Therefore, the reservoir quality for these sandstones is relatively high.

The presence of highly porous (up to 40%), laterally extensive sands in glaciomarine settings indicates that these deposits could potentially serve as high quality reservoirs in petroleum systems. In addition, the persistence of patterns throughout the broad scale and in individual sequences indicates that these trends should hold merit, regardless of the scale of investigation. However, additional processes associated with burial diagenesis must be considered. An increase of cement in various sequence stratigraphic tracts and climatic regimes below c. 700 mbsf suggests that increased residence time with depth increases the likelihood for cementation in all settings, which in turn, reduces the significance of previously identified trends.

In summary, it is evident that the climate sensitivity characteristic of the high latitudes leads to changes in depositional systems, which can, in turn, produce significant heterogeneity in reservoir quality. The propensity for brine formation exists in most glaciomarine systems and should not be overlooked in reservoir assessments of glaciogenic deposits. Results of this study have the potential to change the way burial history and reservoir character are evaluated in sedimentary successions that formed in polar environments.

REFERENCES

Acton, G., Crampton, J., Di Vincenzo, G., Fielding, C.R., Florindo, F., Hannah, M., Harwood, D.M., Ishman, S., Johnson, K., Jovane, L., Levy, R.H., Lum, B., Marcano, M.C., Mukasa, S., Ohneiser, C., Olney, M.P., Riesselman, C., Sagnotti, L., Stefano, C., Strada, E., Taviani, M., Tuzzi, E., Verosub, K.L., Wilson, G.S., Zattin, M., and ANDRILL-SMS Science Team, 2008, Preliminary integrated chronostratigraphy of the AND-2A core, ANDRILL Southern McMurdo Sound Project, Antarctica. Terra Antarctica, v. 15, n. 1, p. 211-220.

Bache, F., Moreau, J., Rubino, J.L., Gorini, C., and Van-Vliet Lanoe, B., 2012, The subsurface record of Late Paleozoic glaciation in the Chaco Basin, Bolivia. Geological Society of London, Special Publications 2012, v.368, p. 257-274.

Baker, J.C., and Fielding, C.R., 1998, Diagenesis of glacimarine Miocene strata in CRP-1, Antarctica. Terra Antarctica, v.5, n. 3, p. 647-653.

Barrett, P.J., 1989, Antarctic Cenozoic history from the CIROS-1 drillhole, McMurdo Sound: New Zealand Department of Scientific and Industrial Research Bulletin, 237.

Barrett, P.J., and Hambrey, M.J., 1992, Plio-Pleistocene sedimentation in Ferrar Fiord, Antarctica. Sedimentology, v. 39, p. 109-123.

Barrett, P.J., 2007, Cenozoic climate and sea level history from glacimarine strata off the Victoria Land coast, Cape Roberts Project, Antarctica. In: Hambrey, M.J., Christoffersen, P., Glasser, N. F., and Hubbart, B., Glacial Processes and Products. International Associate of Sedimentologists Special Publications, v. 39, p. 259-287.

Bartek, L.R., Henrys, S.A., Andersen, J.B., and Barrett, P.J., 1996, Seismic stratigraphy of McMurdo Sound, Antarctica: implications for glacially influenced early Cenozoic eustatic change?. Marine Geology, v. 130, p. 79-98.

Behrendt, J.C., LeMasurier, W.E., Cooper, A.K., Tessensohn, F., Trehu, A., and Damaske, D., 1991, The West Antarctic rift system- A review of geophysical investigations. Antarctic Research Series, v. 53, p. 67-112.

Blackstone, B.A., 2009, Mid-Miocene stratigraphic succession of the Victoria Land Basin in the AND-2A drillcore from Southern McMurdo Sound, Antarctica: sequence stratigraphy, palaeobathymetry and reservoir development. MSc Thesis, University of Nebraska-Lincoln.

Brancolini, G., Cooper, A.K., and Coren, F., 1995 (a), Seismic facies and glacial history in the Western Ross Sea (Antarctica). In: Cooper, A.K., Barker, P.F., and Brancolini, G., Geology and Seismic Stratigraphy of the Antarctic Margin. American Geophysical Union Antarctic Research Series, v. 68. p. 209-233.

Brancolini, G., Busetti, M., et al., 1995 (b), Descriptive text for the seismic stratigraphic atlas of the Ross Sea, Antarctica. In: Cooper, A.K., Barker, P.F., and Brancolini, G., Geology and Seismic Stratigraphy of the Antarctic Margin. American Geophysical Union Antarctic Research Series, v. 68. p. 209-233.

Catuneanu, O., 2006, Principles of Sequence Stratigraphy. Elsevier, 375 p.

Cape Roberts Project Science Team, 1998, Initial report on CRP-1, Cape Roberts Project, Antarctica. Terra Antarctica, v. 5, n. 1, p. 1-187.

Cape Roberts Project Science Team, 1999, Studies from the Cape Roberts Project, Ross Sea, Antarctica: initial reports on CRP-2/2A. Terra Antarctica, v. 6, n. 1/2, p. 1-173.

Cape Roberts Project Science Team, 2000, Studies from the Cape Roberts Project, Ross Sea, Antarctica: initial report on CRP-3. Terra Anarctica, v. 7, n. 1, p. 1-209.

Cooper, A.K., Davey, F.J., and Behrendt, J.C., 1987, Seismic Stratigraphy and Structure of the Victoria Land Basin, Western Ross Sea, Antarctica. CPCEMR Earth Science series, v. 5B, pp. 27-76.

Dickinson W.R., 1985, Interpreting provenance relationships from detrital modes of sandstones. In: Zuffa, G.G., Provenance of Arenites, NATO ASI Series, v. 148, p. 333-361.

Douillet, G., Ghienne, J.F., Geraud, Y., Abueladas, A., Diraison, M., and Al-Zoubi, A., 2012, Late Ordovician tunnel valleys in southern Jordan. Geological Society of London, Special Publications 2012, v.368, p. 275-292.

Dunbar, G., Atkins, C., Magens, D., Niessen, F., and ANDRILL-SMS Science Team, 2008 (a), Physical properties of the AND-2A core, ANDRILL Southern McMurdo Sound Project, Antarctica. Terra Antarctica, v. 15, n. 1, p. 49-56.

Dunbar, G.D., Naish, T.R., Barret, P.J., Fielding, C.R., and Powell, R.D., 2008 (b), Constraining the amplitude of late Oligocene bathymetric changes in western Ross Sea during orbitally-induced oscillations in the East Antarctic Ice Sheet: 1. Implications for glacimarine sequence stratigraphic models. Palaeogeography, Palaeoclimatology, Palaeoecology, v. 260, p. 50-65.

El-Ghali, M.A.K., Mansurbeg, H., Morad, S., Al-Aasm, I., Ramseyer, K., 2006, Distribution of diagenetic alterations in glaciogenic sandstones within a depositional facies and sequence stratigraphic framework: Evidence from the Upper Ordovician of the Murzuq Basin, SW Libya. Sedimentary Geology, v. 190, p. 323-351.

Fielding, C.R., Woolfe, K.J, Purdon, R.G., Lavelle, M., and Howe, J.A., 1997, Sedimentological and stratigraphical re-evaluation of the CIROS-1 core, McMurdo Sound, Antarctica. Terra Antarctica, v. 4, n. 2, p. 149-160.

Fielding, C.R., Wolfe, K.J., Howe, J.A., and Lavelle, M., 1998, Sequence stratigraphic analysis of CRP-1, Cape Roberts Project, McMurdo Sound, Antarctica. Terra Antarctica, v. 5, n. 3, p. 353-361.

Fielding, C.R., Naishe, T.R., Woolfe, K.J., and Lavelle, M., 2000, Facies analysis and sequence stratigraphy of CRP-2/2A, McMurdo Sound, Antarctica. Terra Antarctica, v. 7, n. 3, p. 323-338.

Fielding, C.R., Henrys, S.A., and Wilson, T.J., 2006, Rift history of the western Victoria Land Basin: a new perspective based on integration of cores with seismic reflection data, In: Futterer, D.K., Damaske, D., Kleinschmidt, G., Miller, H., and Tessensohn, F., Antarctica: Contributions to Global Earth Sciences. Springer-Verlag, Berlin, p. 309-318.

Fielding, C.R., Atkins, C.B., et al. ANDRILL-SMS Science Team, 2008 (a), Sedimentology and stratigraphy of the AND-2A core, ANDRILL Southern McMurdo Sound Project, Antarctica. In: Harwood, D.M., Florindo, F., Talarico, F., Levy, R.H., Studies from the ANDRILL, Southern McMurdo Sound Project, Antarctica, Terra Antarctica, v. 15, p. 77-112.

Fielding, C.R, Whittaker, J., Henrys, S.A., Wilson, T.J., and Naish, T.R., 2008 (b), Seismic facies and stratigraphy of the Cenozoic succession in McMurdo Sound, Antarctica: Implications for tectonic, climatic and glacial history. Palaeogeography, Palaeoclimatology, Palaeoecology, v. 260, p. 8–29.

Fielding, C.R., Browne G.H., Field, B., Florindo, F., Harwood, D.M., Krissek, L.A., Levy, R.H., Panter, K.S., Passchier, S., and Pekar, S.F., 2011, Sequence stratigraphy of the ANDRILL AND-2A drill core, Antarctica: A long-term, ice-proximal record of Early to Mid-Miocene climate, sea-level and glacial dynamism. Palaeogeography, Palaeoclimatology, Palaeoecology, v. 305, n. 1, 337-351.

Fielding, C.R, Blackstone, B.A., Frank, T.D., and Gui, Z., 2012, Reservoir potential of sands formed in glaciomarine environments: an analogue study based on Cenozoic examples from McMurdo Sound, Antarctica. Geological Society of London, Special Publications 2012, v.368, p.211-228.

Florindo, F., Harwood, D.M., Talarico, F., Levy, R.H., and ANDRILL-SMS Science Team, 2008, Background to the ANDRILL Southern McMurdo Sound Project, Antarctica. Terra Antarctica, v. 15, p. 13-20.

Folk, R. L., 1980. *Petrology of sedimentary rocks.* Austin, Tex.: Hemphill Pub. Co.

Franca, A.B., and Potter, P.E., 1991, Stratigraphy and reservoir potential of glacial deposits of the Itarare Group (Carboniferous-Permian), Parana Basin, Brazil. AAPG Bulletin, v. 75, p. 62-85.

Frank, T.D, Gui, Z., and the ANDRILL SMS Science Team, 2010, Cryogenic origin for brine in the subsurface of southern McMurdo Sound, Antarctica. Geology, v.38, n.7, p.587-590.

Girard, F., Ghienne, J.F., and Rubino, J.L., 2012, Channelized sandstone bodies ('cordons') in the Tassili N'Ajjer (Algeria & Libya): snapshots of a Late Ordovician proglacial outwash plain. Geological Society of London, Special Publications 2012, v.368, p. 355-379.

Hamilton, R.J., Luyendyk, B.P., Sorlien, C.C., and Bartek, L.R., 2001, Cenozoic tectonics of the Cape Roberts Rift Basin and Transantarctic Mountain Front, southwestern Ross Sea, Antarctica. Tectonics, v. 20, p. 325-342.

Harwood, G., 1988, Microscopical techniques: II. Principles of sedimentary petrography. In: Tucker, R.M., Techniques in Sedimentology, p. 108-173.

Harwood, D.M., Florindo, F., Talarico, F., and Levy, R., 2008, Studies from ANDRILL Southern McMurdo Sound Project, Antarctica. Terra Antarctica, v. 15, p. 1-235.

Henrys, S.A, et al., 2007, Tectonic history of mid-Miocene to present southern Victoria Land Basin, inferred seismic stratigraphy in McMurdo Sound, Antarctica: A keystone in a changing world-Online proceedings of the 10th ISAES, edited by A.K Cooper and Raymond C.R. et al., USGS open file report 2007-1047, short research paper 049, 4p.

Herut, B., Starinsky, A., Katz, A., and Bein, A., 1990, The role of seawater freezing in subsurface brines. Geochimica et Cosmochimica Acta, v. 54, p. 13-21.

Hirst, J.P.P., Benbakir, A., Payne, D.F., and Westlake, I.R., 2002, Tunnel valleys and density flow processes in the Upper Ordovician glacial succession, Illizi Basin, Algeria. Journal of Petroleum Geology, v. 25, p. 297-324.

Hirst, J.P.P., 2012, Ordovician proglacial sediments in Algeria: insights into the controls on hydrocarbon reservoirs in the In Amenas field, Illizi Basin. Geological Society of London, Special Publications 2012, v.368, p. 319-353.

Lang, J., Dixon, R.J., Le Heron, D.P., and Winsemann, J., 2012, Depositional architecture and sequence stratigraphic correlation of Upper Ordovician glaciogenic deposits, Illizi Basin, Algeria. Geological Society of London, Special Publications 2012, v.368, p. 293-317.

Levell, B.K., Braakman, J.H., and Rutten, K.W., 1988, Oil-bearing sediments of Gondwana glaciation in Oman. AAPG Bulletin, v. 72, p. 775-796.

McGinnis L.D., 1981, Dry Valley Drilling Project. American Geophysical Union Antarctic Research Series, 33. Washington, D.C. 465 pp.

Melvin, J., and Norton, K., 2013, Advances in Arabian stratigraphy: Comparative studies of glaciogenic Juwayl and lower Unayzah strata (Carboniferous-Permian) of Saudi Arabia. GeoArabia, v. 18, p. 97-134.

Melvin, J., Sprague, R.A., and Heine, C.J., 2010, From bergs to ergs: The late Paleozoic Gondwanan glaciation and its aftermath in Saudi Arabia. Geological Society of American Special Papers, v. 468, p. 37-80.

Miller, J., 1988, Microscopical techniques: I. Slices, slides, staind and peels, In: Tucker, R.M., Techniques in Sedimentology, p. 86-1097.

Naish, T.R., Powell, R.D., and Levy, R., 2007, Studies from the ANDRILL McMurdo Ice Shelf Project, Antarctica. Terra Antarctica, v. 14, n. 3, p. 110-328.

Ottesen, D., Dowdeswell, J.A., Rise, L., and Bugge, T., 2012, Large scale development of the mid-Norwegian shelf over the last three million years and potential for hydrocarbon reservoirs in glacial sediments. Geological Society of London, Special Publications 2012, v.368, p. 53-73.

Panter, K.S., Talarico, F., et al. ANDRILL-SMS Science Team, 2008, Petrologic and geochemical composition of the AND-2A core, ANDRILL Southern McMurdo Sound Project, Antarctica. In: Harwood, D.M., Florindo, F., Talarico, F., Levy, R.H., Studies from the ANRILL, Southern McMurdo Sound Project, Antarctica, Terra Antarctica, v. 15, p. 147-192.

Passchier, S., Browne, G., Field, B., Fielding, C.R., Krissek, L.A., Panter, K., Pekar, S.F., ANDRILL-SMS Science Team, 2012, Early and Middle Miocene Antarctic glacial history from the sedimentary facies distribution in AND-2A, Ross Sea, Antarctica. GSA Bulletin, v. 123, p. 2352-2365.

Rocha-Campos, A.C., 1967, The Tubarao Group in the Brazillian portion of the Parana Basin. In: Bigarella, J.J., Becker, R.D., Pinto, I.D., Problems in Brazillian Gondwana Geology, p. 27-102.

Talarico, F.M., and Sandroni, S., 2011, Early Miocene basement clasts in ANDRILL AND-2A core and their implications for paleoenvironmental changes in the McMurdo Sound region (western Ross Sea, Antarctica). Global and Planetary Change, v. 78, n. 1-2, p. 23-35.

Tessensohn, F.G., and Wörner, 1991, The Ross sea rift system. In: Thomson, M.R.A, Crame, J.A., and Thomson, J.W., Geological Evolution of Antarctica, p. 273-271.

Tournier, F., Pagel, M., Portier, E., Wazir, I., and Fiet, N., 2010, Relationship between deep diagenetic quartz cementation and sedimentary facies in a Late Ordovician glacial environment. Search and Discovery, Abstract #50263.

Vail, P.R., Audemard, F., Bowman, S.A., Eisner, P.N., and Perez-Cruz, C., 1991, The stratigraphic signatures of tectonics, eustasy and sedimentology- an overview. In: Einsele, G., Ricken, W., and Seilacher, A., Cycles and Events in Stratigraphy, p. 617-659.

Vesely, F.F. and Assine, M.L., 2006, Deglaciation sequences in the Permo-Carboniferous Itarare Group, Parana Basin, southern Brazil. Journal of South American Earth Sciences, v. 22, p. 156-168.

Vesely, F.F., Rostirolla, S.P., Appi, C.J., and Kraft, R.P, 2007, Late Paleozoic glacially related sandstones reservoirs in the Parana Basin, Brazil. AAPG Bulletin, v. 91, n. 2, p. 151-160.

FIGURES AND TABLES

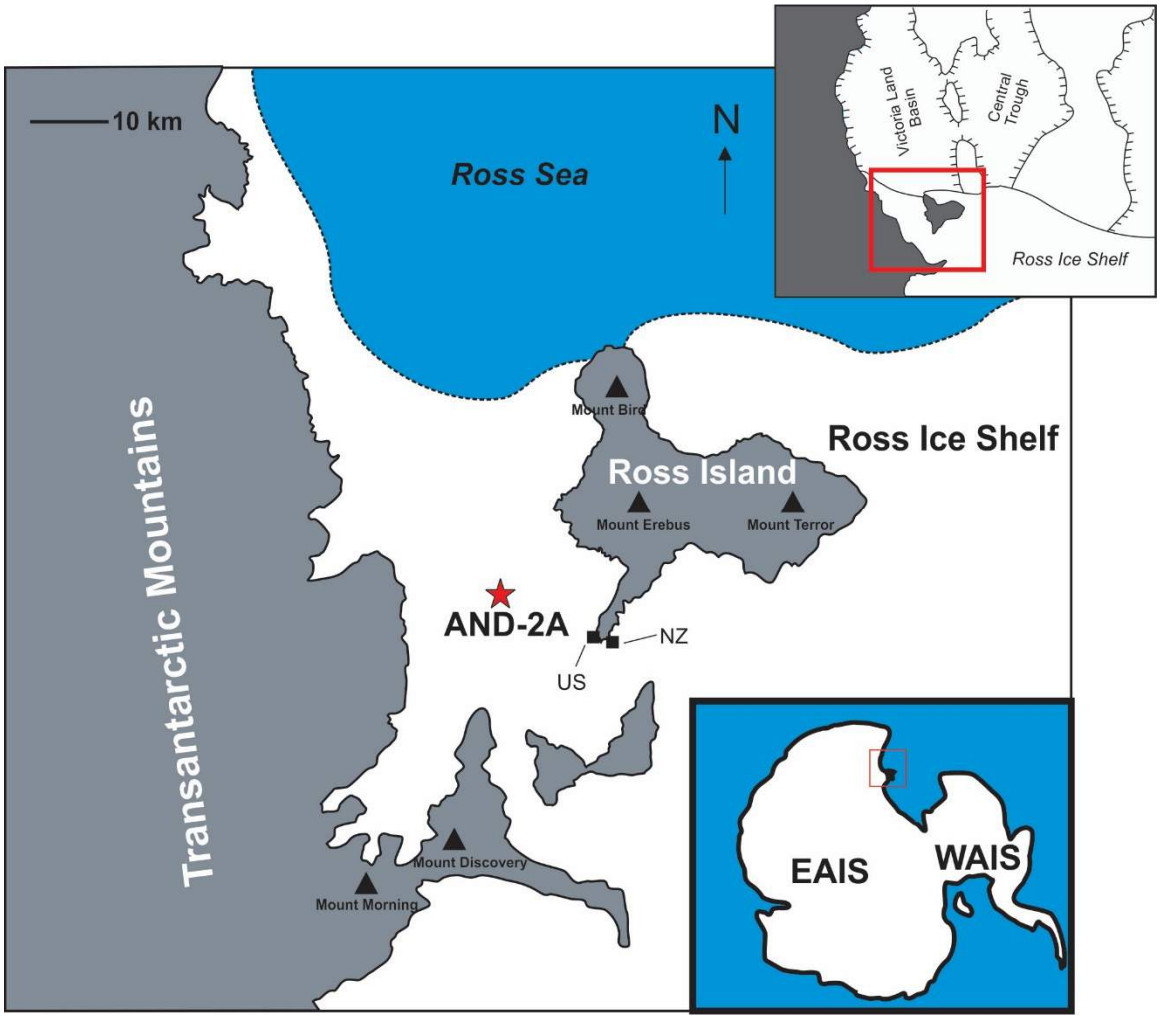

Figure 1: Location map showing geologic context of Southern McMurdo Sound, Antarctica (inset), the location of the AND-2A core (red star), Neogene, rift-related volcanic edifices (black triangles), and principle research bases in the area (black squares).

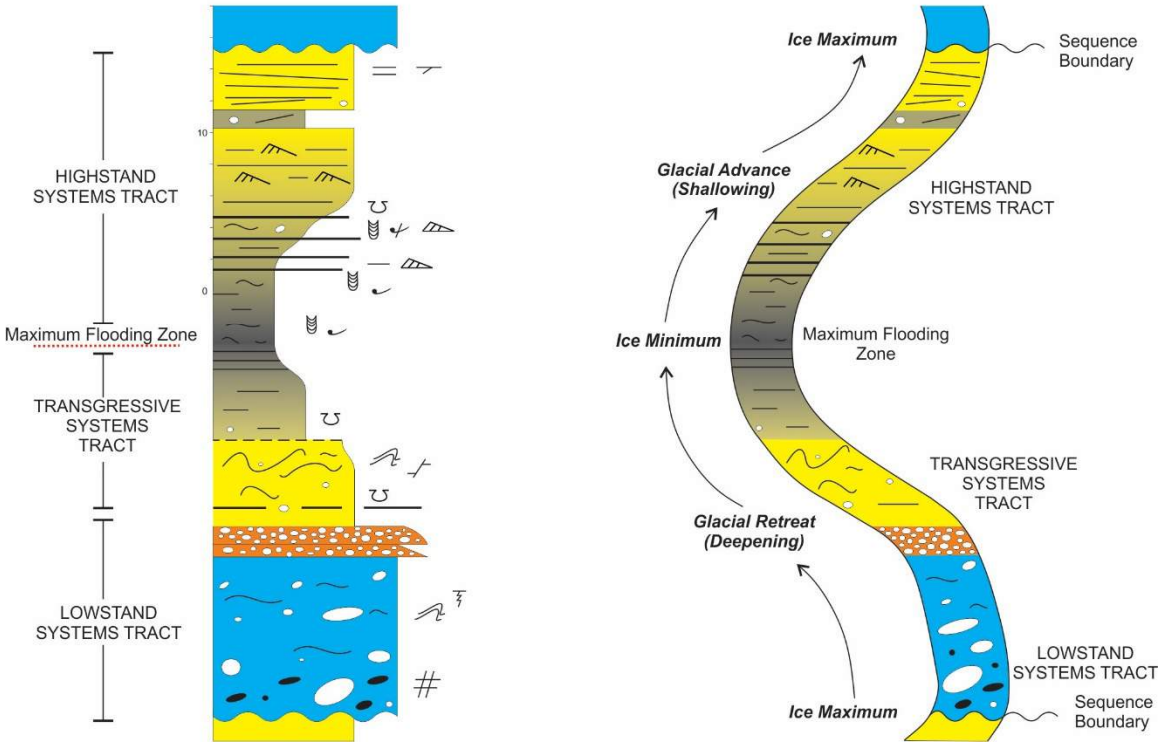

Figure 2: The idealized depositional sequence of the Cenozoic succession of Southern McMurdo Sound modified from Fielding et al. (2011). Vertical stacking patterns, depositional environments, and systems tracts are shown.

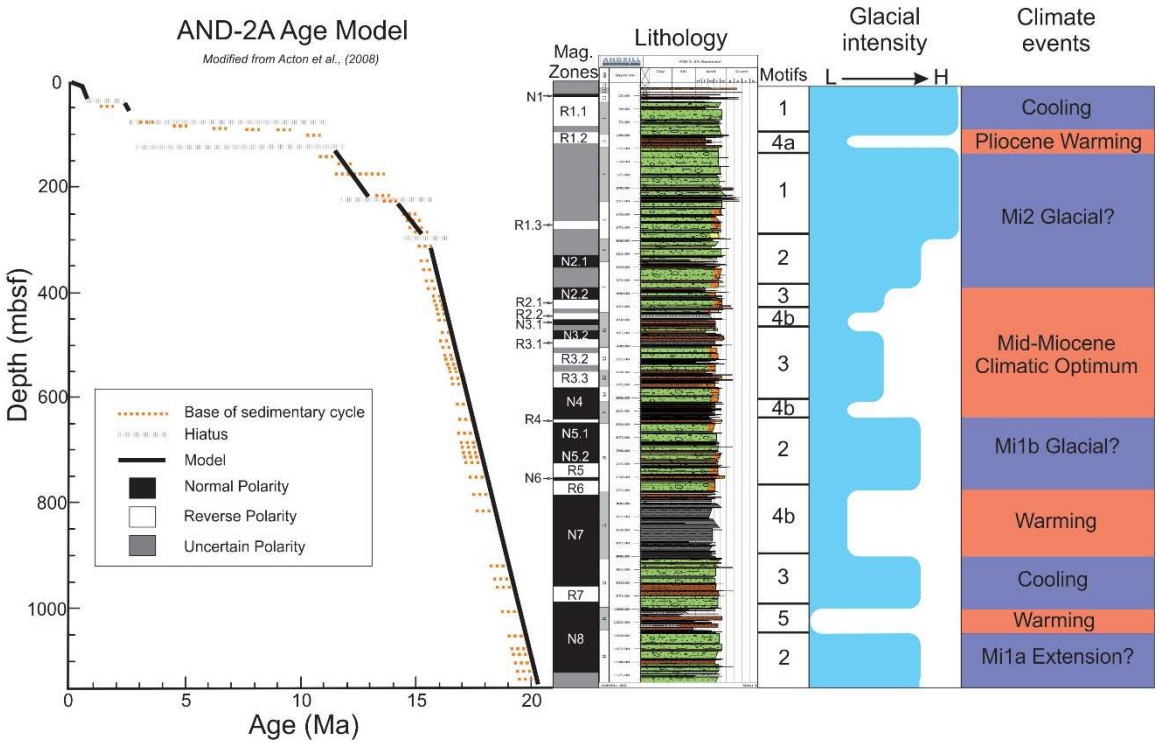

Figure 3: Paleoclimate record for the AND-2A core developed using stacking patterns of the six stratigraphic motifs of Fielding et al. (2011). The interpreted paleoclimate record matches accordingly to known climatic events during the Neogene. Chronostratigraphic data (magnetostratigraphy, diatom FAD or LAD, *Neogloboquadrina pachyderma* forams, ^{40}Ar-^{39}Ar, Strontium, sedimentary cycles) are modified from Acton et al. (2008)

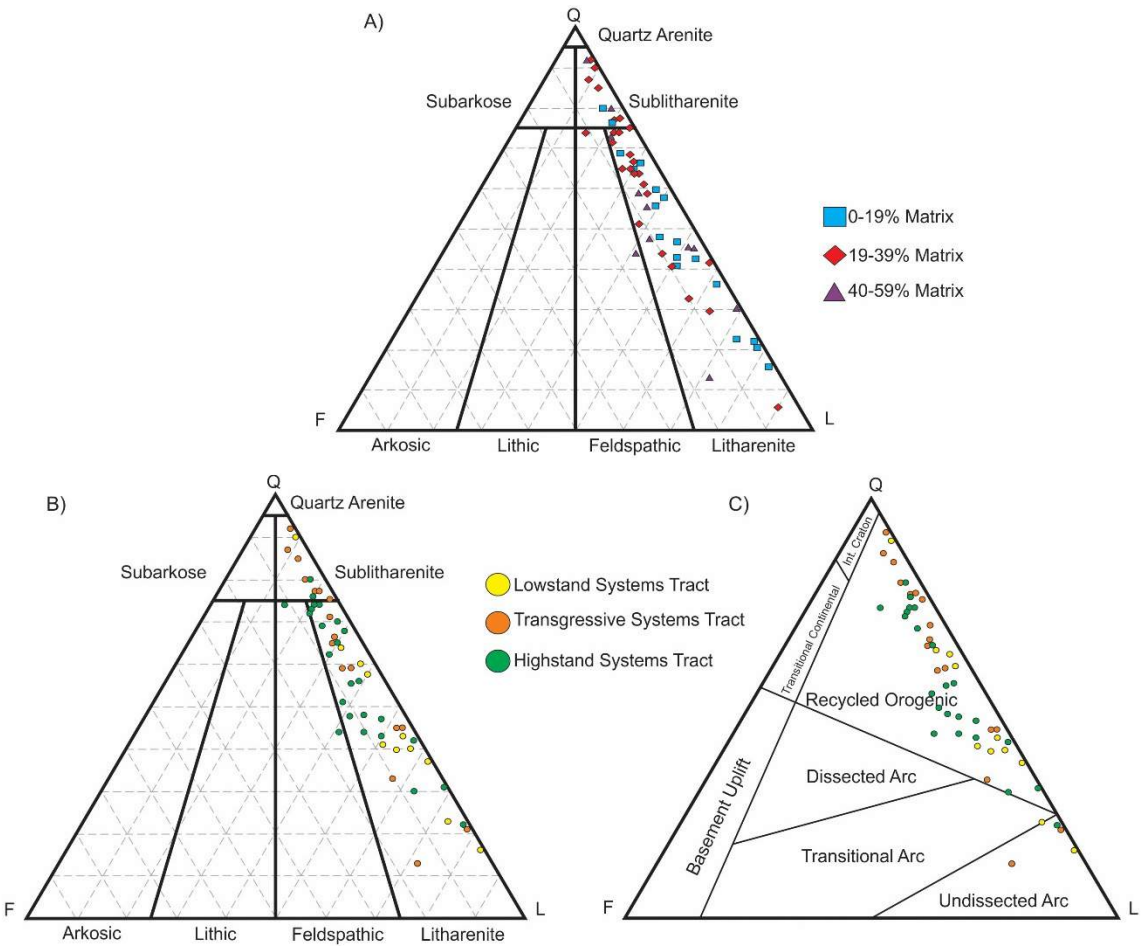

Figure 4: Ternary plots of (a) sandstone types with matrix incorporated, (b) sandstone types with their associated sequence tracts, and (c) provenance based on results of point counting.

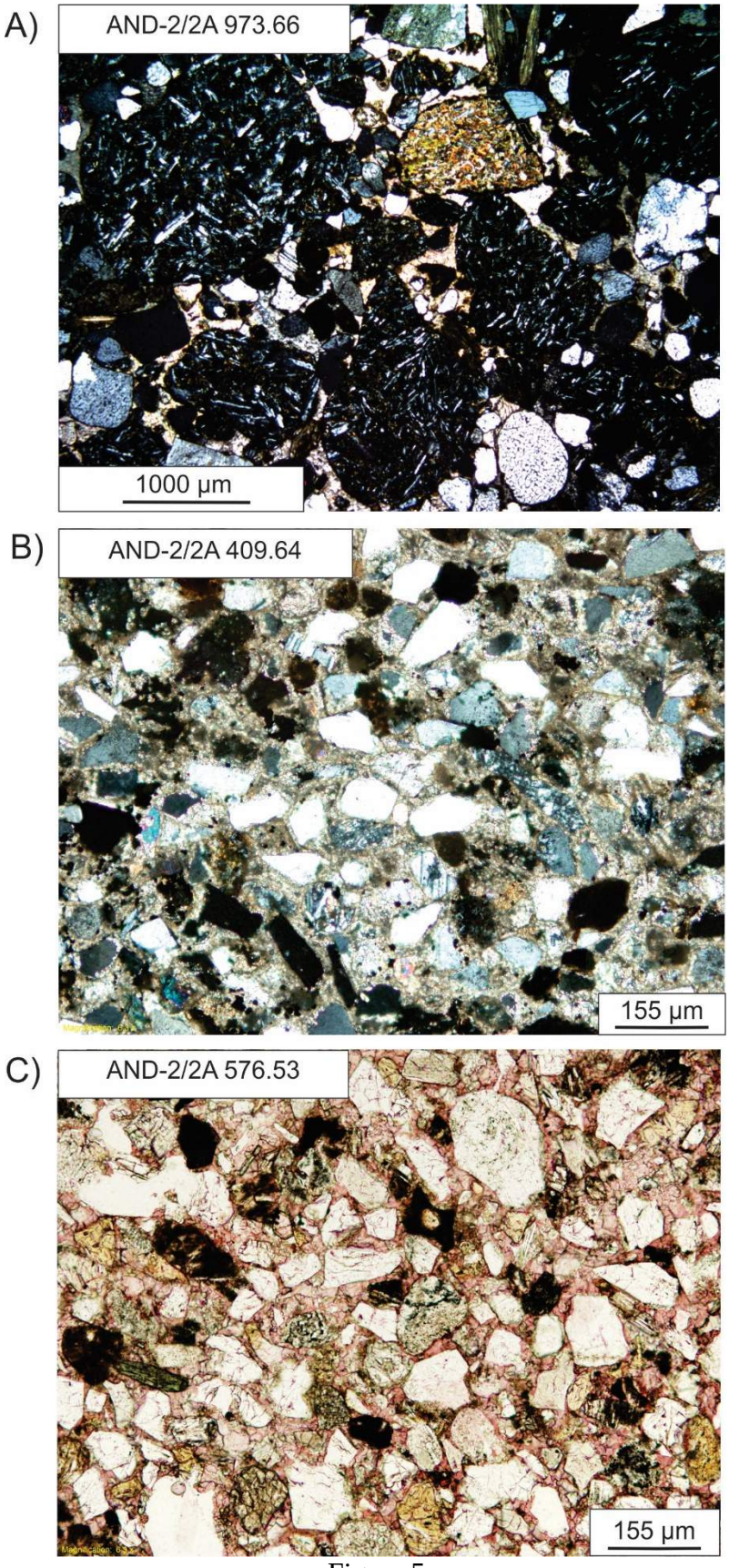
A)
AND-2/2A 973.66
1000 µm
B)
AND-2/2A 409.64
155 µm
C)
AND-2/2A 576.53
155 µm

Figure 5

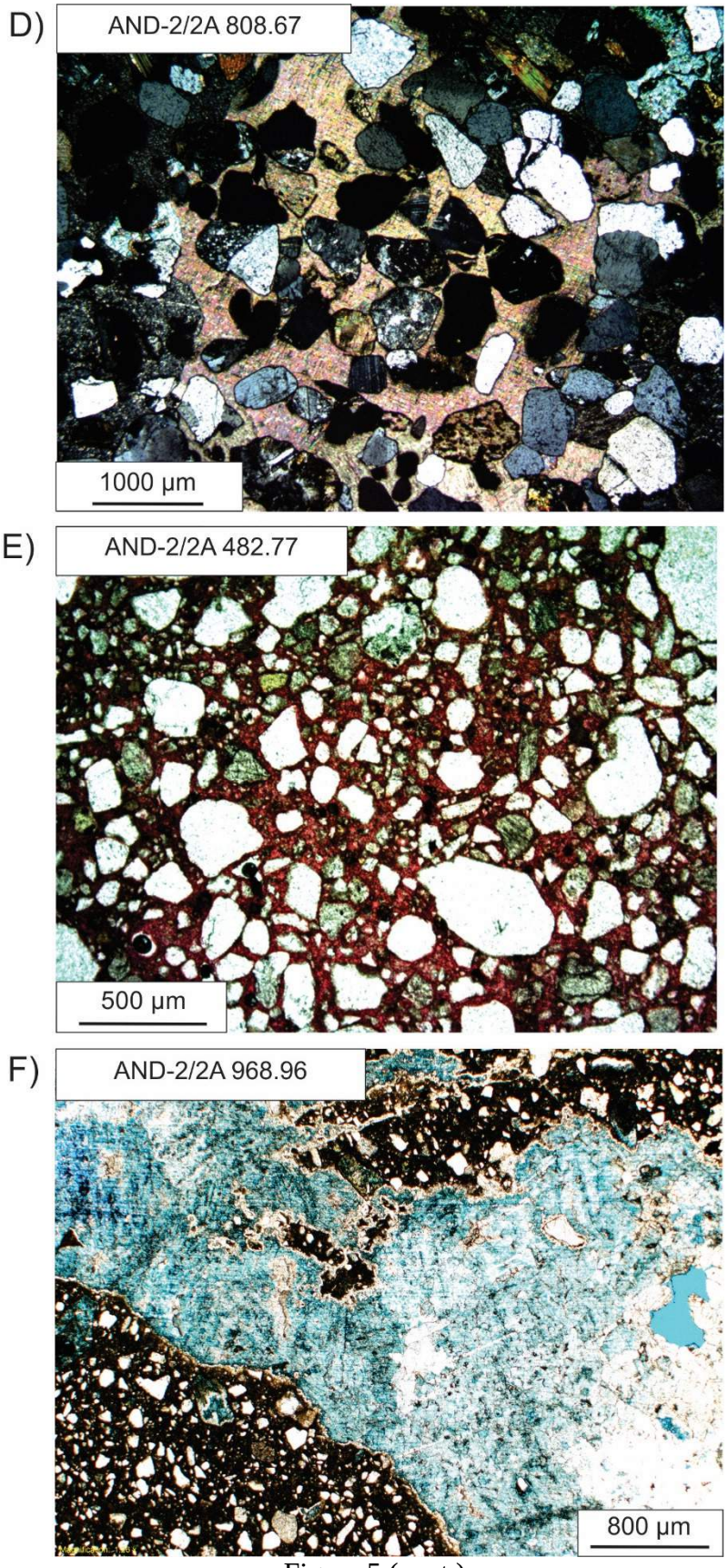

Figure 5 (cont.)

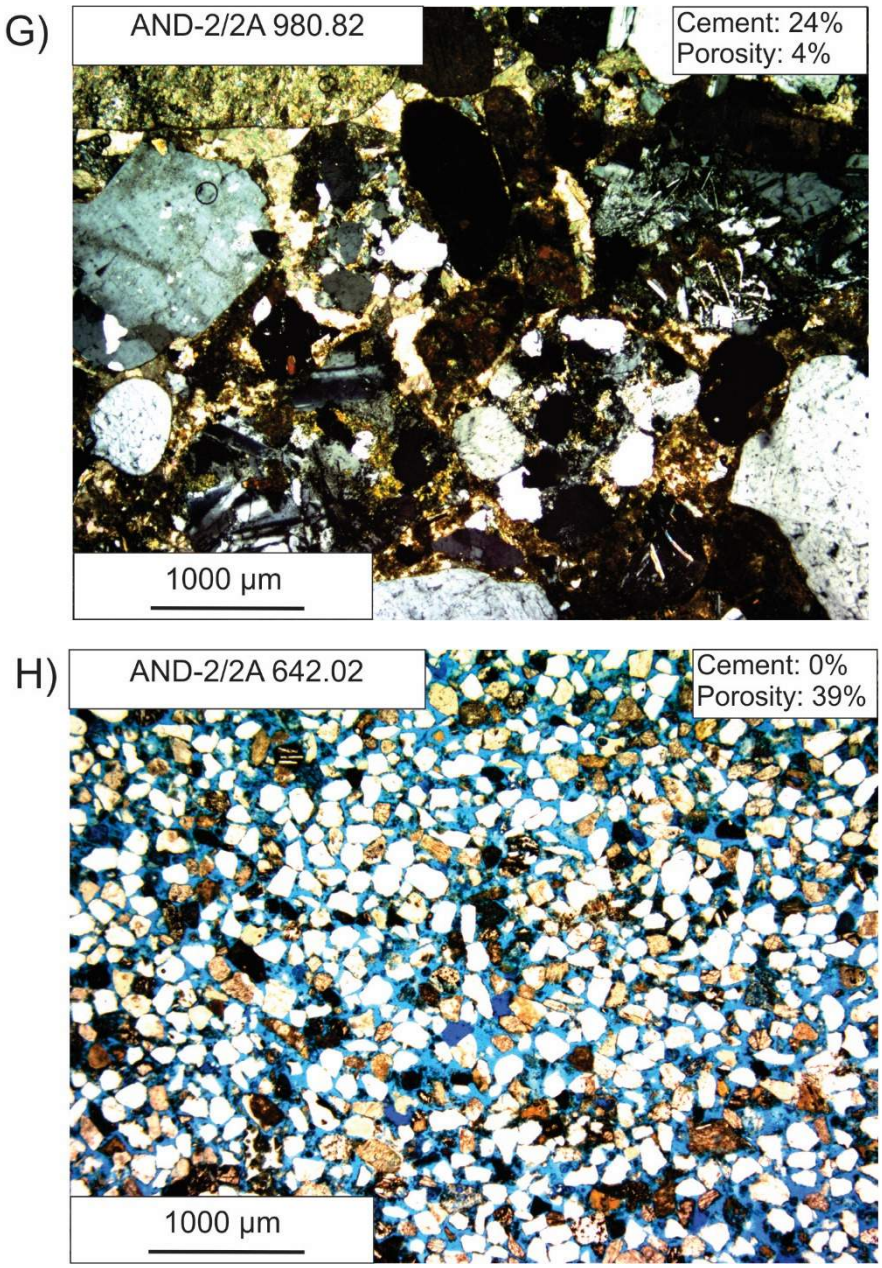

Figure 5 (cont.): Photomicrographs of cements and framework grains of AND-2A samples. (a) Labile framework grains derived from crystalline basement and other volcanics are well preserved. Three carbonate cement morphologies are present: (b) microcrystalline, (c) blocky, and (d) poikilotopic. Calcite (e) is the dominant carbonate phase, but ferroan dolomite is also present, usually as coarse fracture fill (f). Cement and porosity values are highly variable and range from heavily occluded (g), to highly porous with no cementation (h).

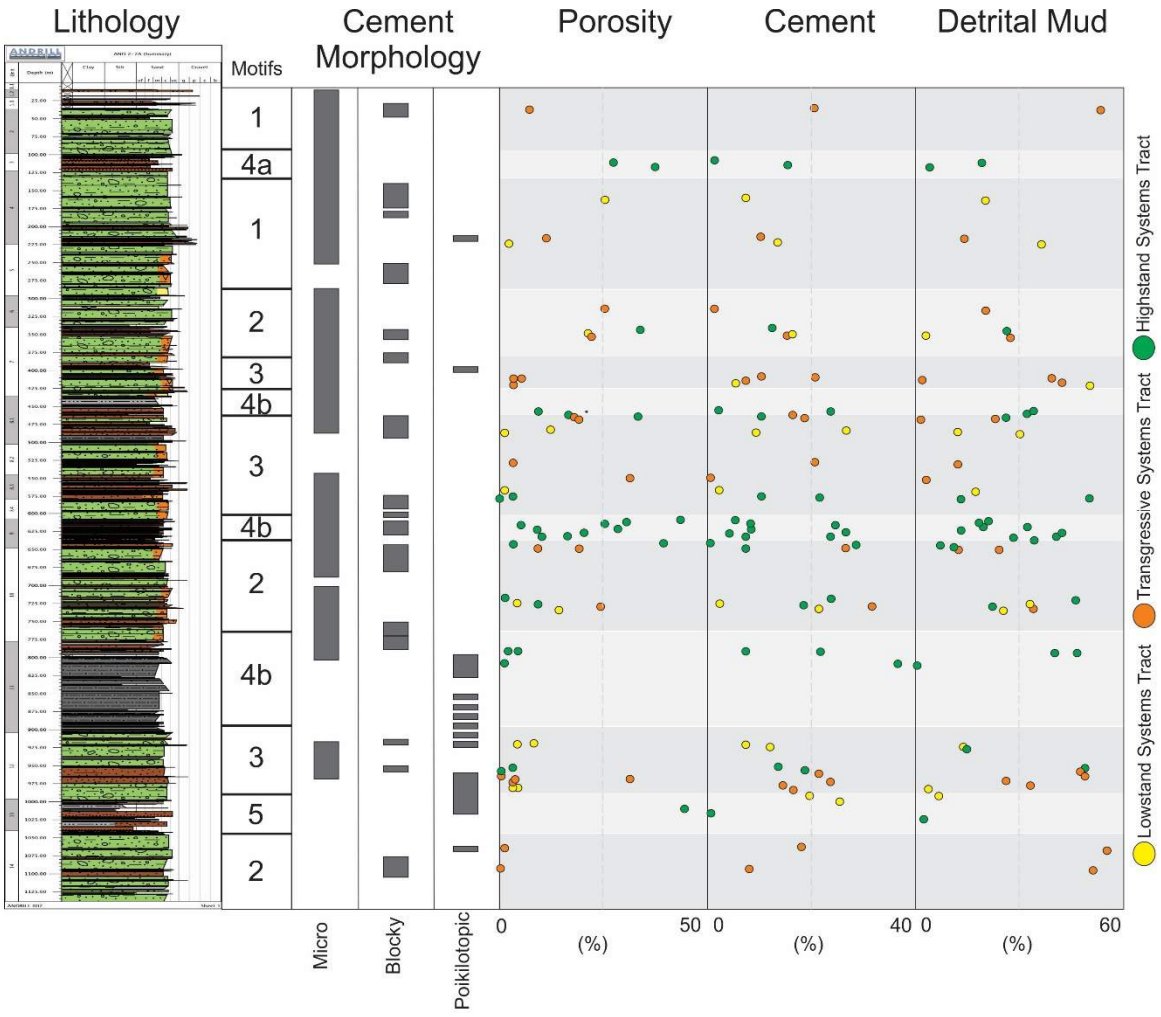

Figure 6: Distribution of cement morphologies, cement, porosity, and detrital mud in sandstone samples throughout the AND-2A succession.

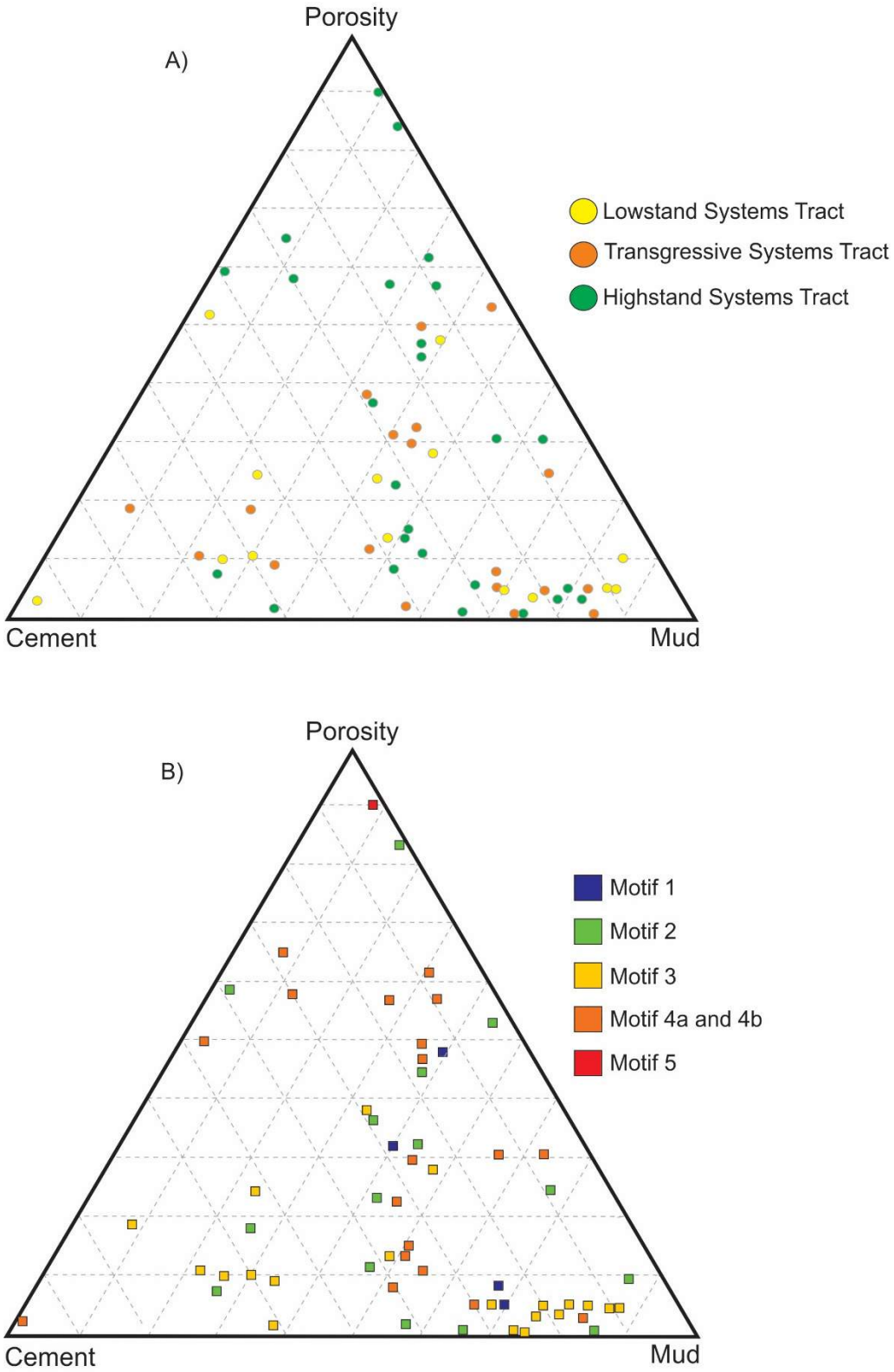

Figure 7: Porosity, cement, and detrital mud distribution based on a) systems tract and b) stratigraphic motifs.

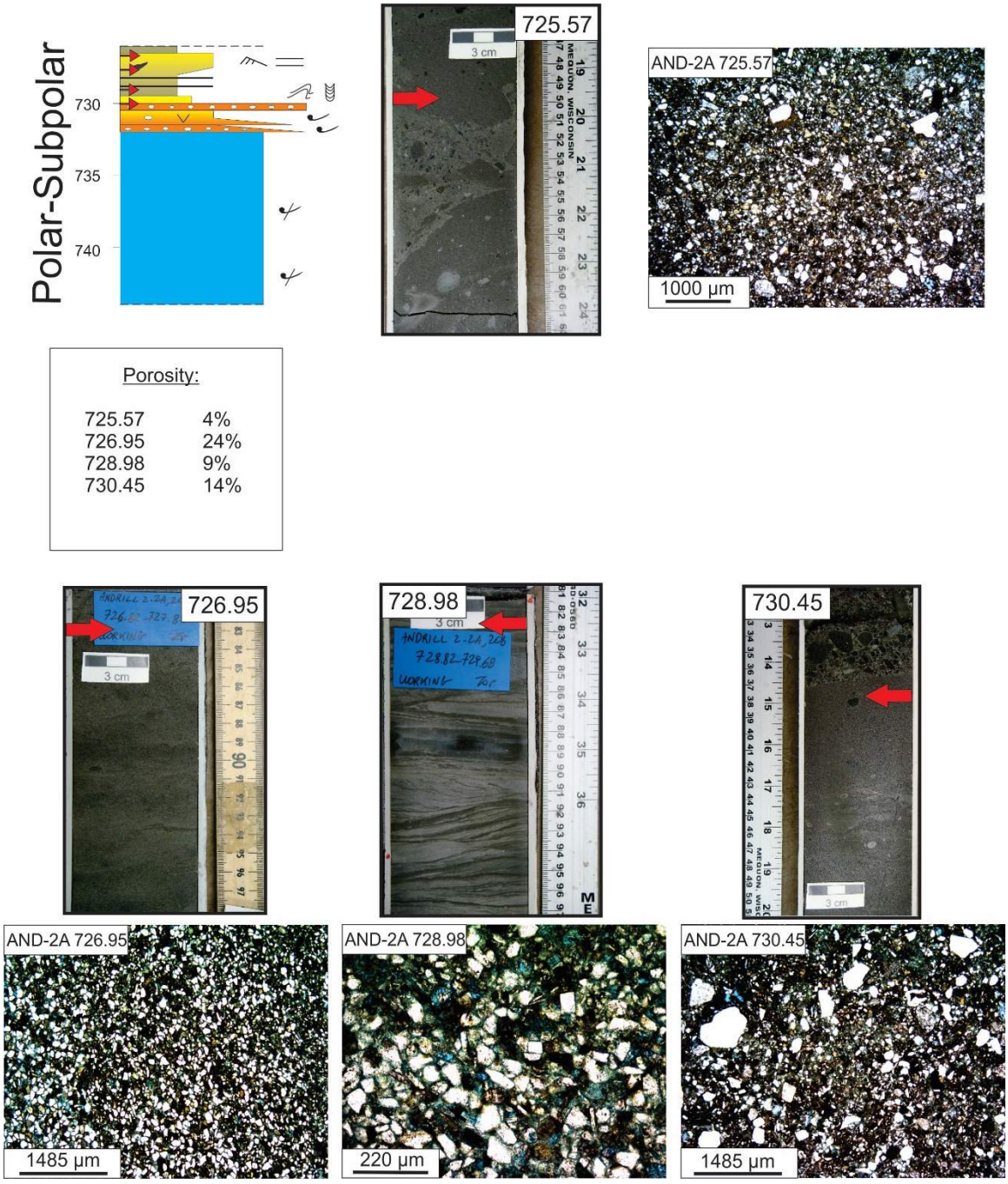

Figure 8a: Porosity distribution within sequences deposited during polar-subpolar glacial regimes demonstrating a negative influence from a lack of muddy lithologies that serve as a porosity preservation mechanism in temperate systems. Red arrows indicate location of polar-subpolar samples.

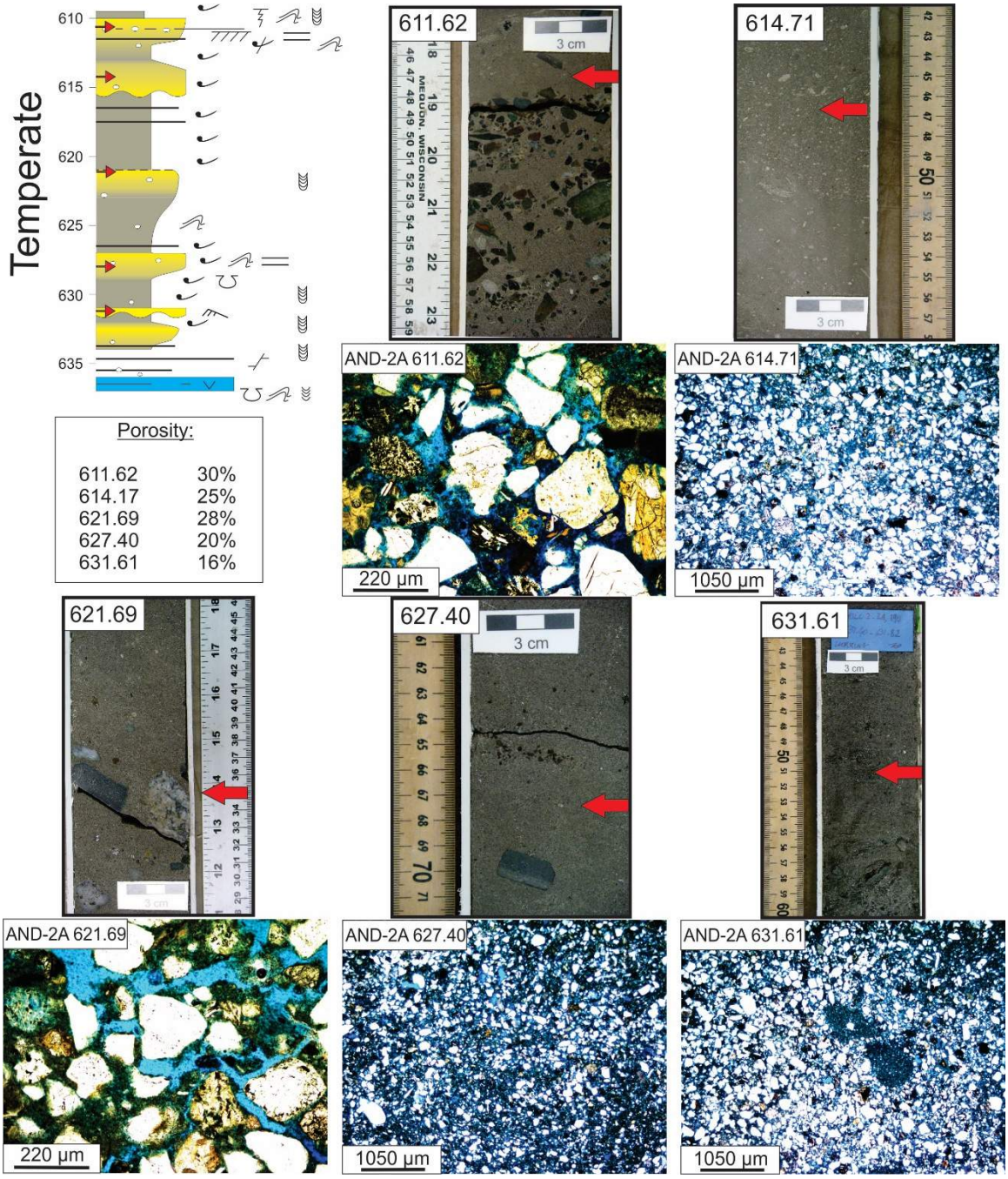

Figure 8b: Porosity distribution within sequences deposited during temperate glacial regimes demonstrating positive influence from muddy lithologies that serve as a porosity preservation mechanism in temperate systems. Red arrows indicate location of temperate samples.

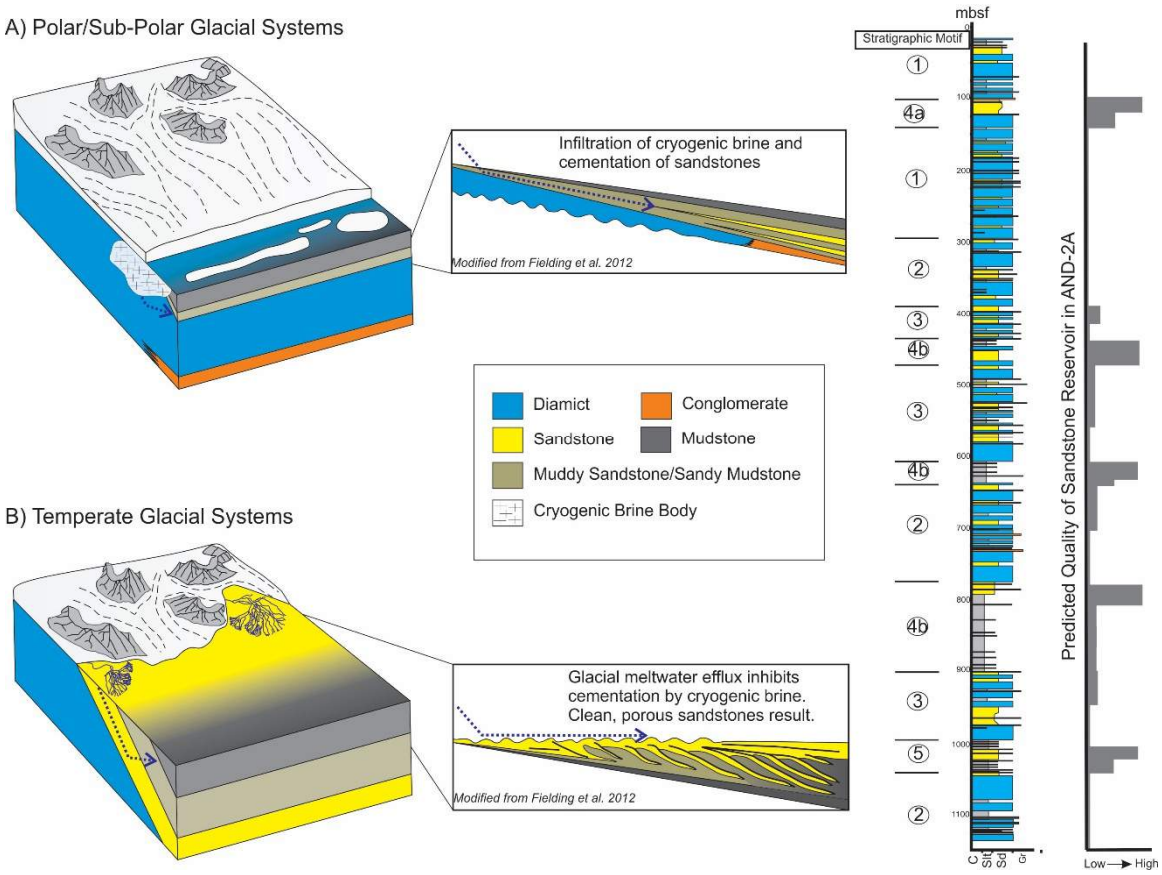

Figure 9: (a) Depositional model and dip parallel schematic for the lowstand and transgressive systems tracts of polar/sub-polar glaciomarine systems based on AND-2A. Lowstand and transgressive systems tract lithofacies will produce a diamict dominated succession with a minor sand constituent. Sandstone from polar and sub-polar glaciomarine systems will be clean, but heavily cemented, resulting in poor reservoirs in these settings. (b) Depositional model and dip parallel schematic for the highstand systems tracts of temperate glaciomarine systems based on AND-2A. Highstand systems tract lithofacies are dominated by sandstone and mudstone. Sandstone from temperate glaciomarine systems will be clean and porous, resulting in high quality reservoirs in these settings. The quality of sandstone reservoirs in the AND-2A core can be predicted using trends seen in paleoclimate and sequence stratigraphy.

Motif	Lithological Characteristics	Deposition	Regime Interpretation
1	Diamictite dominated. Diamictite displays shear and brecciation fabrics and are amalgamated. Limited range and thickness of other lithologies.	Ice-proximal, marine proglacial-subglacial.	Cold, polar-subpolar glacial regime with minor meltwater involvement.
2	Diamictite dominated. Diamictite are more variable and are less amalgamated. Greater range and abundance of other lithologies.	Ice-proximal, marine proglacial-subglacial.	Subpolar glacial regime with increased meltwater involvement.
3	Diverse lithologies including diamictite of varying character, not diamictite dominated.	Periodic advancement of tidewater glaciers into the basin.	High-latitude temperate glacial regime, proximal wet based glaciers.
4a	Contains basal diamictite but dominated by stratified sandstones.	Nearshore marine sediment surface, with minimal glacial influence	High-latitude temperate glacial regime, distant wet based glaciers.
4b	Contains basal diamictite but dominated by bioturbated and fossiliferous mudrock.	Offshore marine shelf with distant glacial activity.	High-latitude temperate glacial regime, distant wet based glaciers.
5	Contains thin basal diamictite or conglomerate but dominated by sandstone and mudrock.	Distal glaciomarine during periods of ice advance and open marine conditions.	Minimal glacial influence.

Table 1: Characteristics and interpretations of stratigraphic motifs in AND-2A core (from Fielding et al., 2011).

Depth (mbsf)	Sandstone	Morphology	Cement Type	Seq Strat	Motif	%Porosity	%Cement	%Matrix
37.04	Lithic Wacke	Microgranular	Calcite	TST	1	7	20	53
109.70	Lithic Wacke	Porous	Dolomite	HST	4a	27	1	19
115.38	Litharenite	Microscrystalline	Dolomite	HST	4a	37	15	4
161.78	Lithic Wacke	Microcrystalline	Calcite	LST	1	25	7	20
215.49	Litharenite	Poikilotopic	Dolomite	TST	1	11	10	14
223.20	Lithic Wacke	Microgranular	Calcite	LST	1	2	13	36
314.30	Lithic Wacke	Matrix	None	TST	2	25	1	20
341.75	Lithic Wacke	Microcrystalline	Calcite	HST	2	31	12	26
350.07	Litharenite	Blocky	Calcite	LST	2	22	16	3
353.32	Lithic Wacke	Microcrystalline	Calcite	TST	2	21	15	27
409.64	Sublithic Wacke	Microgranular	Dolomite	TST	3	3	10	39
410.40	Litharenite	Poikilotopic	Calcite	TST	3	5	20	2
414.04	Sublithic Wacke	Microcrystalline	Dolomite	TST	3	3	7	42
417.83	Sublithic Wacke	Microcrystalline	Calcite	LST	3	3	5	50
455.05	Lithic Wacke	Microcrystalline	Calcite	HST	4b	9	2	34
458.30	Sublithic Wacke	Microscrystalline	Calcite	HST	4b	17	23	32
462.33	Lithic Wacke	Microcrystalline	Calcite	TST	4b	18	16	26
463.61	Sublithic Wacke	Microcrystalline	Calcite	TST	4b	33	10	23
465.53	Sublitharenite	Microgranular	Dolomite	TST	4b	19	18	1
482.77	Litharenite	Micro-poikilotopic	Calcite	LST	3	12	26	12
486.46	Sublithic Wacke	Microcrystalline	Dolomite	LST	3	1	9	30
527.56	Sublitharenite	.Blocky-Poik	Dolomite	TST	3	3	20	12
549.95	Sublitharenite	Porous	None	TST	3	31	0	3
566.10	Lithic Wacke	Micro-blocky	None	LST	3	1	2	17
575.26	Lithic Wacke	Microcrystalline	Calcite vein	HST	3	3	10	50
576.53	Litharenite	Blocky-microgranular	Calcite	HST	3	<1	21	13
609.03	Sublithic Wacke	Microgranular	None	HST	4b	43	5	21
611.62	Lithic Wacke	Microcrystalline	None	HST	4b	30	5	18
614.71	Lithic Wacke	Microcrystalline	None	HST	4b	25	8	19
616.36	Lithic Wacke	Microgranular	Calcite	HST	4b	5	24	32
621.69	Litharenite	Microcrystalline	None	HST	4b	28	8	13
625.07	Lithic Wacke	Microcrystalline	Calcite	HST	4b	9	26	42
627.40	Sublithic Wacke	Microcrystalline	None	HST	4b	20	4	41
631.61	Sublithic Wacke	Microgranular	Calcite	HST	4b	16	7	28
633.11	Lithic Wacke	Microscrystalline	Calcite	HST	4b	10	23	34
642.02	Sublitharenite	Porous	None	HST	2	39	0	7
642.52	Litharenite	Blocky-micro	Calcite	HST	2	3	28	11
647.78	Litharenite	Blocky-Micro	Dolomite	TST	2	9	26	12
648.49	Lithic Wacke	Microgranular	None	TST	2	19	7	24
718.22	Lithic Wacke	Microcrystalline	Calcite	HST	2	1	23	46
725.57	Lithic Wacke	Matrix	None	LST	2	4	2	33
726.95	Lithic Wacke	Microgranular-Blocky	Calcite	HST	2	24	18	22
728.98	Sublithic Wacke	Microcrystalline	Calcite	TST	2	9	31	34
730.45	Lithic Wacke	Microgranular	Calcite	LST	2	14	21	25
790.86	Lithic Wacke	Micro-Matrix	Calcite	HST	4b	2	7	40
791.13	Lithic Wacke	Microcrystalline	Calcite	HST	4b	4	21	46
808.67	Litharenite	Poikilotopic	Calcite	HST	4b	1	36	0
919.59	Litharenite	Microcrystalline	Dolomite	LST	3	8	7	14
921.13	Litharenite	Micro-Blocky-Poik	Dolomite	LST	3	4	12	15
954.37	Lithic Wacke	Microgranular	Calcite	HST	3	3	13	58
958.70	V.F wacke	Blocky	Calcite vein	HST	3	0	18	54
963.54	V.F wacke	Microcrystalline	Calcite	TST	3	0	21	59
968.96	Sublithic Wacke	Microcrystalline	Dolomite vein	TST	3	31	23	26
970.64	Lithic Wacke	Microcrystalline	Dolomite	TST	3	3	14	36
973.66	Litharenite	Poikilotopic	Calcite	TST	3	3	16	5
979.66	Litharenite	Poikilotopic	Calcite	LST	3	3	19	10
980.82	Litharenite	Poikilotopic	Calcite	LST	3	4	24	10
1011.00	Litharenite	Porous	None	HST	5	44	0	4
1065.75	Lithic Wacke	Microgranular	Calcite	TST	2	1	18	57
1093.61	Lithic Wacke	Porous	Calcite	TST	2	0	7	55

Table 2: List of samples and their associated properties.

APPENDIX A:

Raw Data for QFL Point Counts and Porosity, Cement, and Matrix Point Counts

Data was collected using a maximum grid spacing that encompassed the entire thin section. Three hundred counts were taken at 20x magnification for each sample. Sandstone type was determined based on relative percentages of quartz, feldspar, and lithics (ex. %Q = Q/Q+F+L). Porosity, cement, and matrix volumes were determined based on the number of points for each variable divided by 300 (ex. %Porosity = Pore Space/300).

Depth (mbsf)	Q	L	F	Other
37.04	0	148	0	152
109.70	33	115	2	150
115.38	53	62	9	176
161.78	54	76	4	166
215.49	50	183	2	65
223.20	90	43	7	160
314.30	61	106	18	115
341.75	61	15	8	216
350.07	101	60	7	132
353.32	65	29	7	199
409.64	122	13	6	159
410.40	94	111	5	90
414.04	130	10	2	158
417.83	120	9	1	170
455.05	65	20	8	207
458.30	63	15	3	219
462.33	84	25	7	184
463.61	49	7	2	242
465.53	146	26	10	118
482.77	86	145	2	67
486.46	153	16	2	129
527.56	109	50	5	136
549.95	157	32	8	103
566.10	36	182	1	81
575.26	77	52	9	162
576.53	67	68	7	158
609.03	109	32	7	152
611.62	111	41	9	139
614.71	104	72	10	114
616.36	50	14	5	231
621.69	129	36	11	124
625.07	33	23	9	235
627.40	131	27	18	124
631.61	134	39	8	119
633.11	43	38	11	208
642.02	126	27	5	142
642.52	86	39	7	168
647.78	52	61	3	184
648.49	112	47	7	134
718.22	37	51	1	211
725.57	27	34	5	234

Depth (mbsf)	Q	L	F	Other
726.95	69	23	5	203
730.45	48	57	12	183
790.86	21	44	5	230
791.13	59	63	14	164
808.67	66	149	1	84
919.59	48	153	8	91
921.13	78	97	15	190
954.37	31	29	10	230
958.70	30	30	30	210
963.54	x	x	x	x
968.96	27	12	1	260
970.64	70	31	6	193
973.66	48	179	2	71
979.66	112	70	5	113
980.82	82	103	6	109
1011.00	65	60	11	164
1065.75	7	39	8	246
1093.61	64	37	8	191

Depth (mbsf)	Pore Space	Cement	Matrix	Grain
37.04	20	60	161	59
109.70	86	43	18	153
115.38	112	46	13	129
161.78	74	20	60	146
215.49	33	29	42	196
223.20	7	39	107	147
314.30	75	4	61	160
341.75	94	36	78	92
350.07	67	49	10	174
353.32	63	46	82	109
409.64	8	30	116	146
410.40	16	61	7	216
414.04	8	20	125	147
417.83	8	15	149	128
455.05	28	70	101	101
458.30	50	69	97	84
462.33	54	47	78	121
463.61	99	29	69	103
465.53	58	53	4	185
482.77	37	77	35	151
486.46	4	26	91	179
527.56	10	60	36	194
549.95	93	0	8	199
566.10	3	6	52	239
575.26	10	30	150	110
576.53	2	64	40	194
609.03	128	16	62	94
611.62	91	14	53	142
614.71	74	25	57	144
616.36	16	73	95	116
621.69	84	23	39	154
625.07	26	78	125	71
627.40	61	13	122	104
631.61	47	20	84	149
633.11	31	68	101	100
642.02	116	0	21	163
642.52	10	84	34	172
647.78	27	79	37	157
648.49	57	20	150	73

Depth (mbsf)	Pore Space	Cement	Matrix	Grain
718.22	3	70	138	89
725.57	12	6	100	182
726.95	72	55	67	106
728.98	27	92	103	78
730.45	43	62	75	120
790.86	5	22	121	152
791.13	13	62	138	87
808.67	4	107	0	189
919.59	25	21	42	212
921.13	13	36	46	205
954.37	8	40	173	79
958.70	0	54	161	85
963.54	0	63	176	61
968.96	93	69	79	59
970.64	9	42	109	140
973.66	8	48	16	228
979.66	10	57	29	204
980.82	11	71	29	189
1011.00	131	0	14	155
1065.75	3	53	73	171
1093.61	0	20	113	167

APPENDIX B:

Thin Section Scans

Thin section scans from the AND-2A core, Victoria Land Basin, Antarctica. Sample numbers reflect the depth in meters below sea floor (mbsf). Scans encompass the entire thin section at 4x magnification.

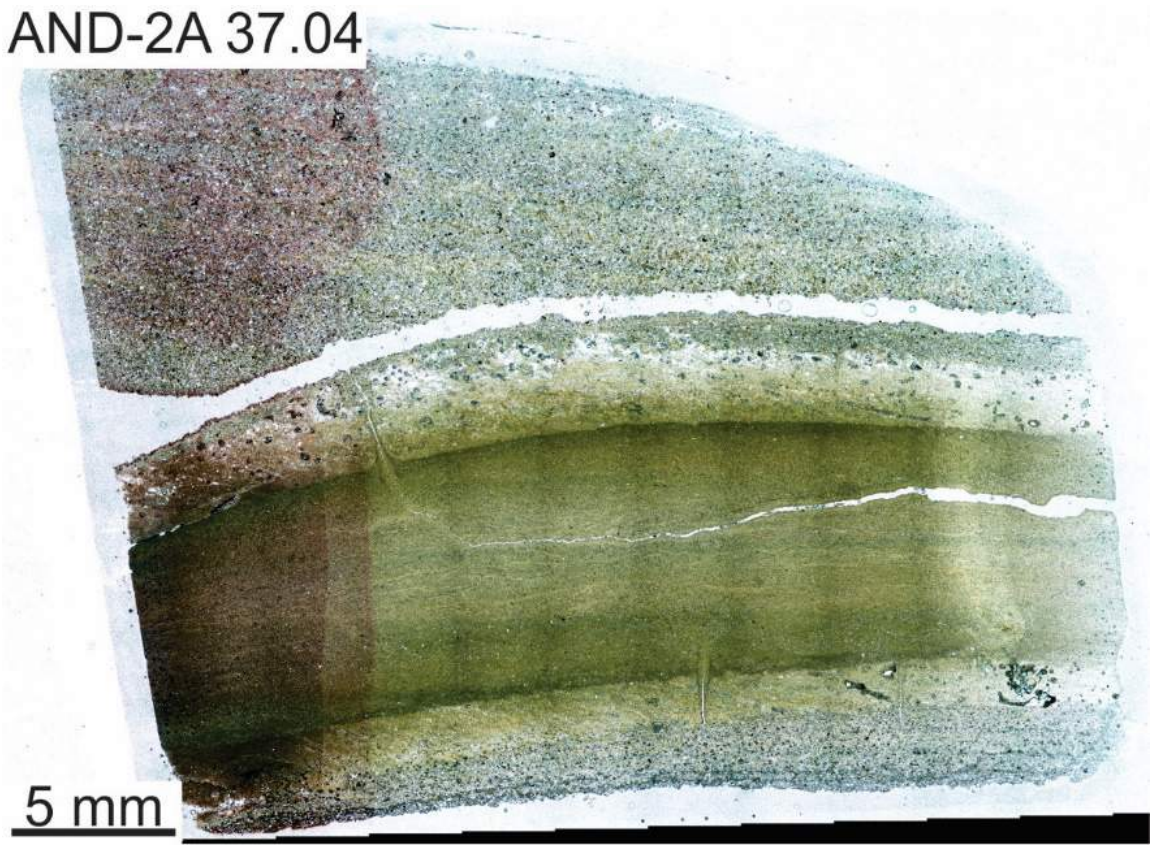
AND-2A 37.04
5 mm

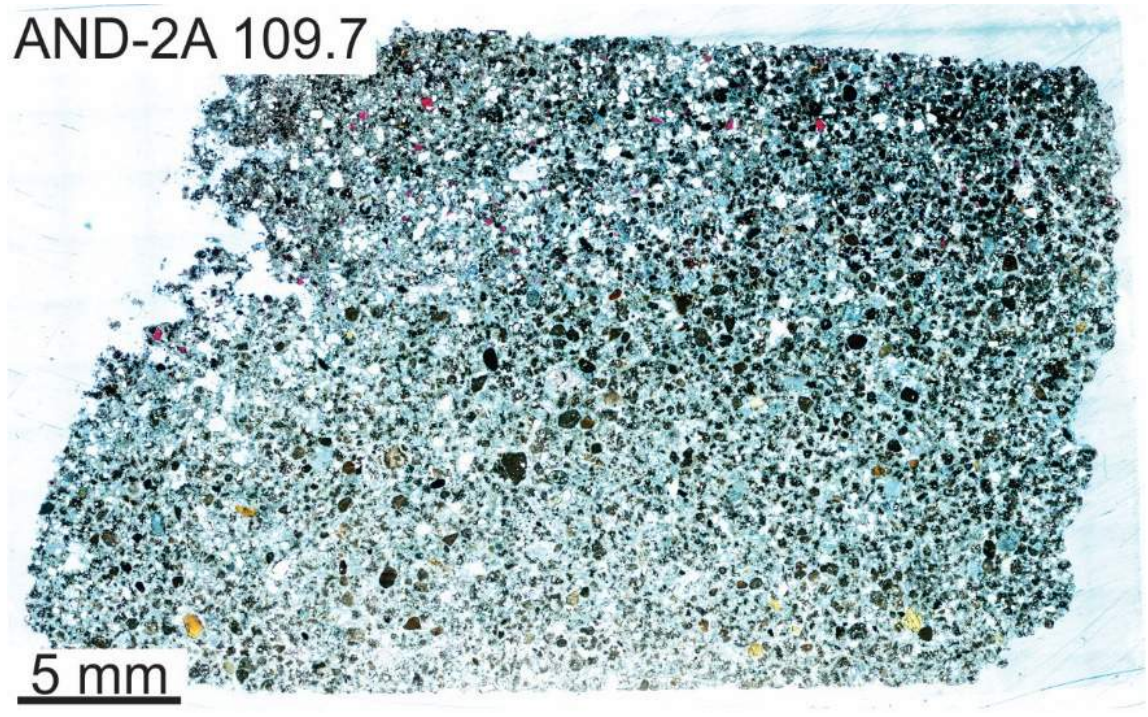
AND-2A 109.7
5 mm


AND-2A 115.38
5 mm

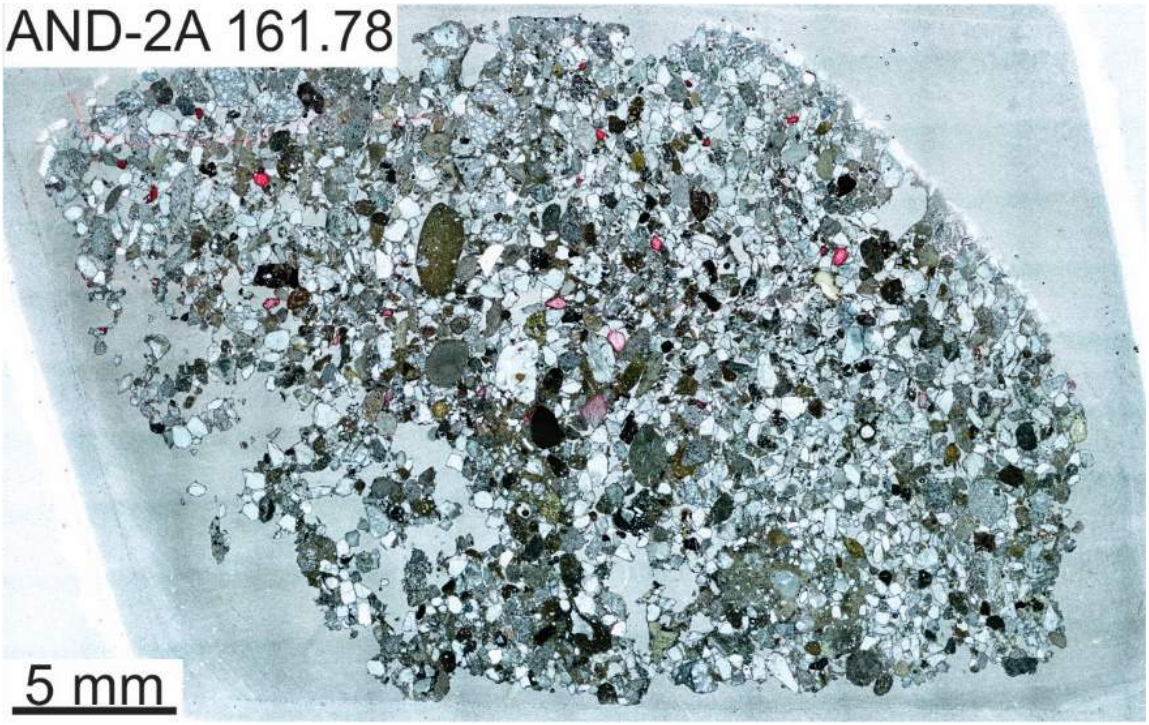
AND-2A 161.78
5 mm

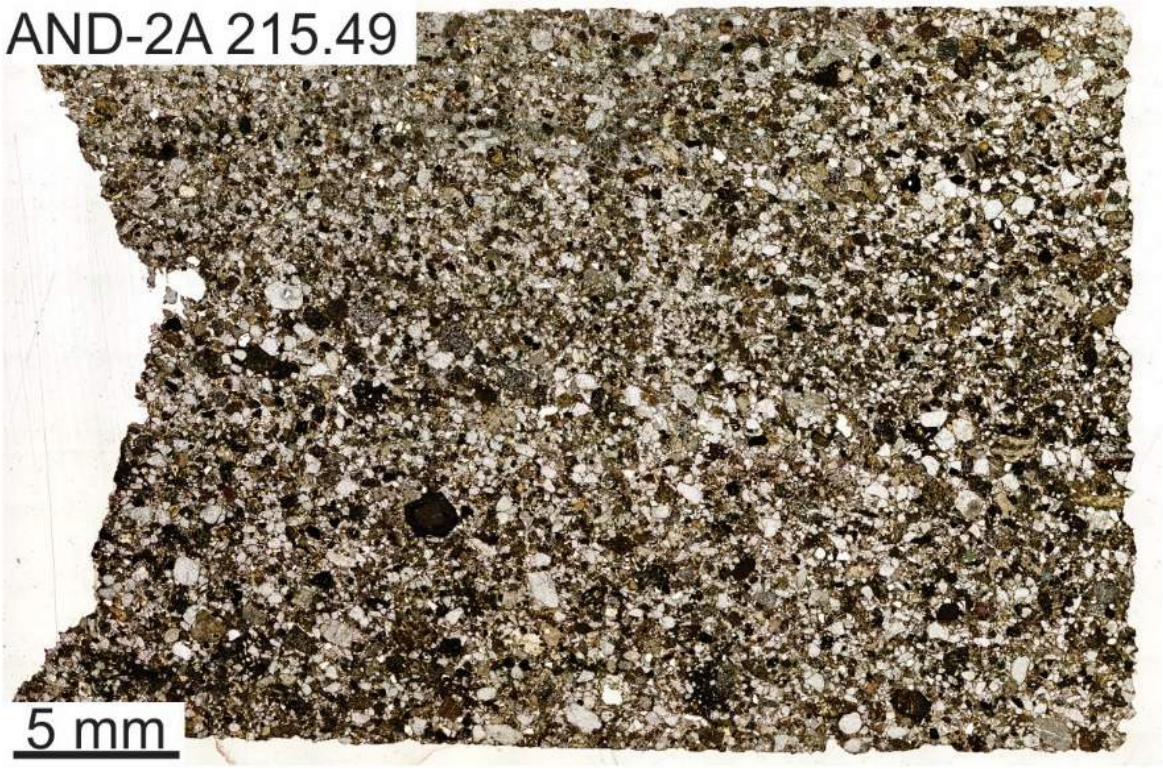
AND-2A 215.49
5 mm

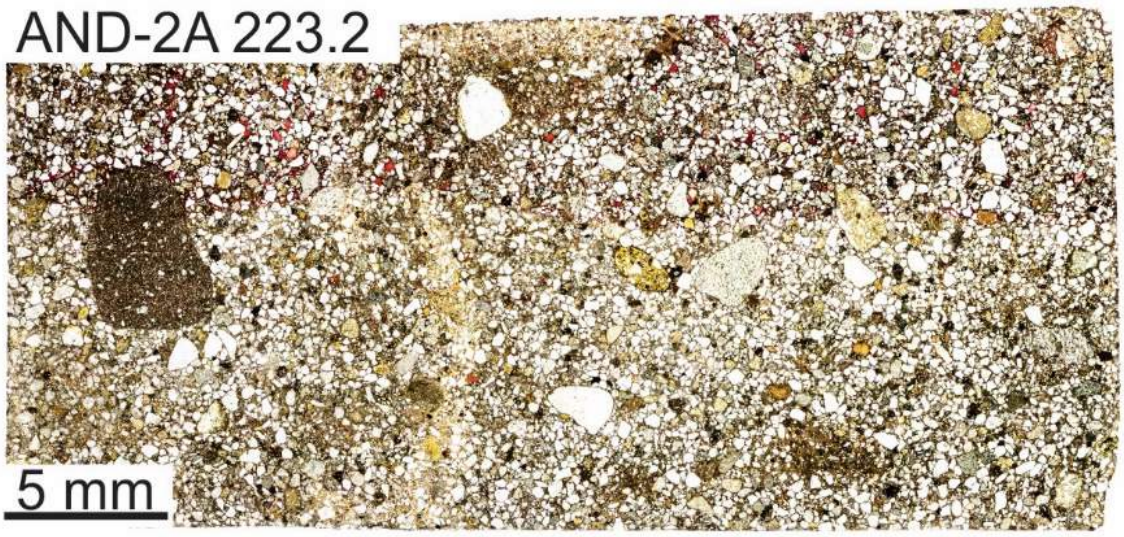
AND-2A 223.2
5 mm

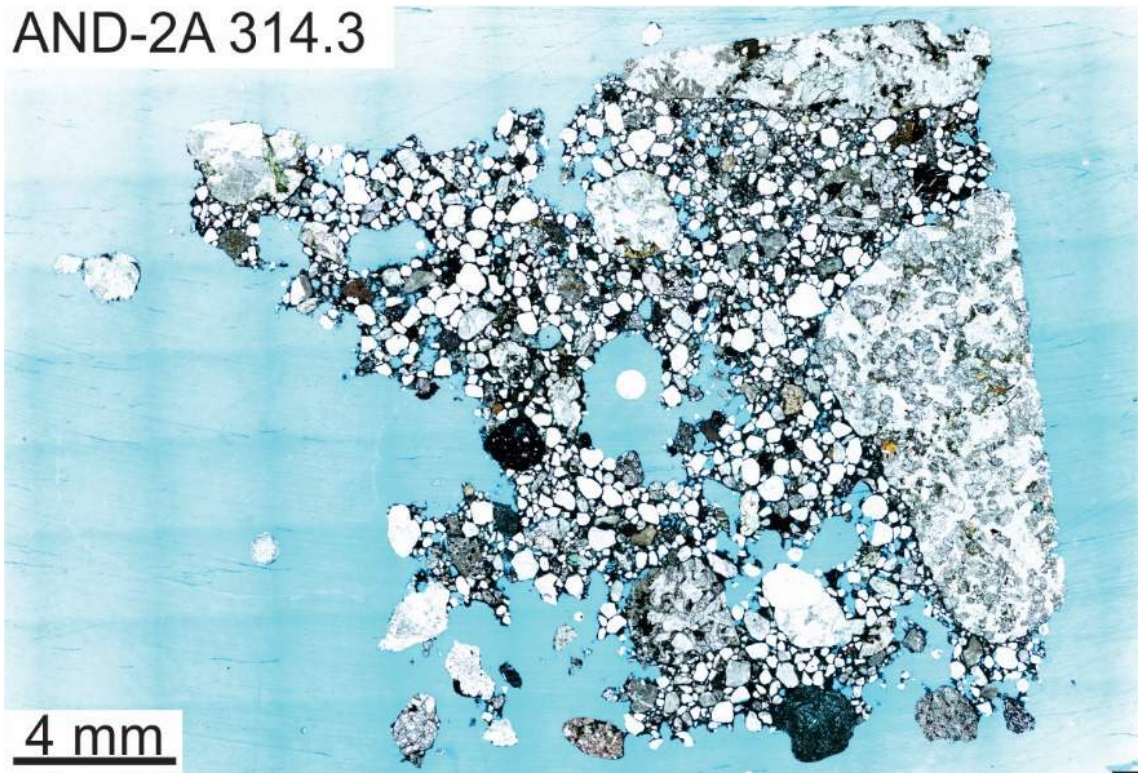
AND-2A 314.3
4 mm


AND-2A 341.75
5 mm

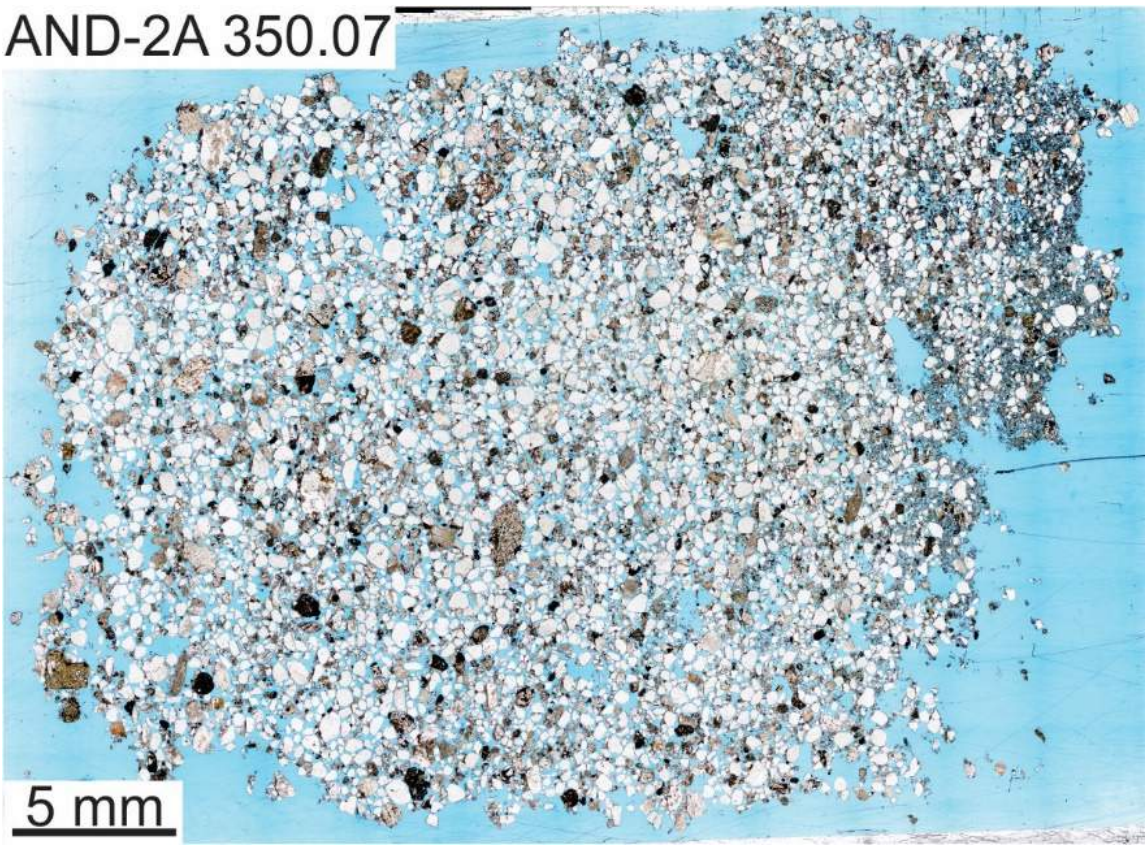
AND-2A 350.07
5 mm

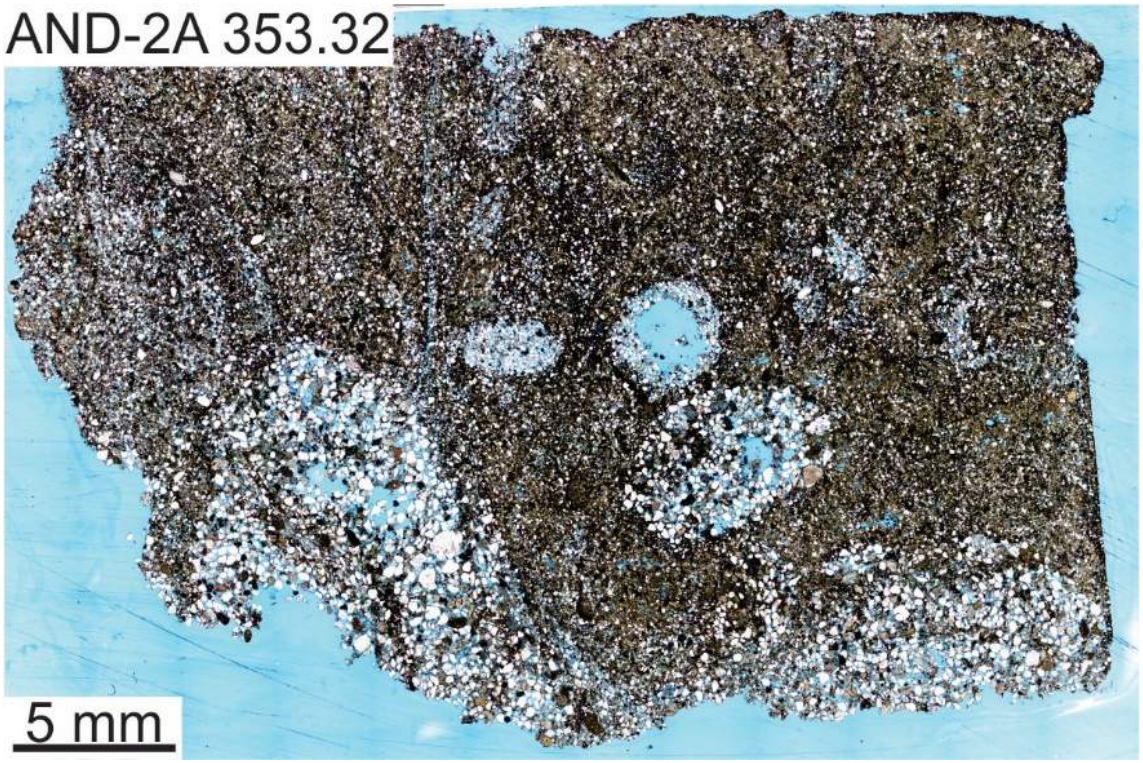
AND-2A 353.32
5 mm


AND-2A 409.64
5 mm

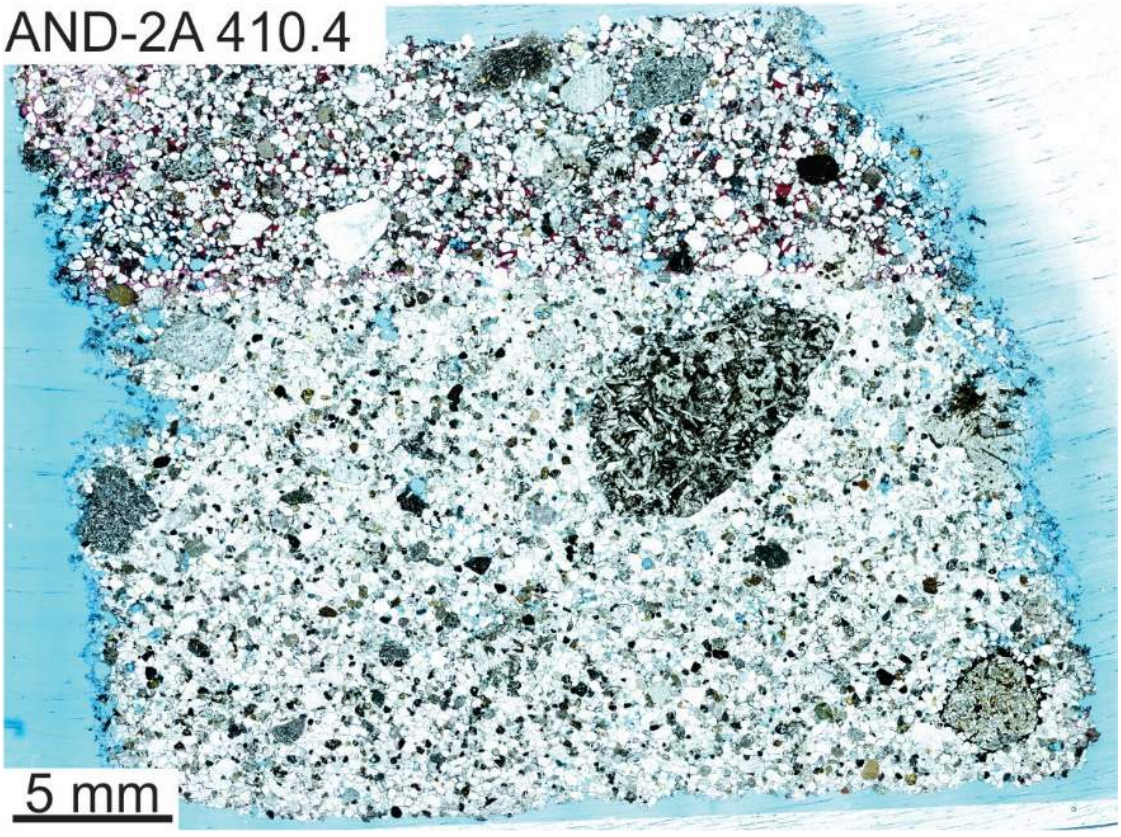
AND-2A 410.4
5 mm

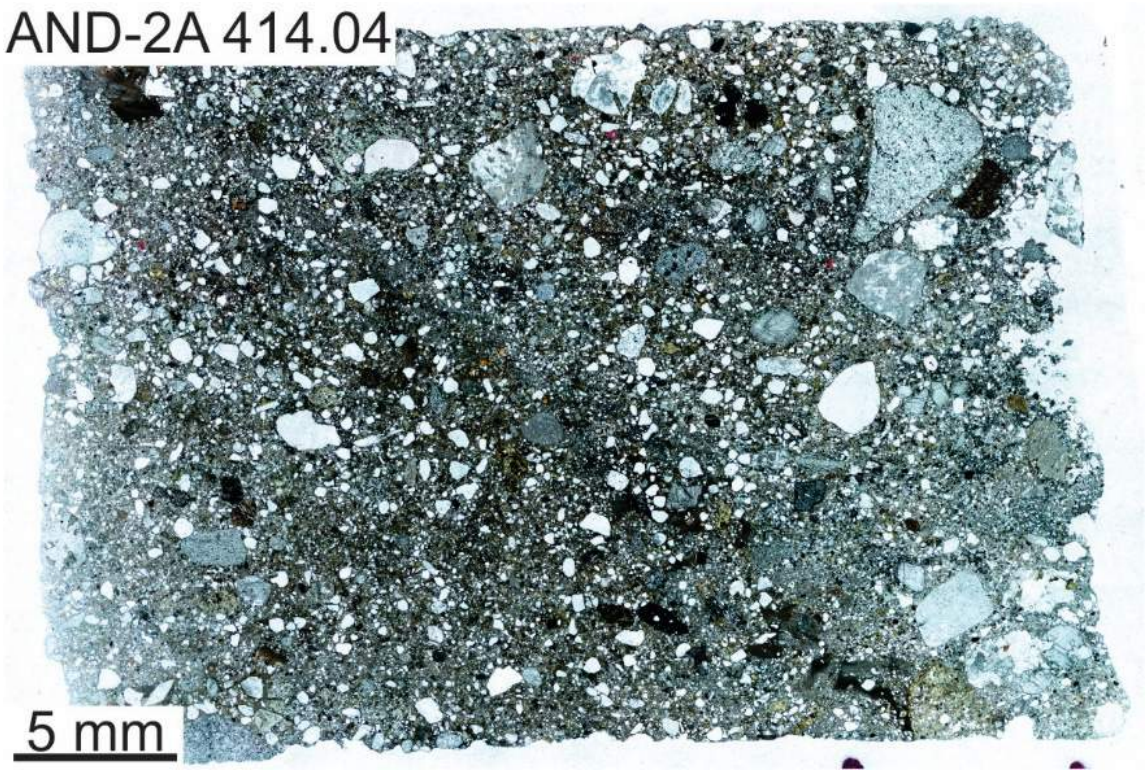
AND-2A 414.04
5 mm


AND-2A 417.83
5 mm


AND-2A 455.05
5 mm

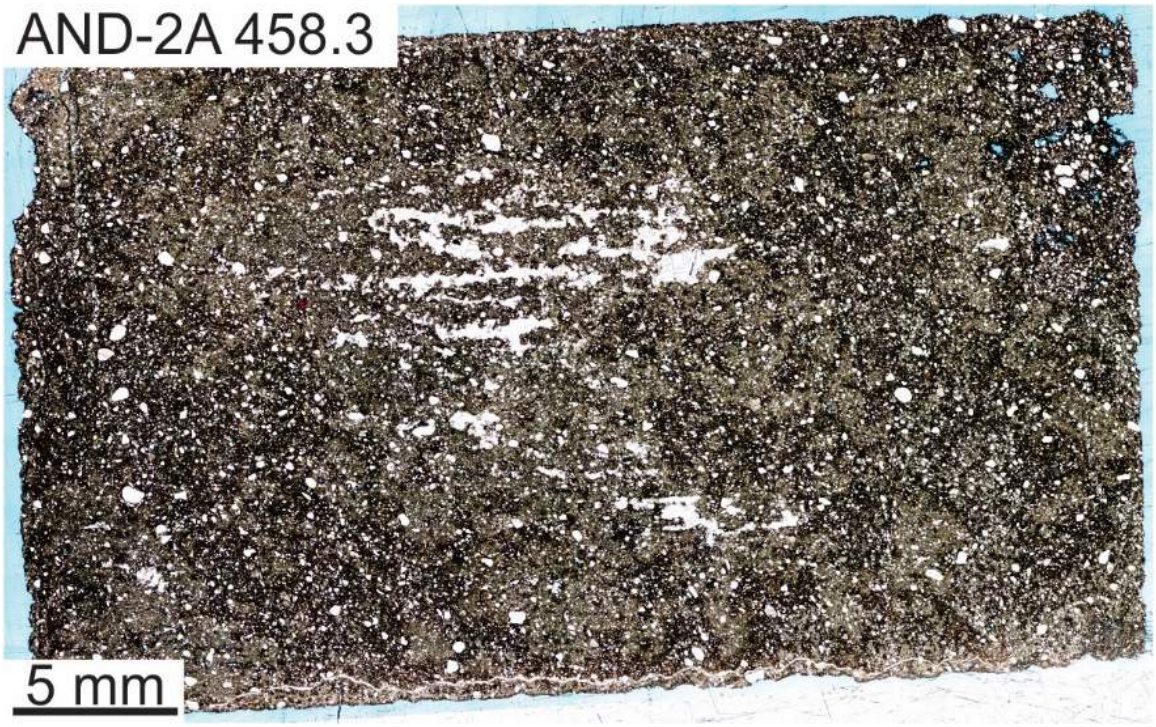
AND-2A 458.3
5 mm


AND-2A 462.33
5 mm

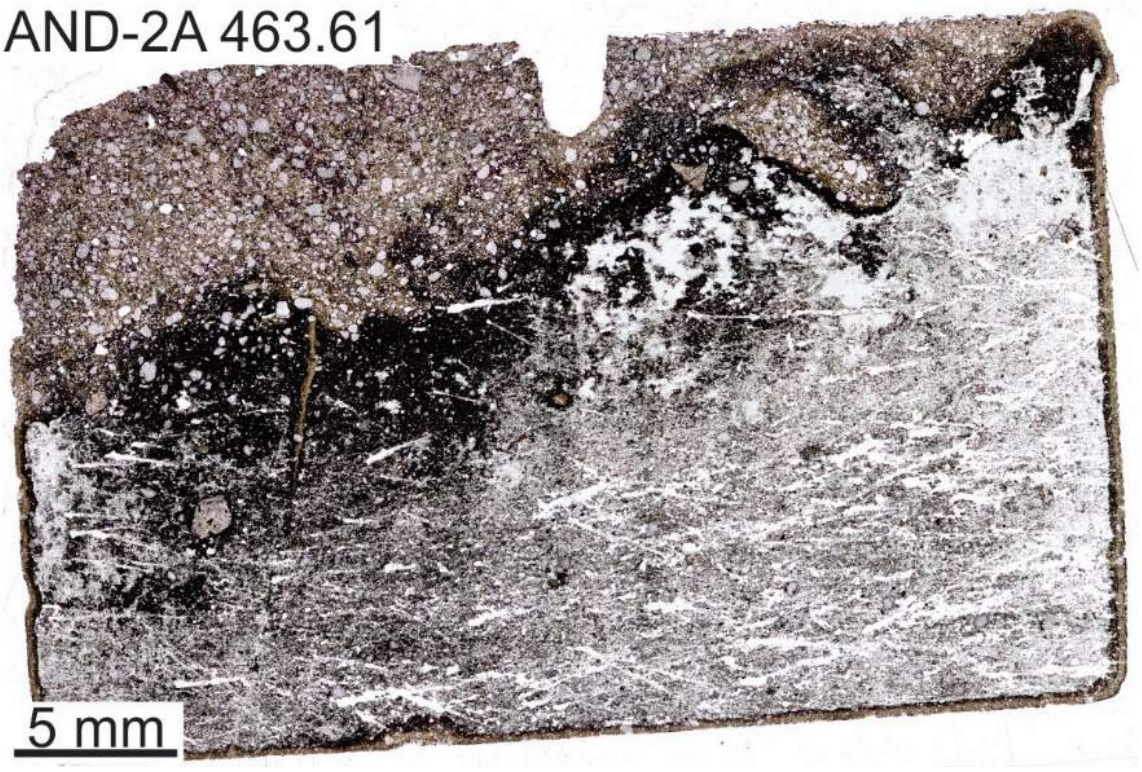
AND-2A 463.61
5 mm

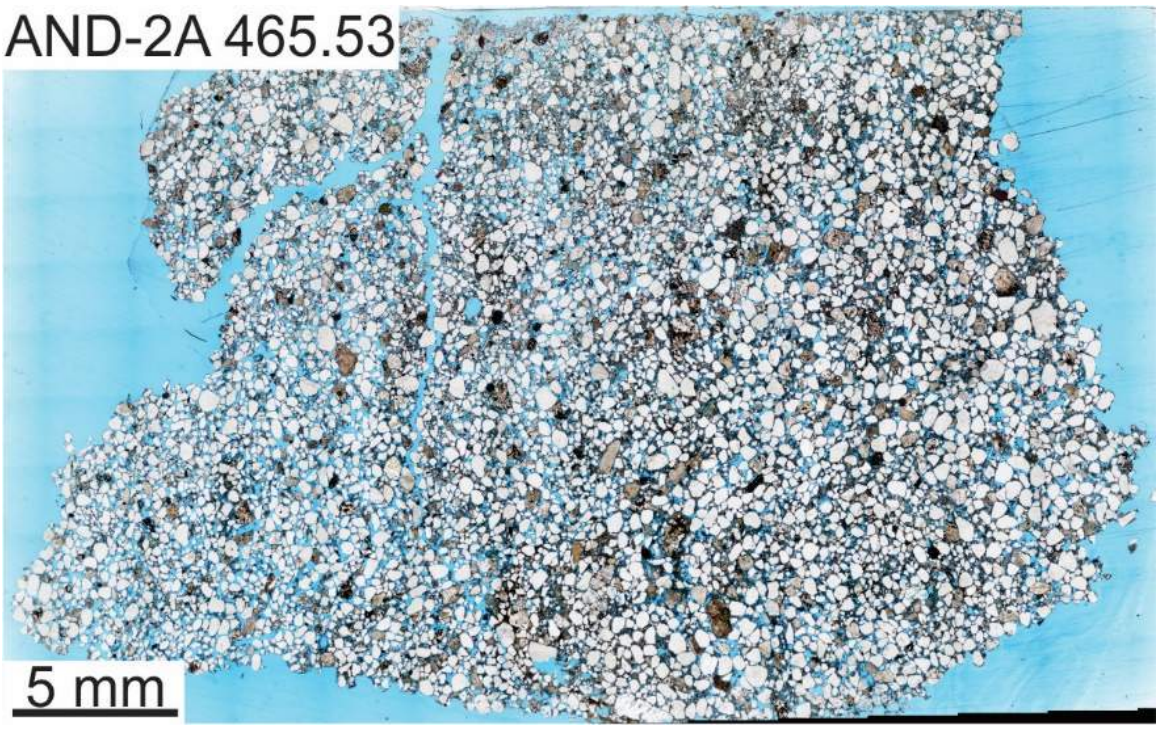
AND-2A 465.53
5 mm

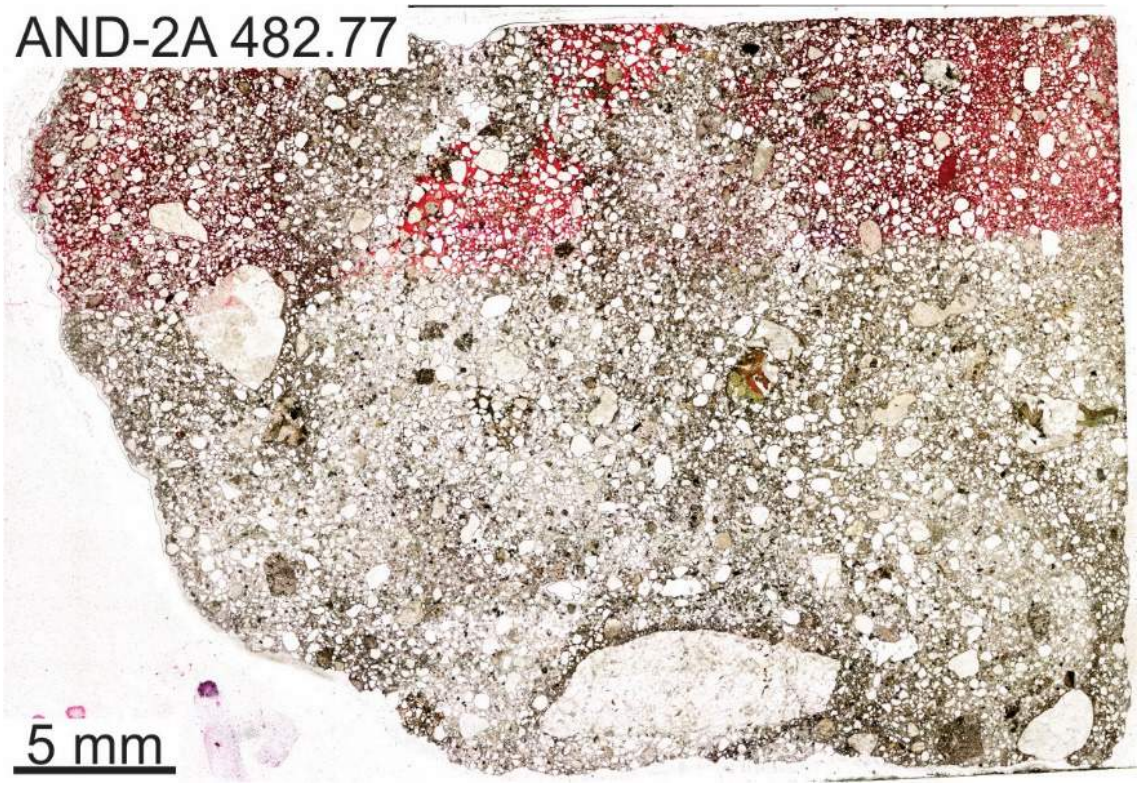
AND-2A 482.77
5 mm

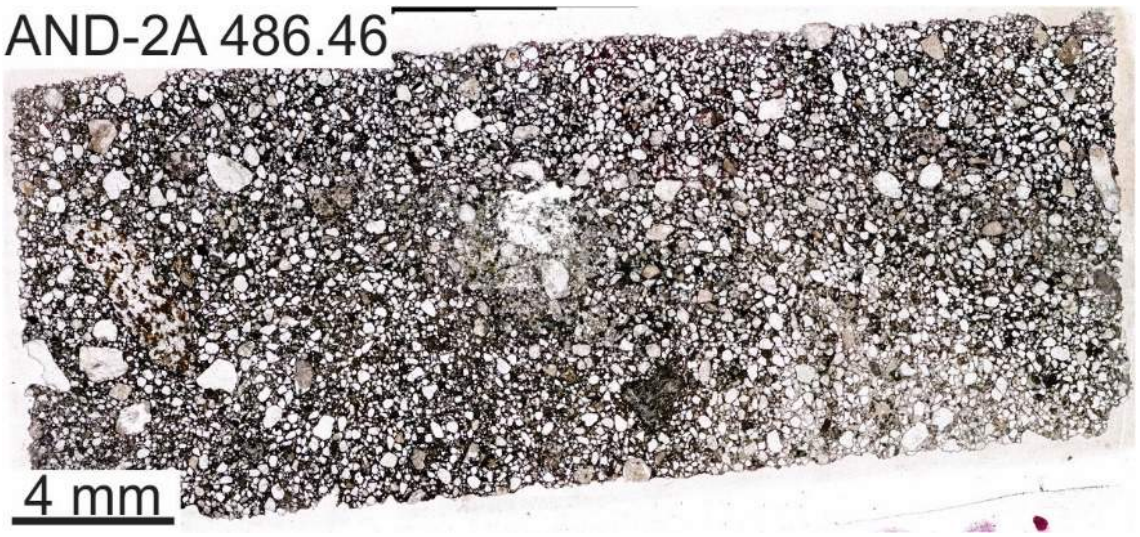
AND-2A 486.46
4 mm

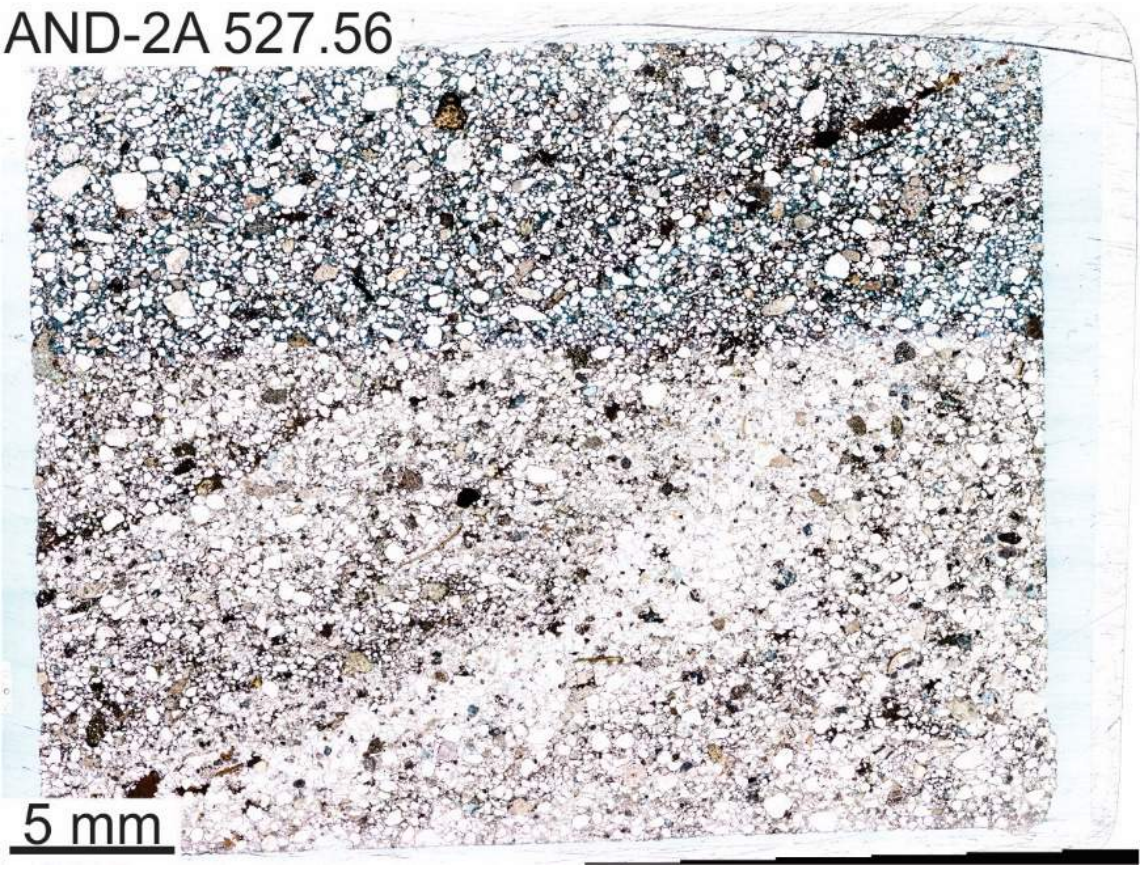
AND-2A 527.56
5 mm

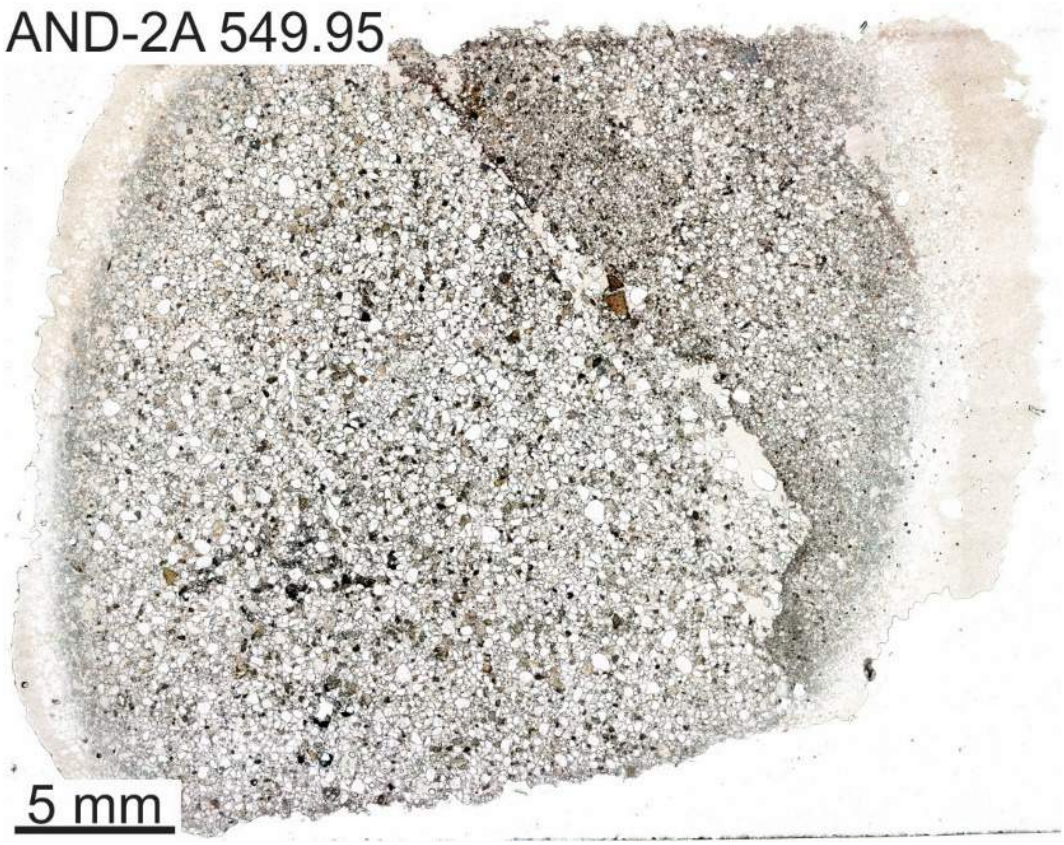
AND-2A 549.95
5 mm

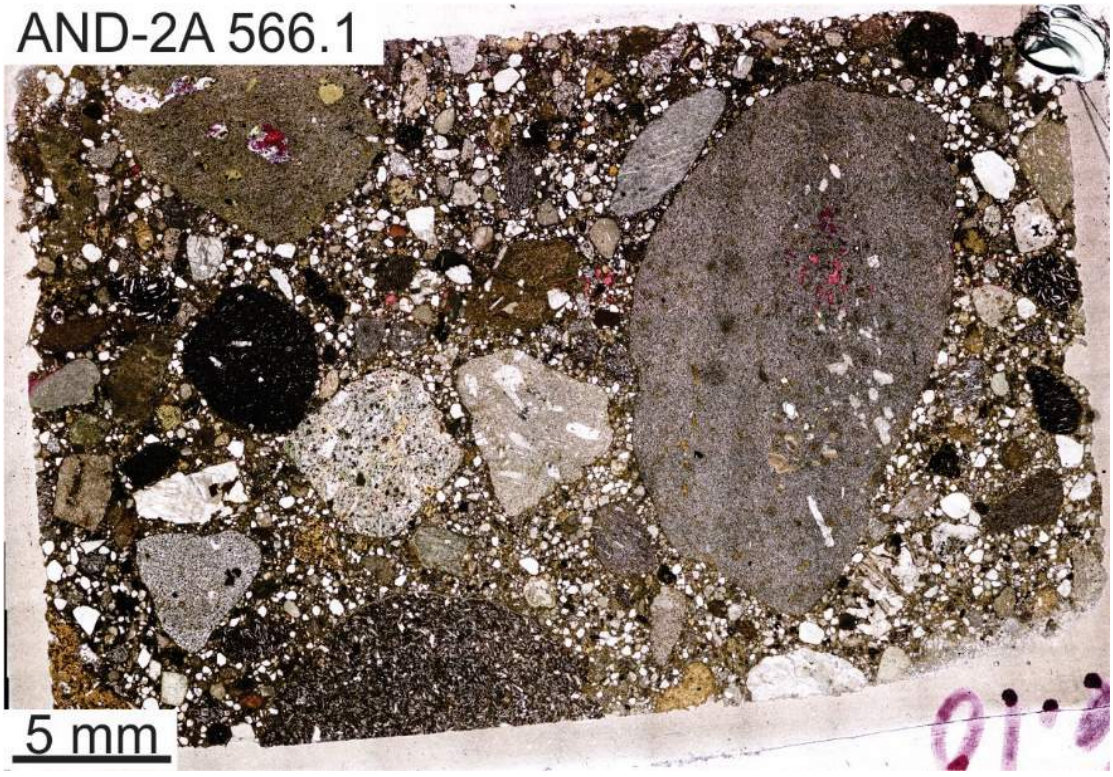
AND-2A 566.1
5 mm

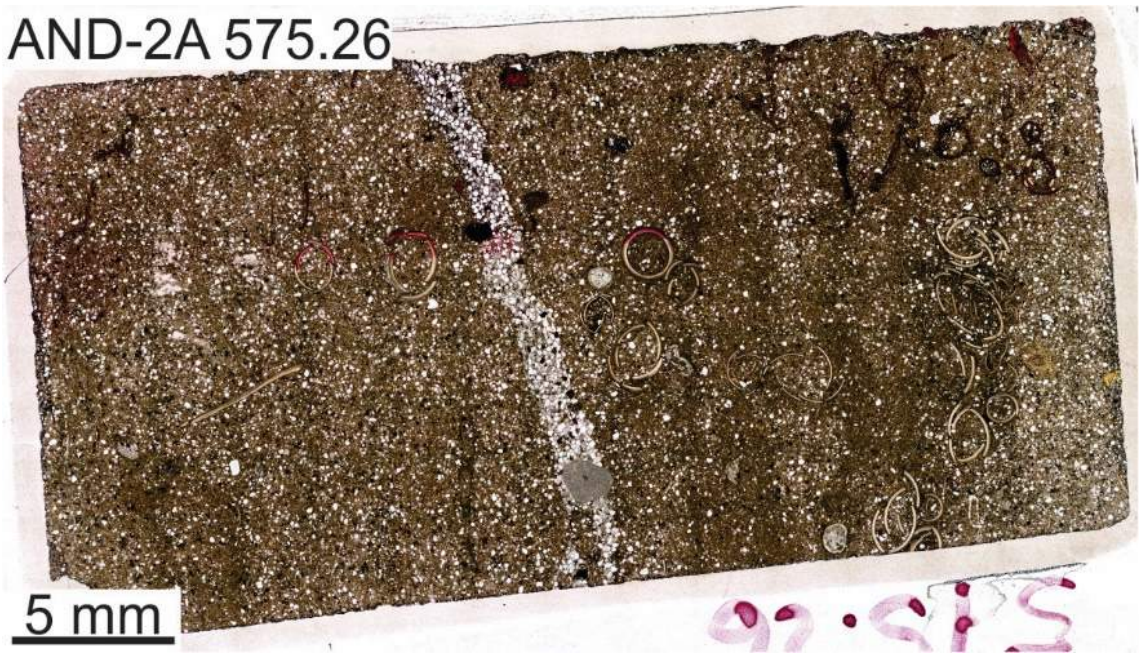
AND-2A 575.26
5 mm


AND-2A 576.53
5 mm

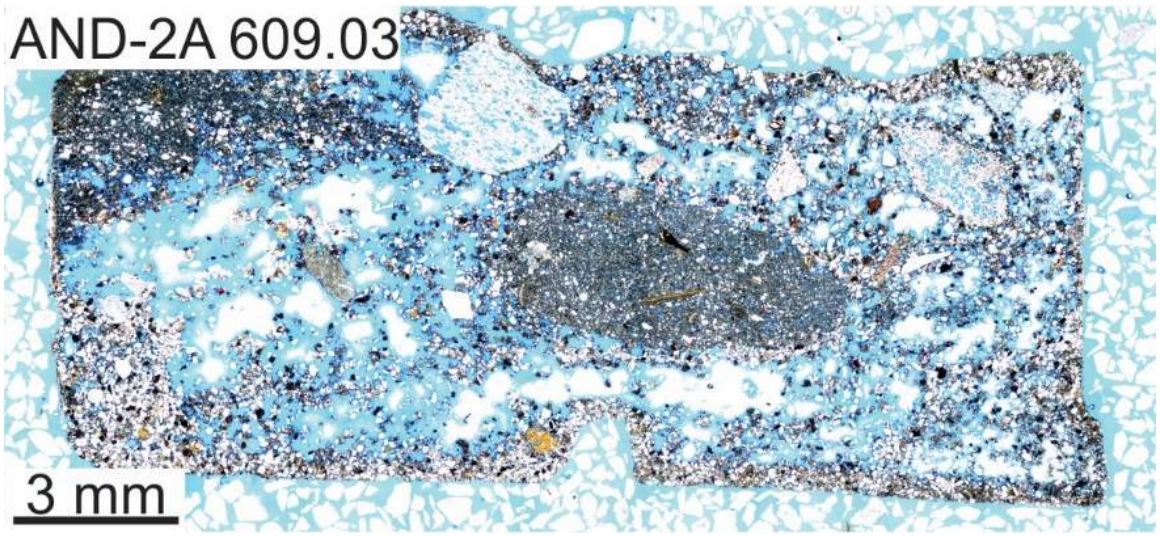
AND-2A 609.03
3 mm

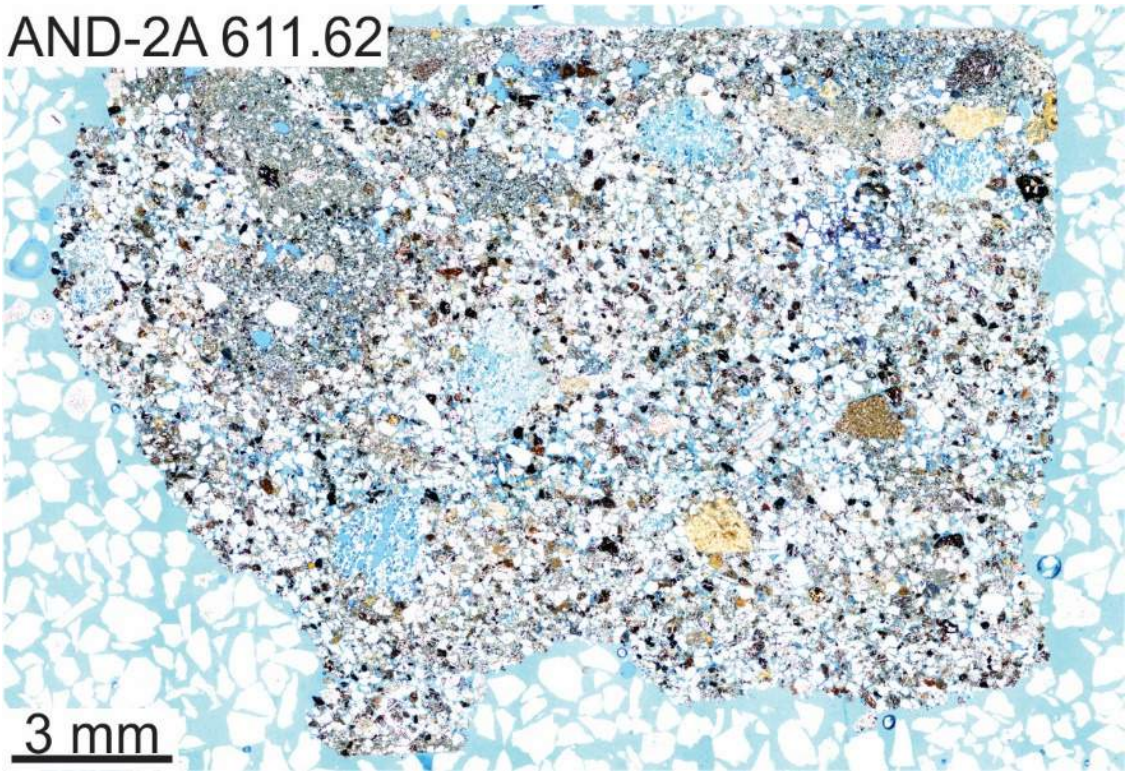
AND-2A 611.62
3 mm


AND-2A 614.71
3 mm

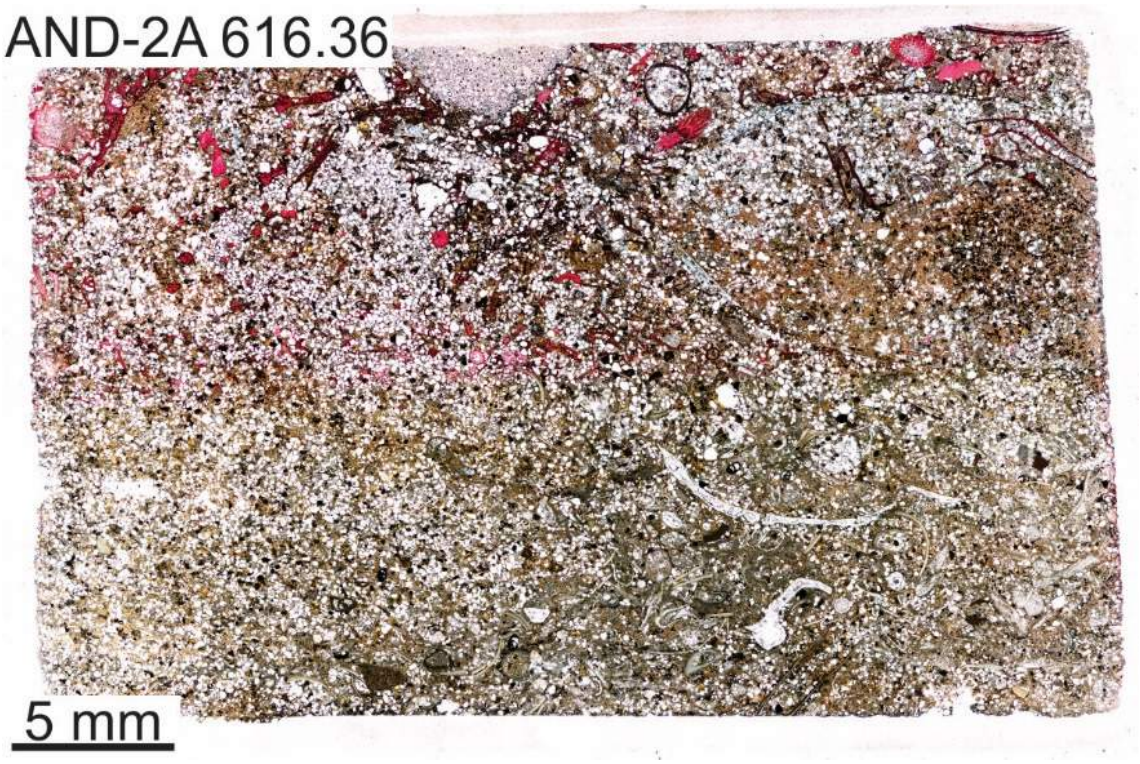
AND-2A 616.36
5 mm

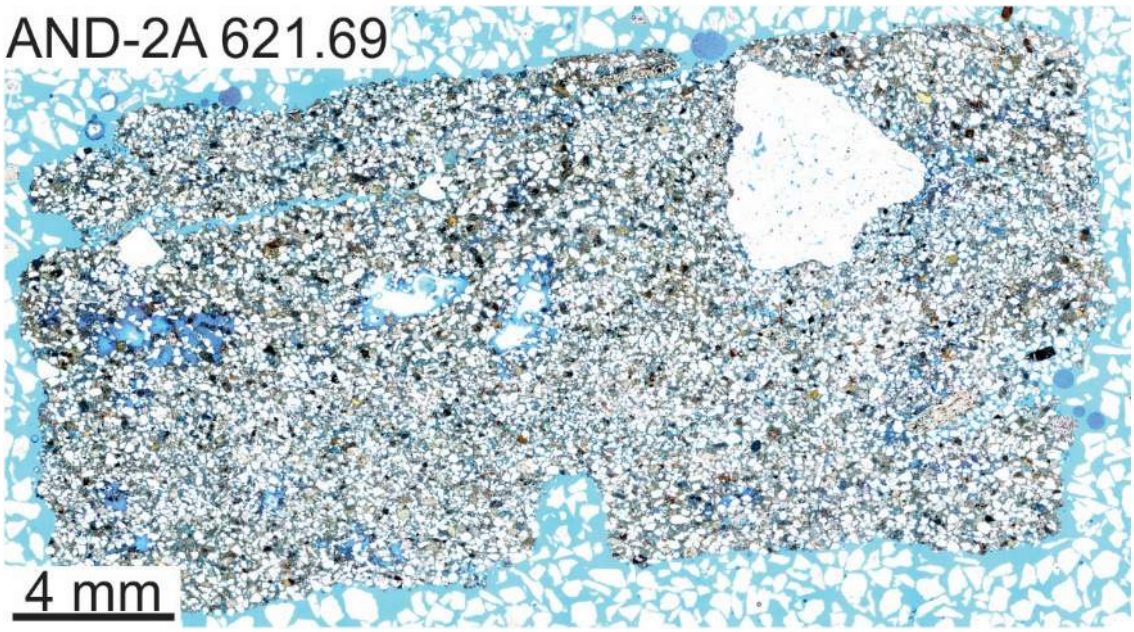
AND-2A 621.69
4 mm

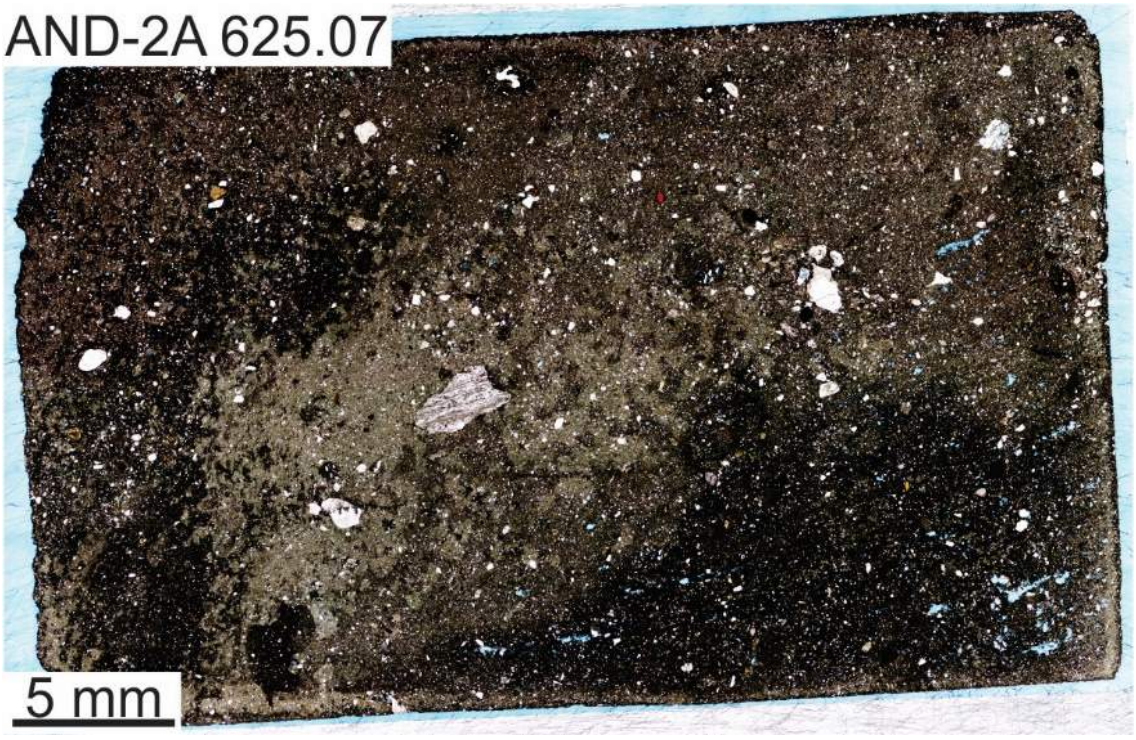
AND-2A 625.07
5 mm

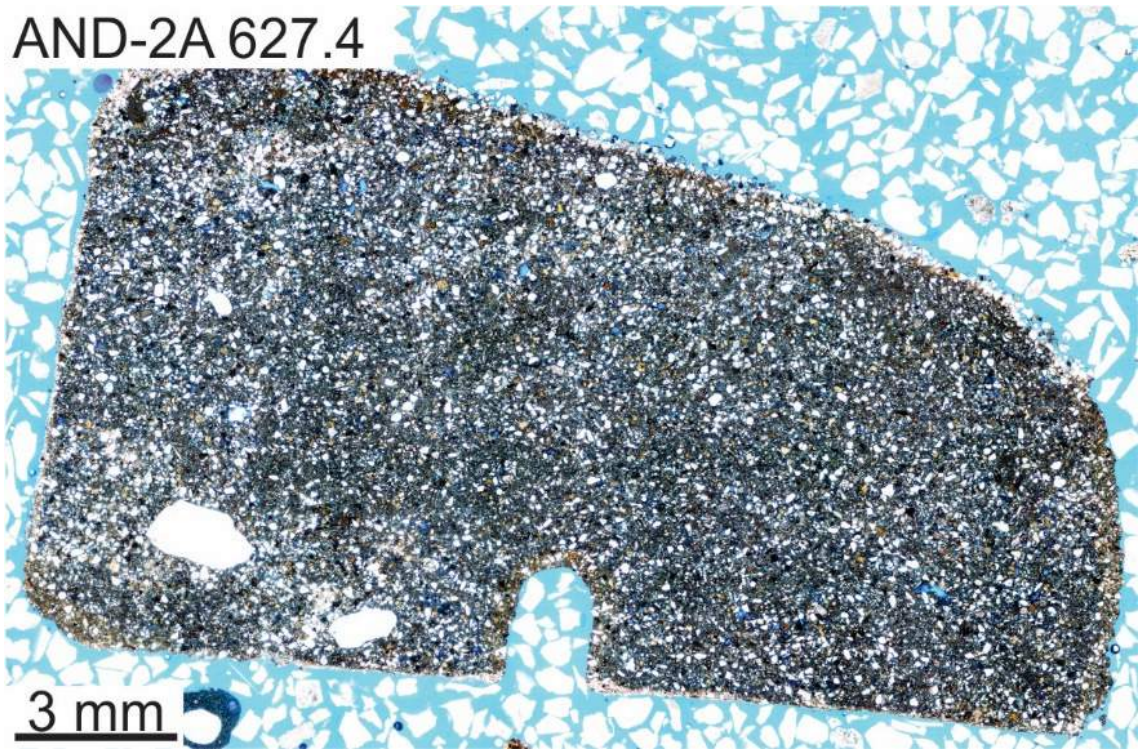
AND-2A 627.4
3 mm

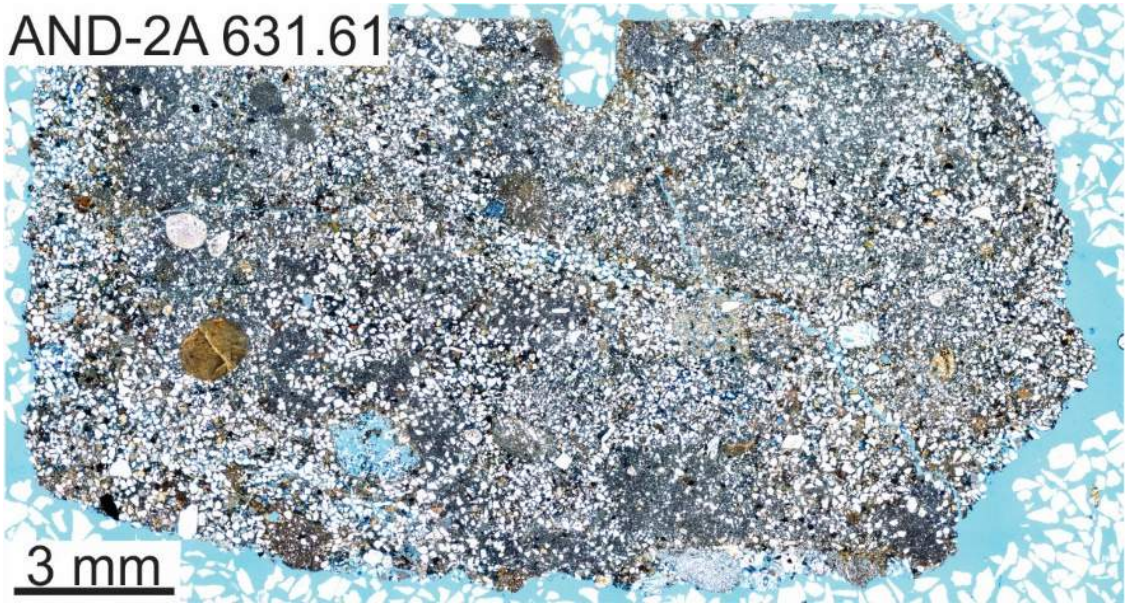
AND-2A 631.61
3 mm

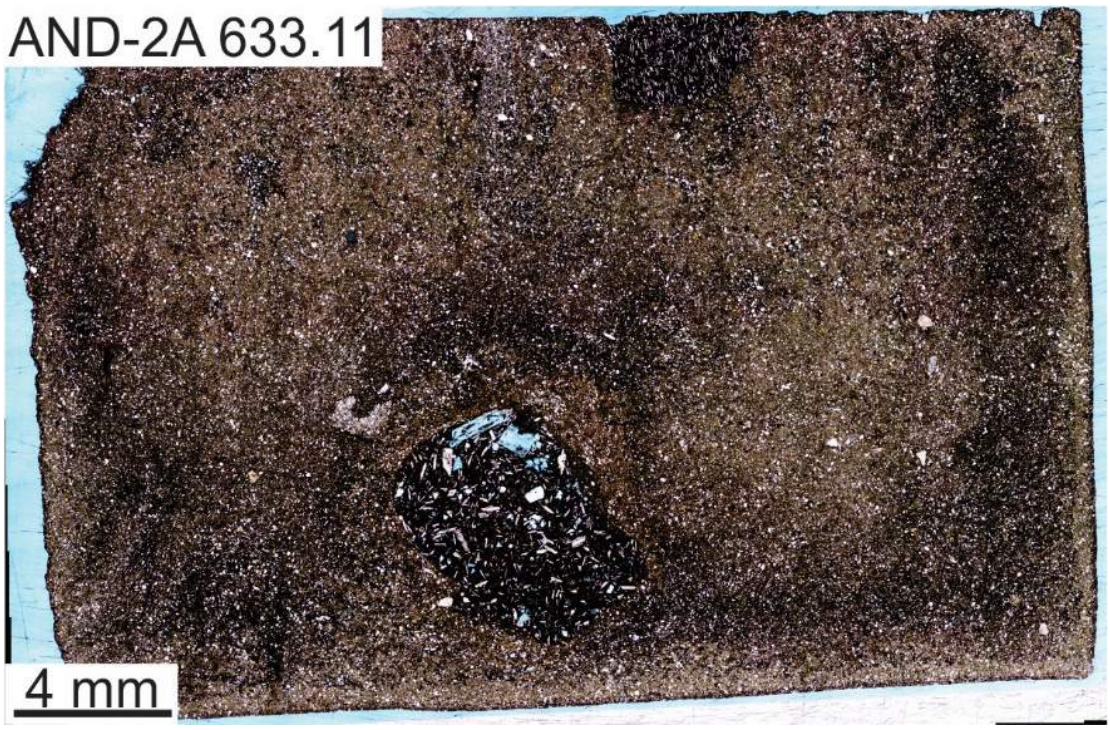
AND-2A 633.11
4 mm

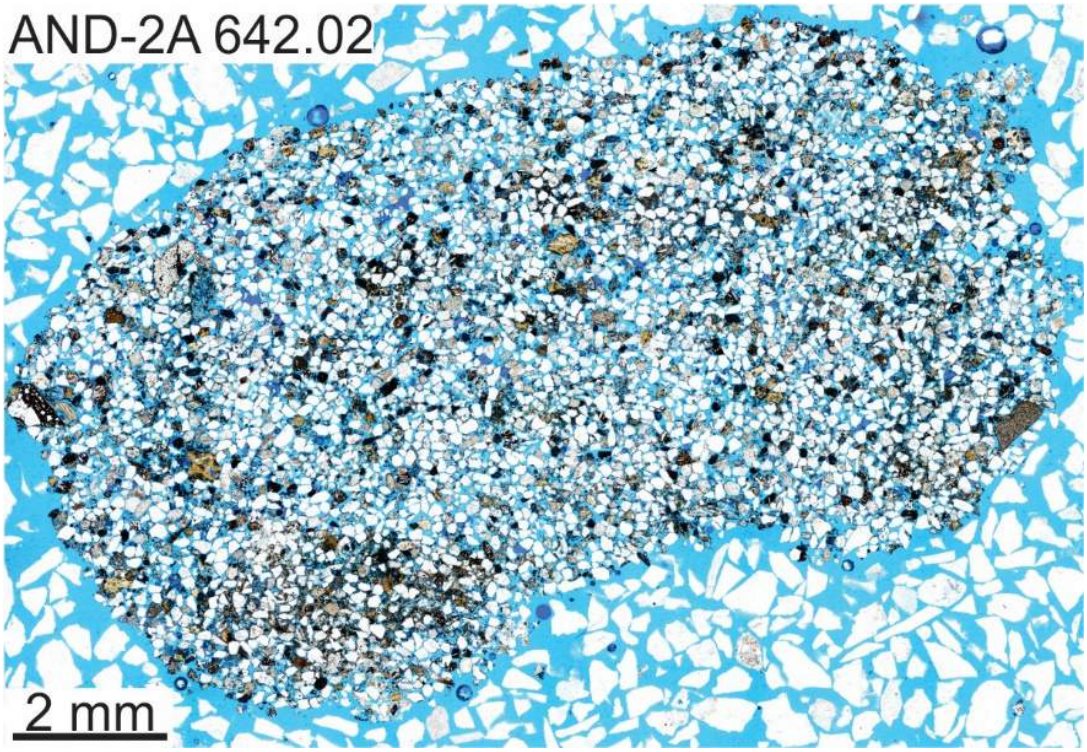
AND-2A 642.02
2 mm

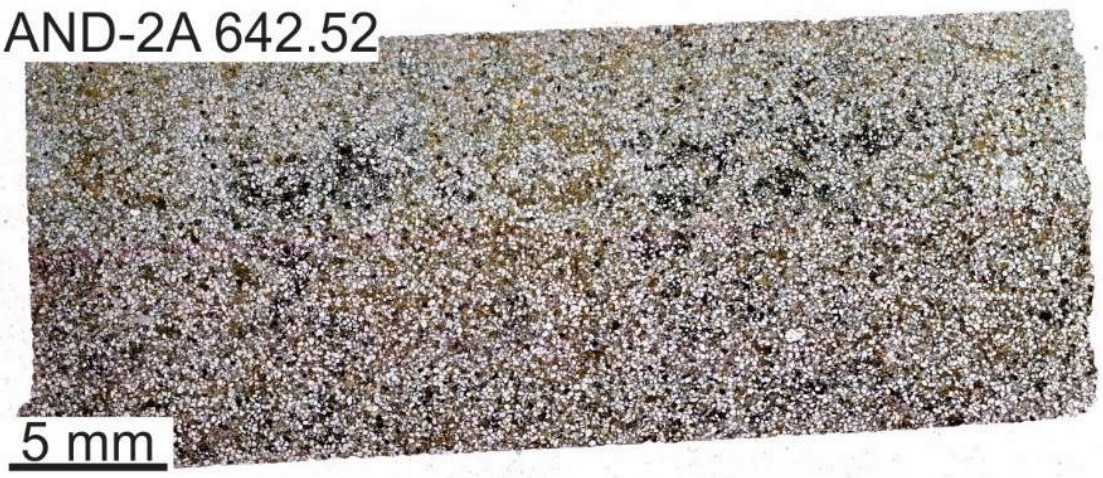
AND-2A 642.52
5 mm

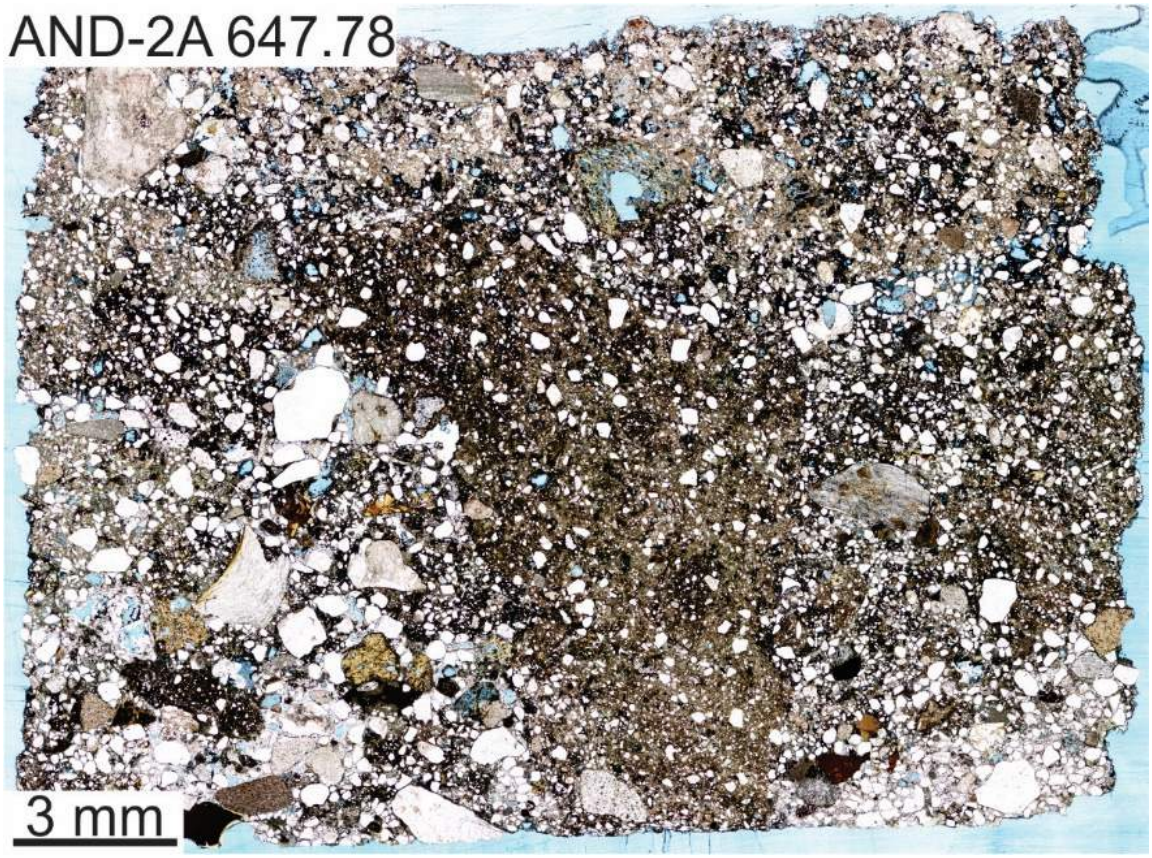
AND-2A 647.78
3 mm

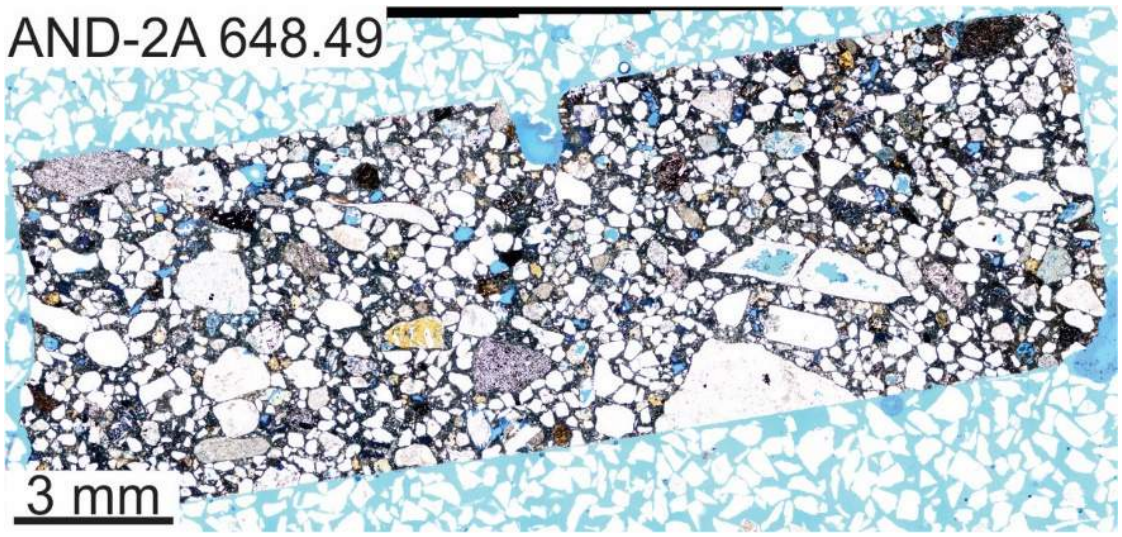
AND-2A 648.49
3 mm

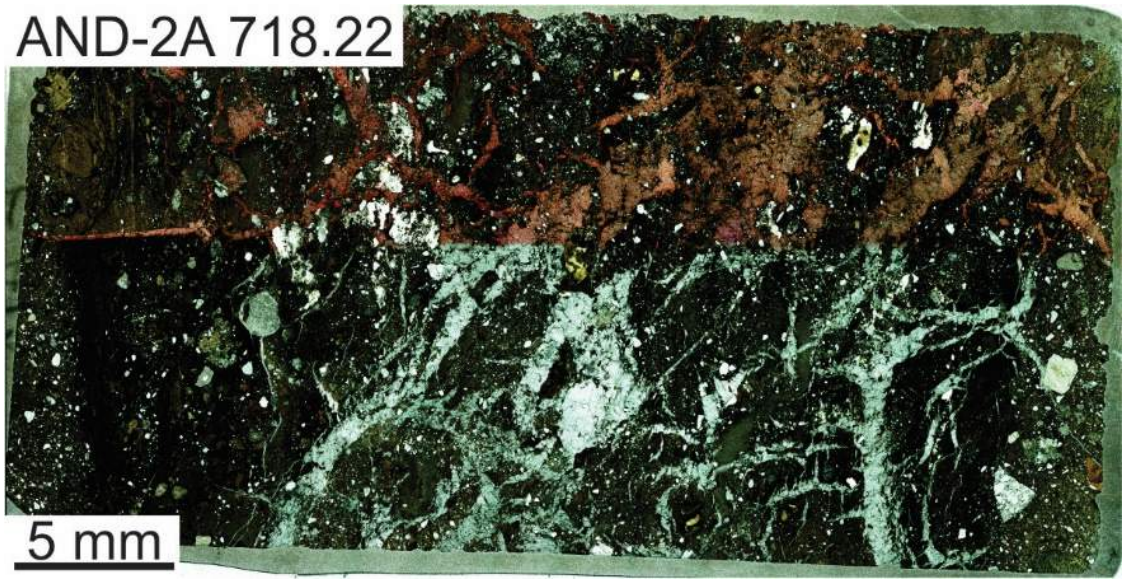
AND-2A 718.22
5 mm


AND-2A 725.57
3 mm

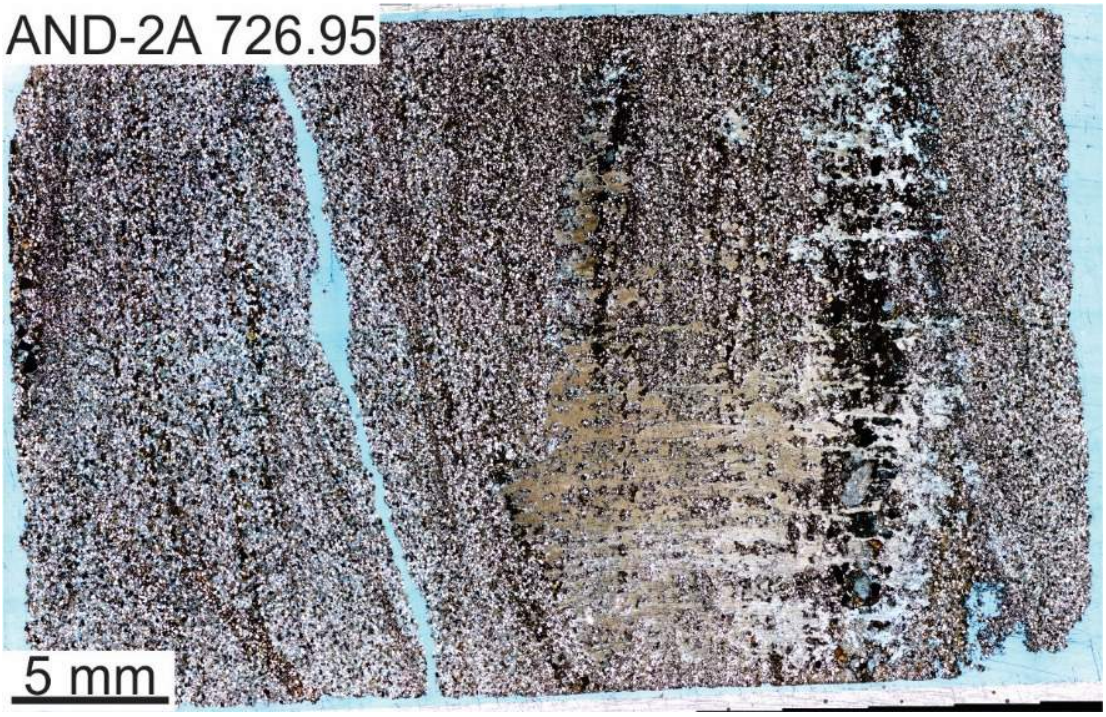
AND-2A 726.95
5 mm


AND-2A 728.98
5 mm


AND-2A 730.45
5 mm


AND-2A 790.86
4 mm

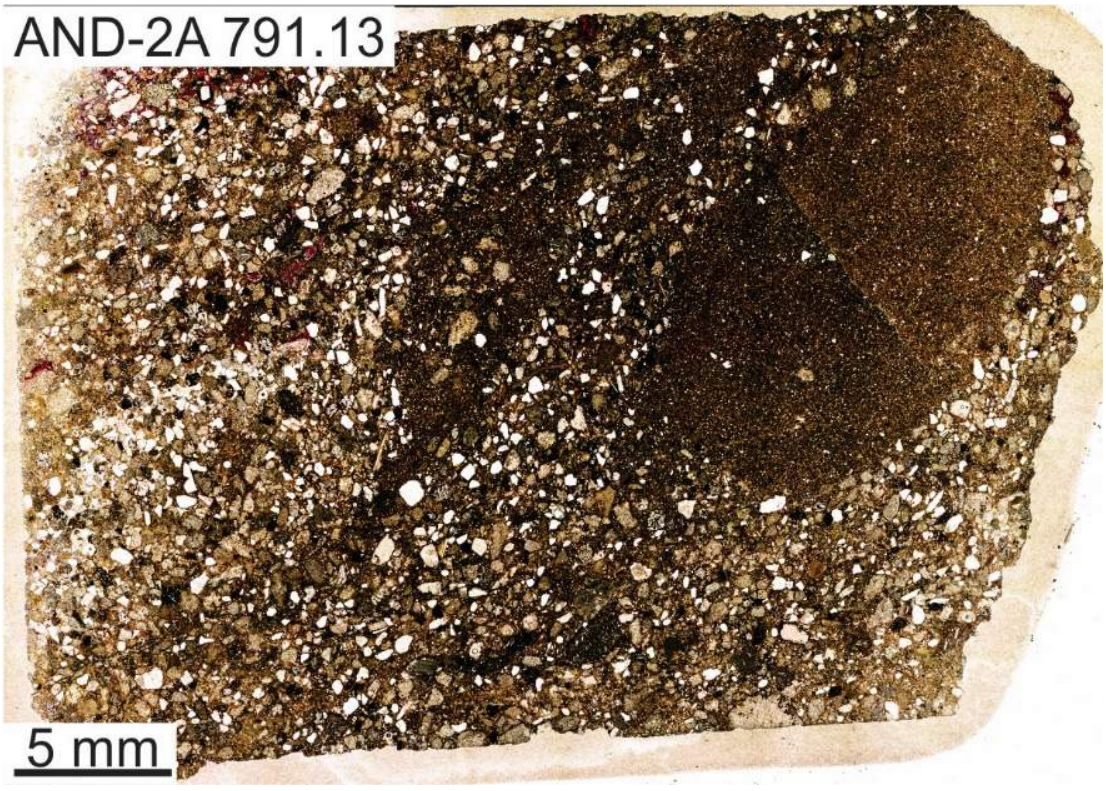
AND-2A 791.13
5 mm

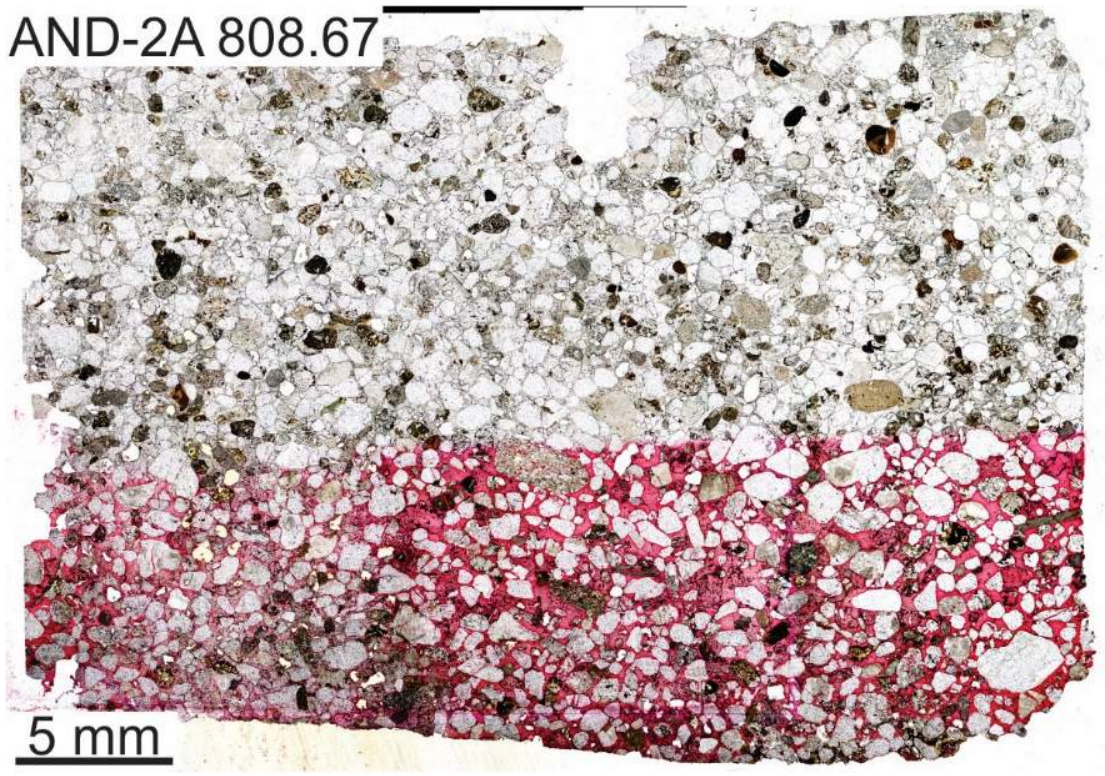
AND-2A 808.67
5 mm

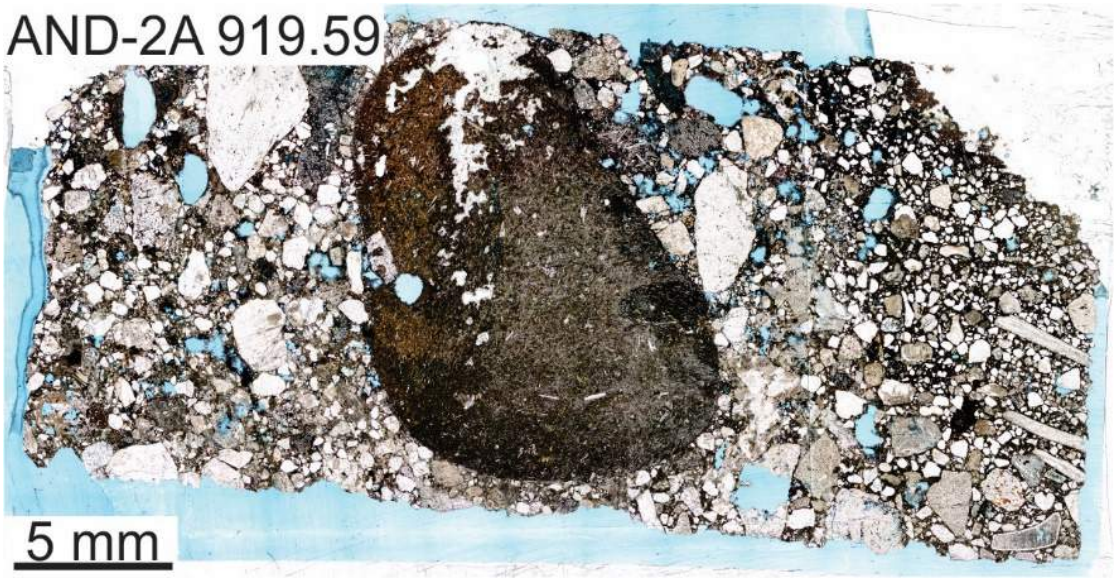
AND-2A 919.59
5 mm

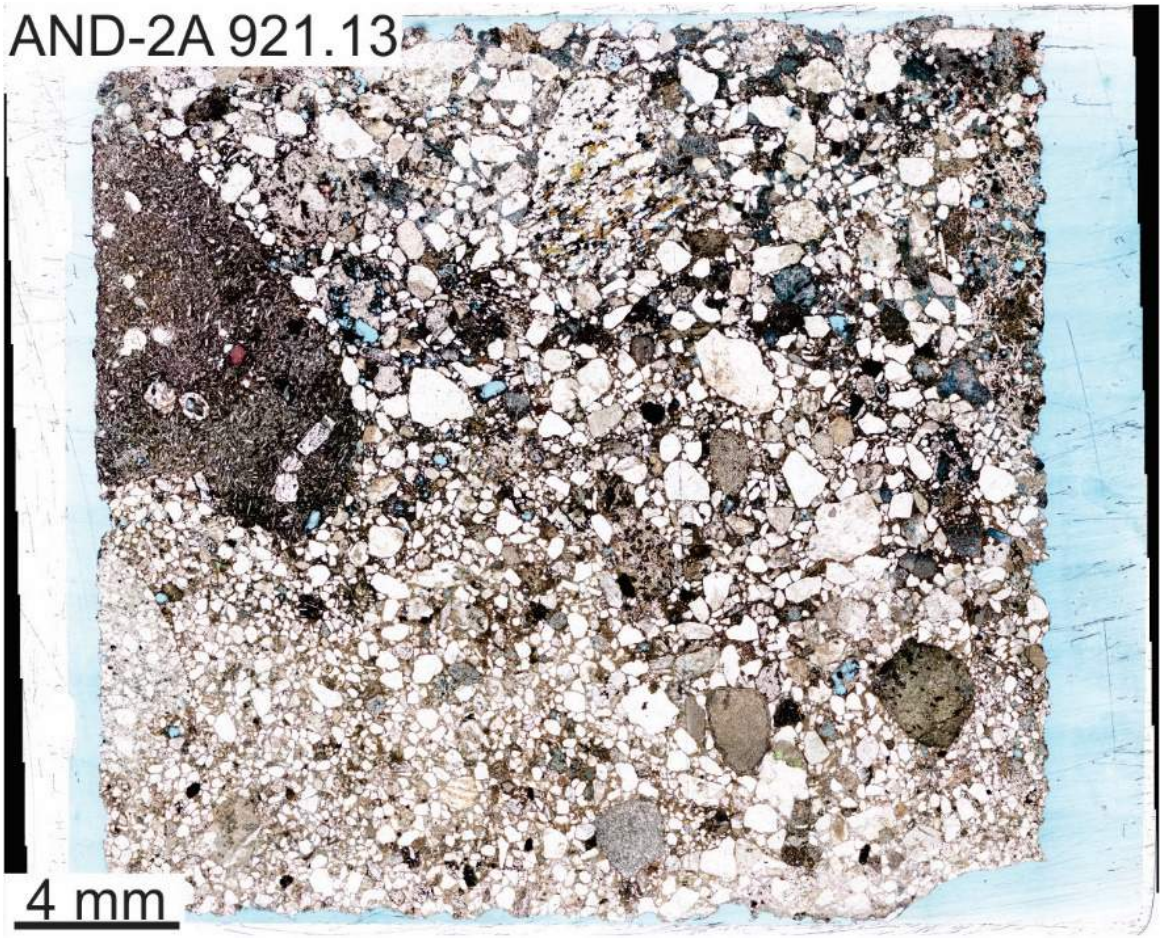
AND-2A 921.13
4 mm

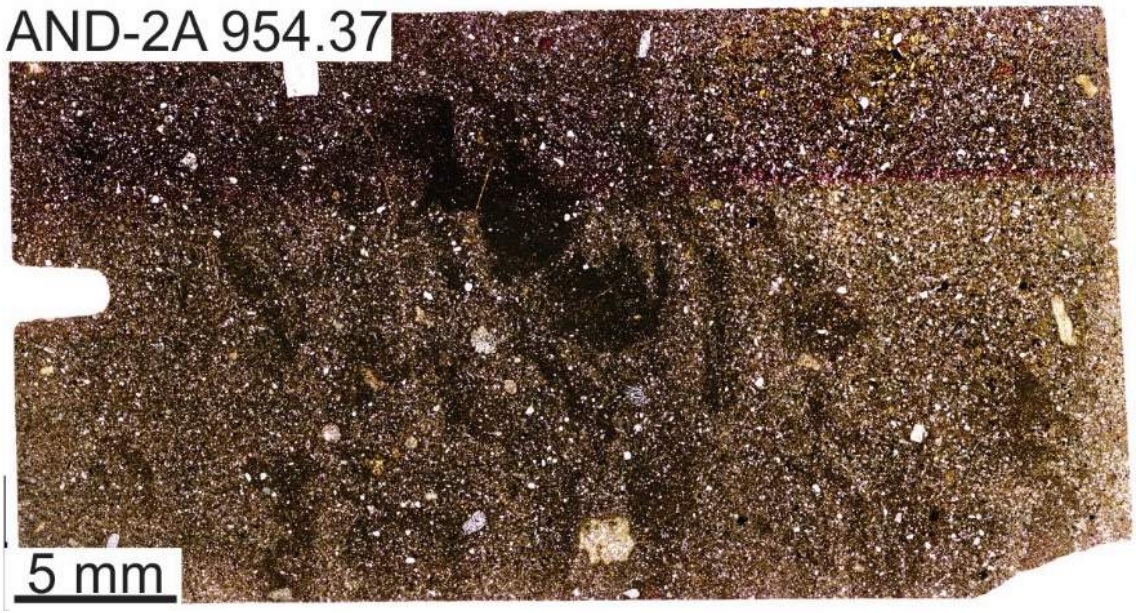
AND-2A 954.37
5 mm

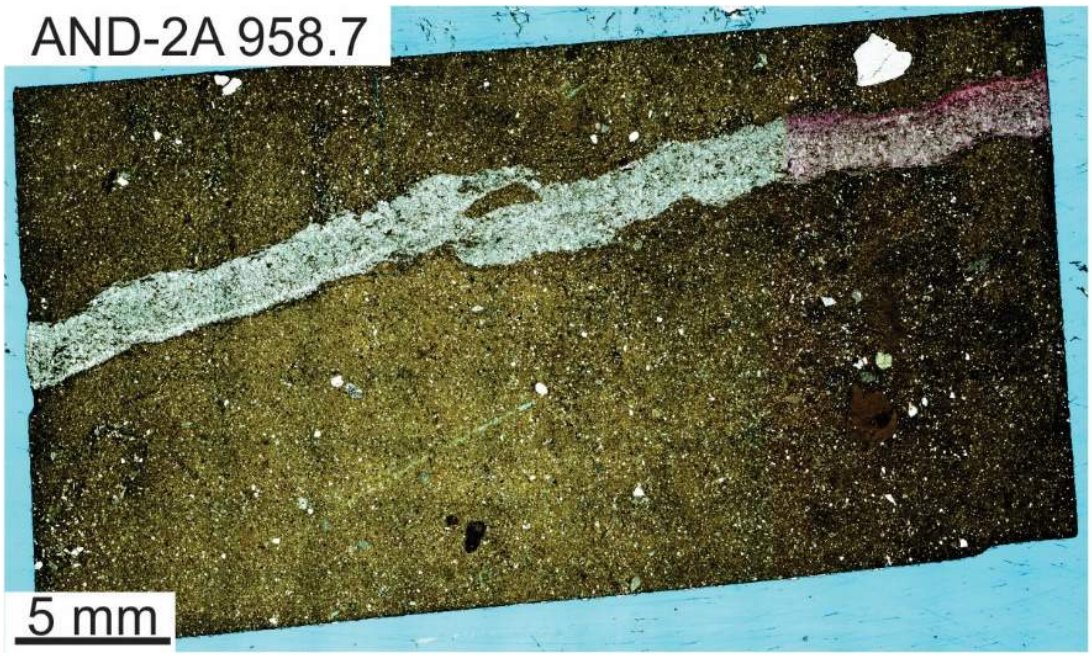
AND-2A 958.7
5 mm

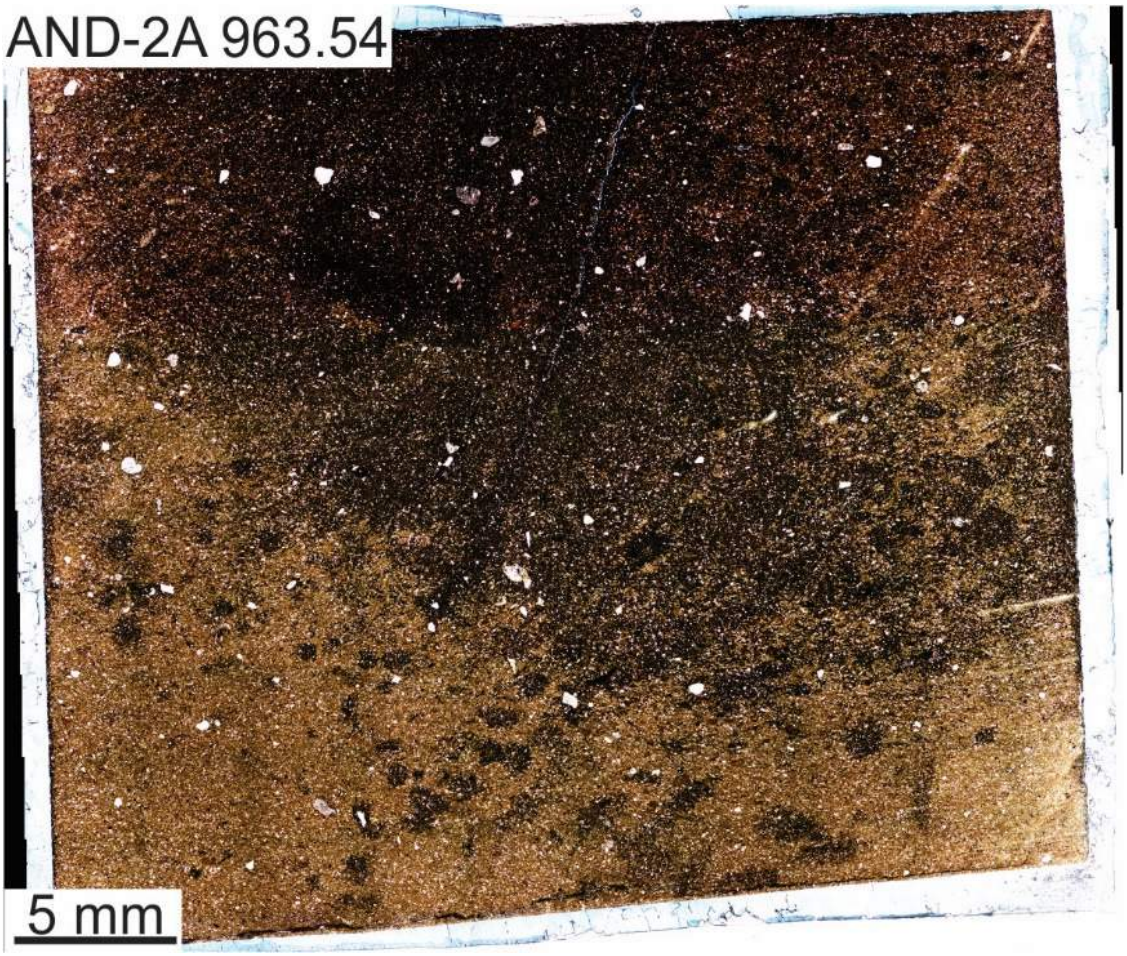
AND-2A 963.54
5 mm

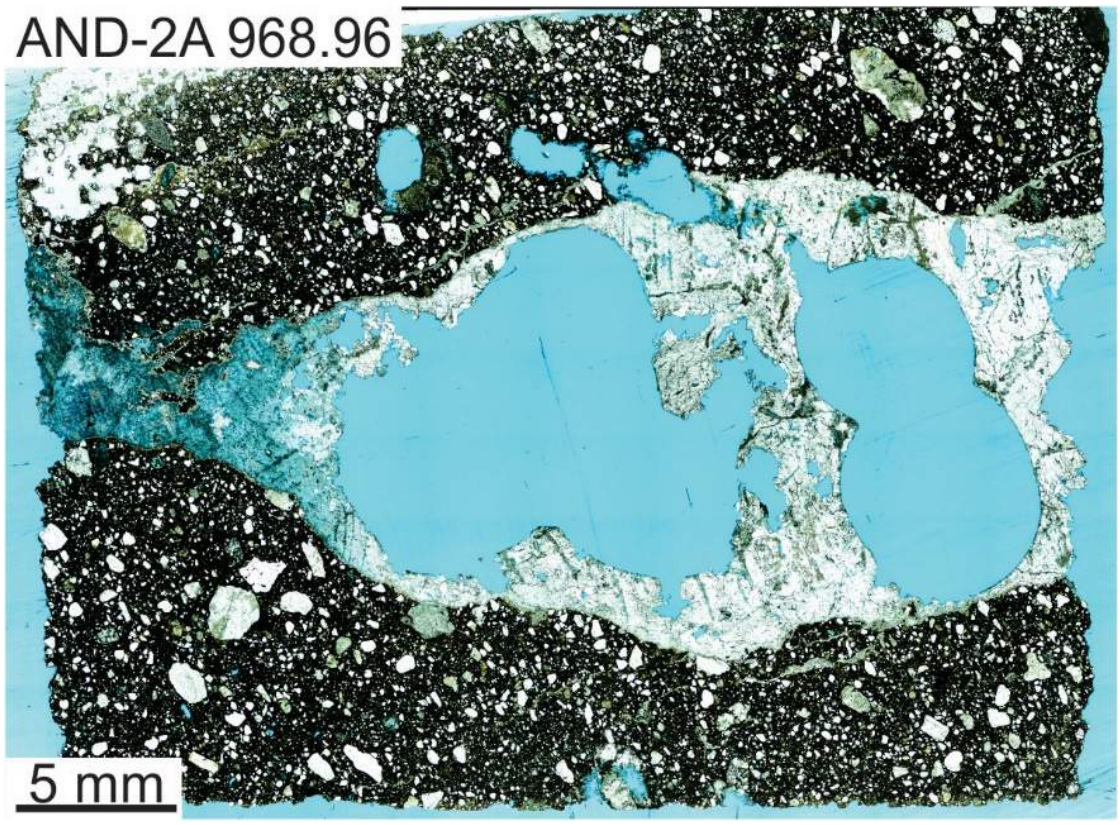
AND-2A 968.96
5 mm

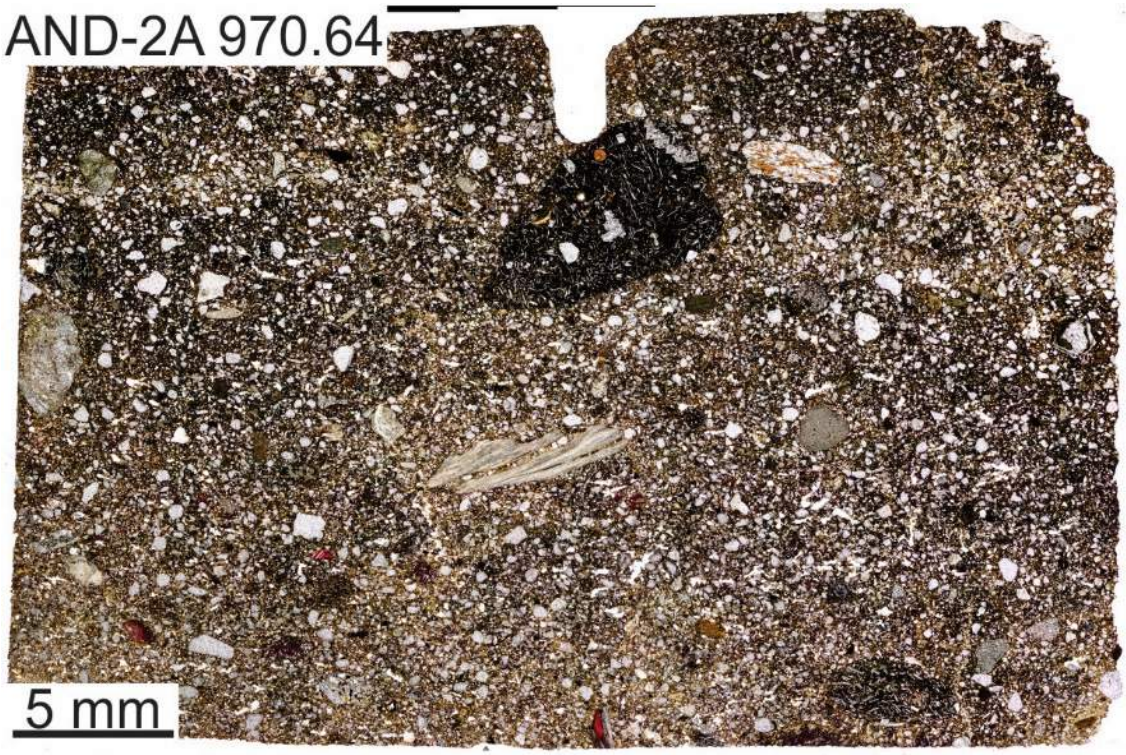
AND-2A 970.64
5 mm

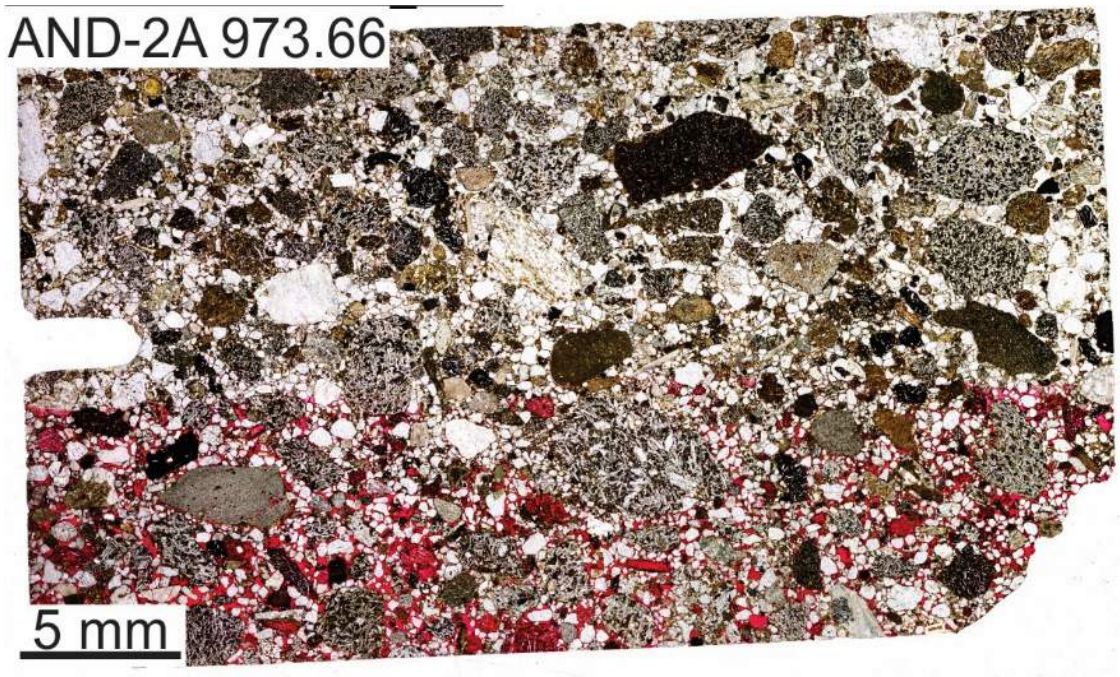
AND-2A 973.66
5 mm


AND-2A 979.66
5 mm

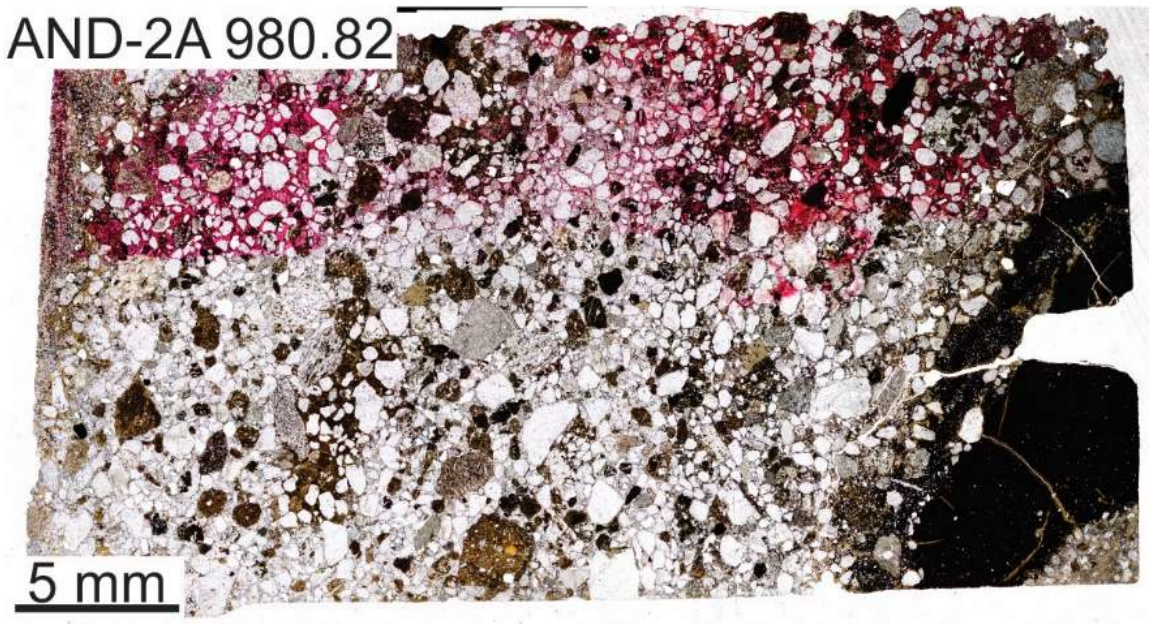
AND-2A 980.82
5 mm

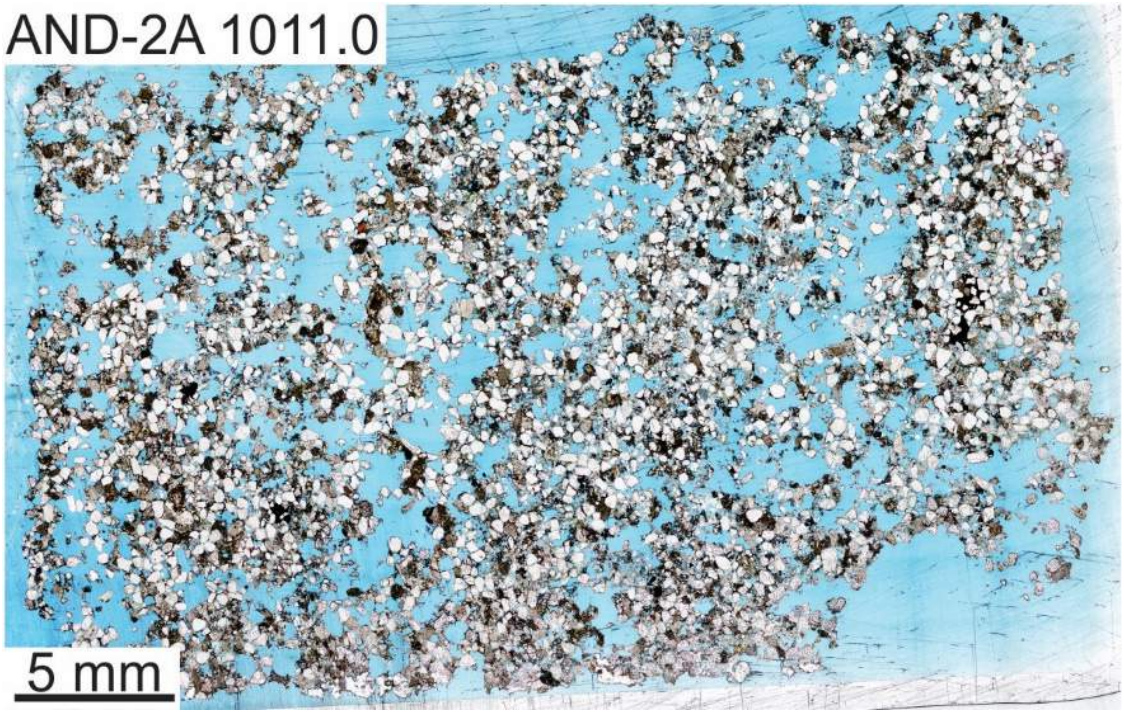
AND-2A 1011.0
5 mm

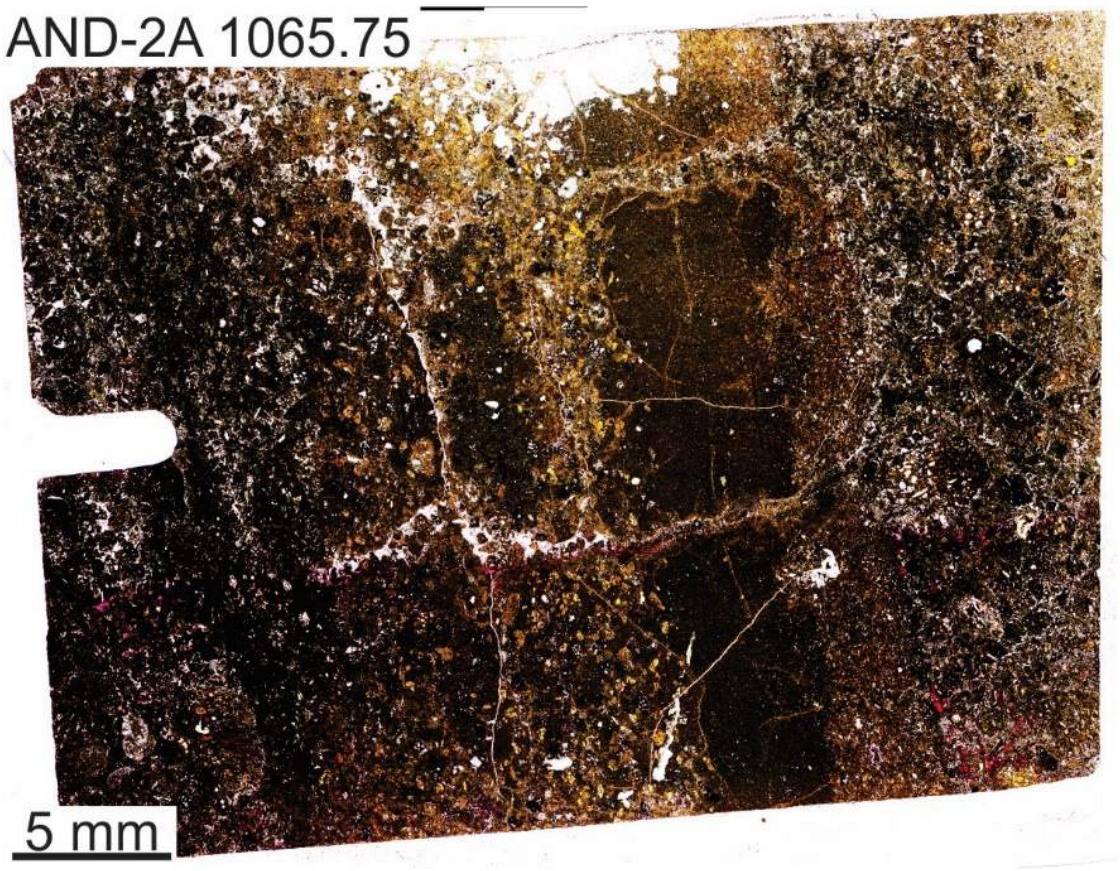
AND-2A 1065.75
5 mm

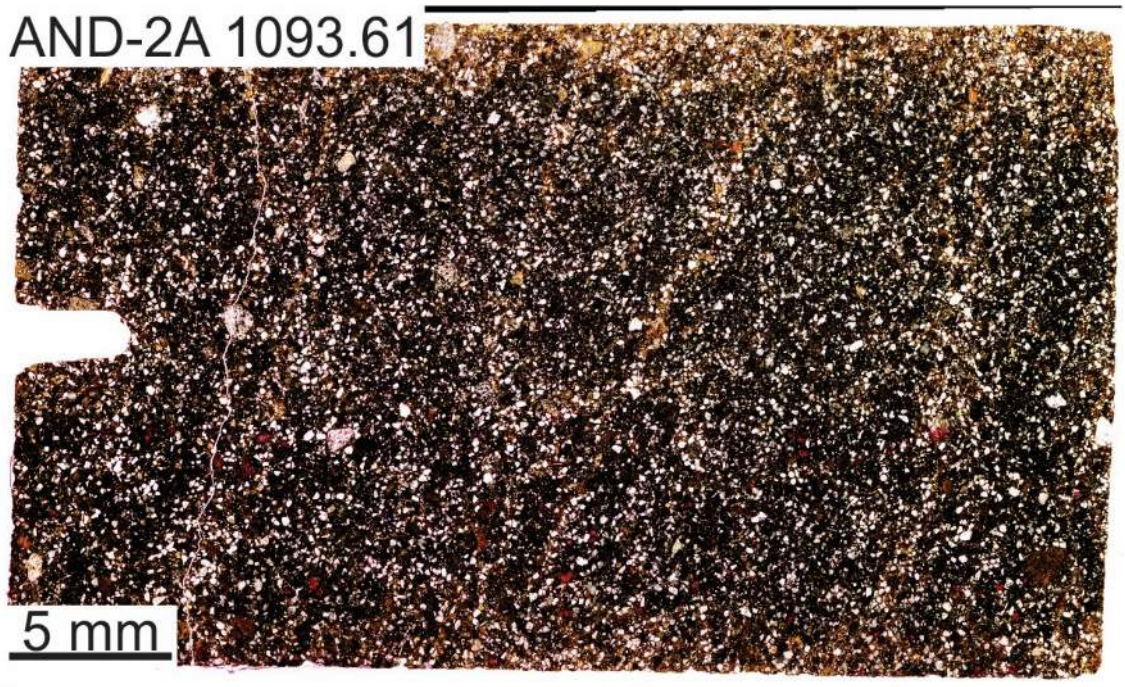
AND-2A 1093.61
5 mm

APPENDIX C:

Photomicrographs

Photomicrographs from the AND-2A core, Victoria Land Basin, Antarctica. Sample numbers reflect the depth in meters below sea floor (mbsf).

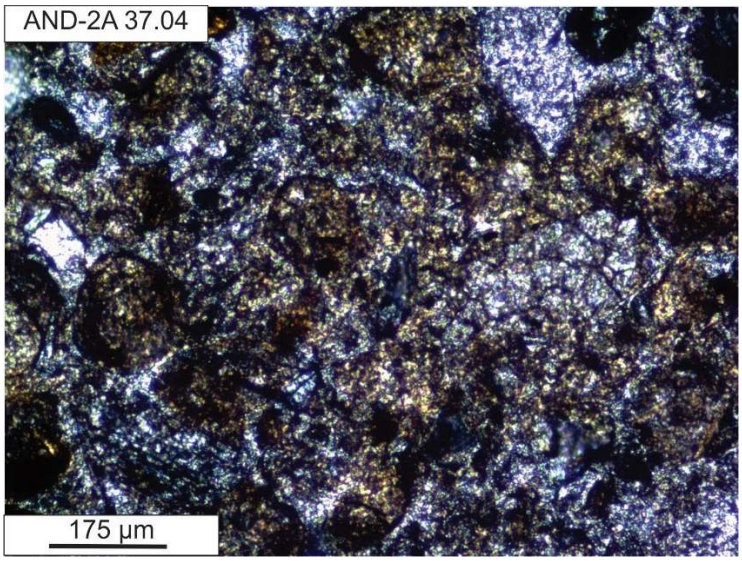
AND-2A 37.04
175 µm

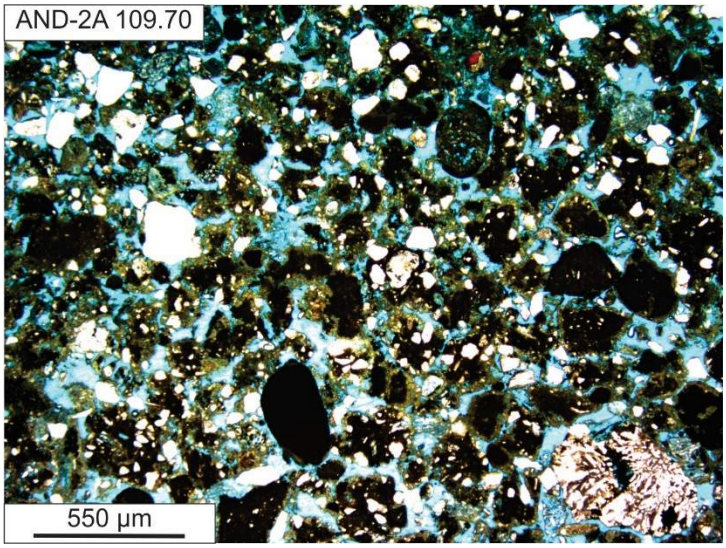
AND-2A 109.70
550 µm

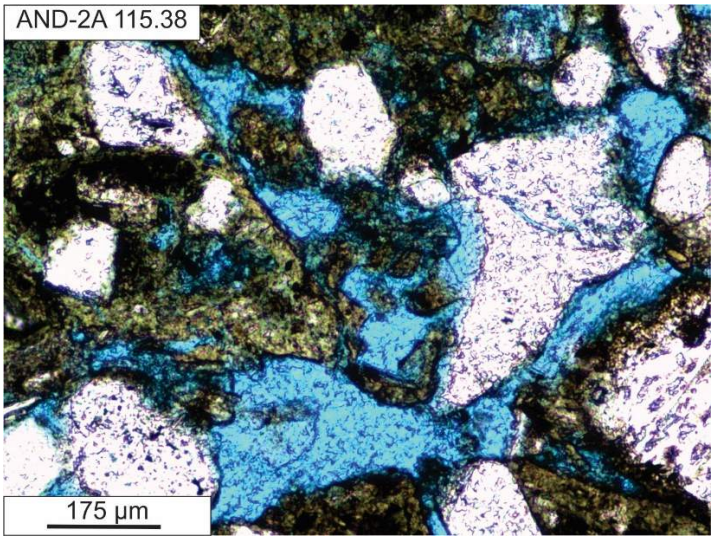
AND-2A 115.38
175 µm

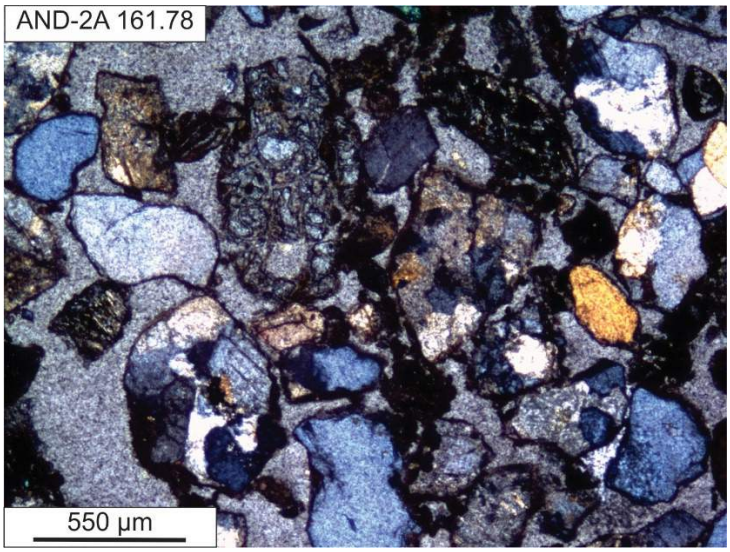
AND-2A 161.78
550 µm

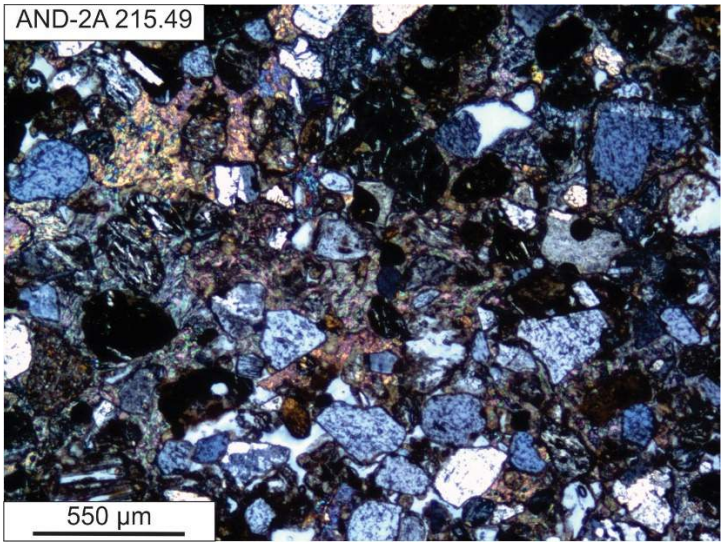
AND-2A 215.49
550 µm

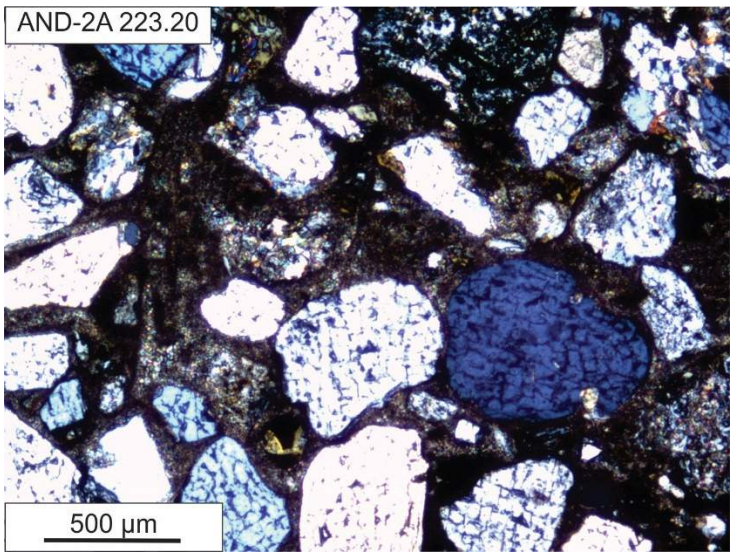
AND-2A 223.20
500 µm

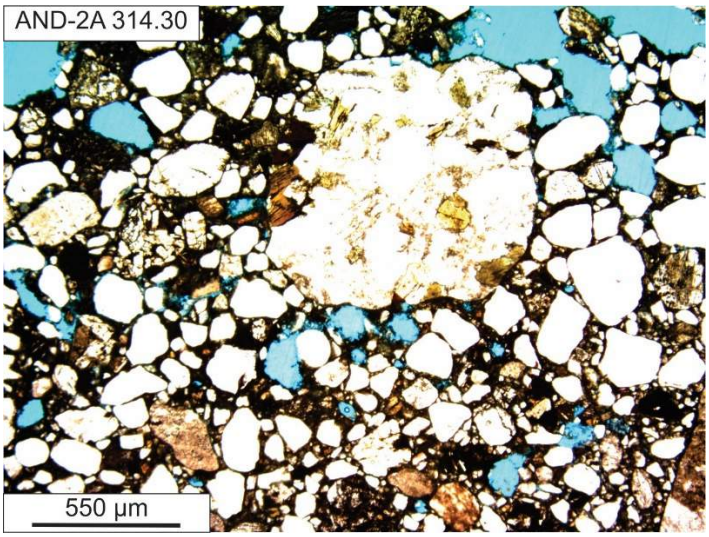
AND-2A 314.30
550 µm

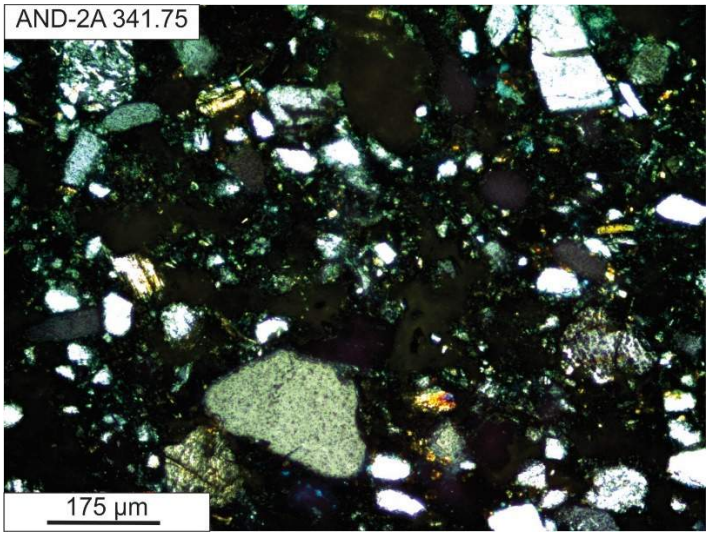
AND-2A 341.75
175 µm

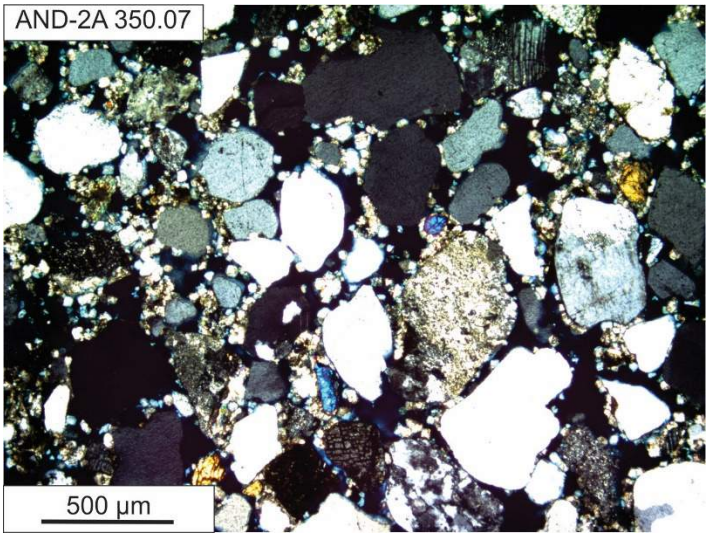
AND-2A 350.07
500 µm

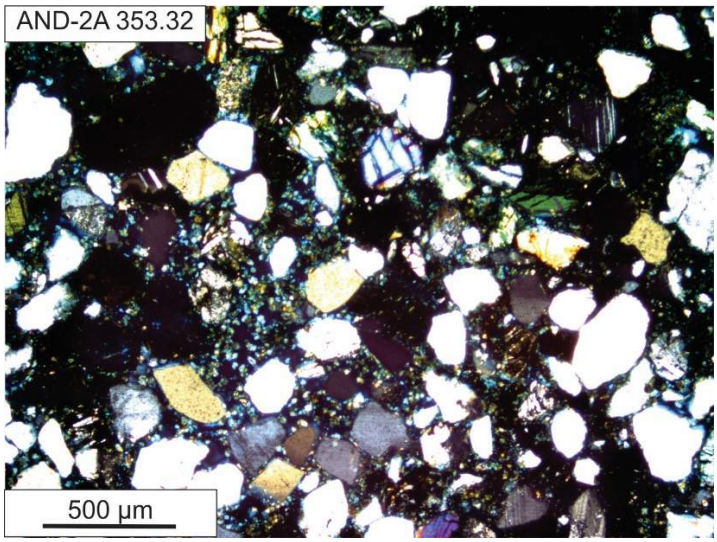
AND-2A 353.32
500 µm

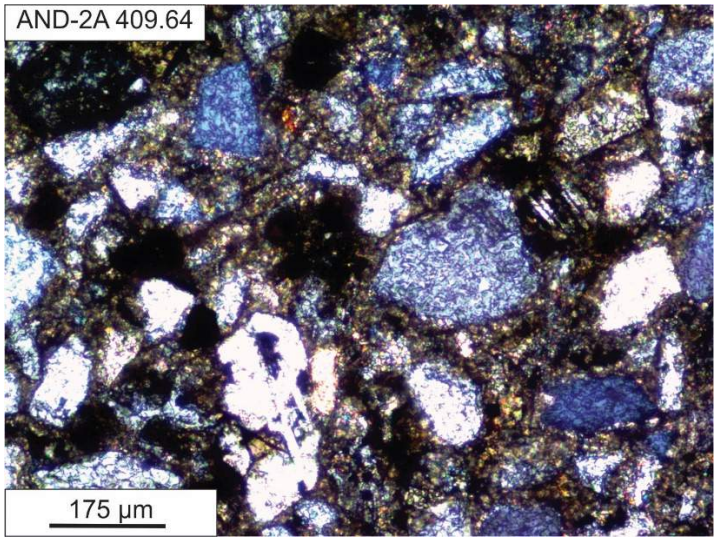
AND-2A 409.64
175 µm

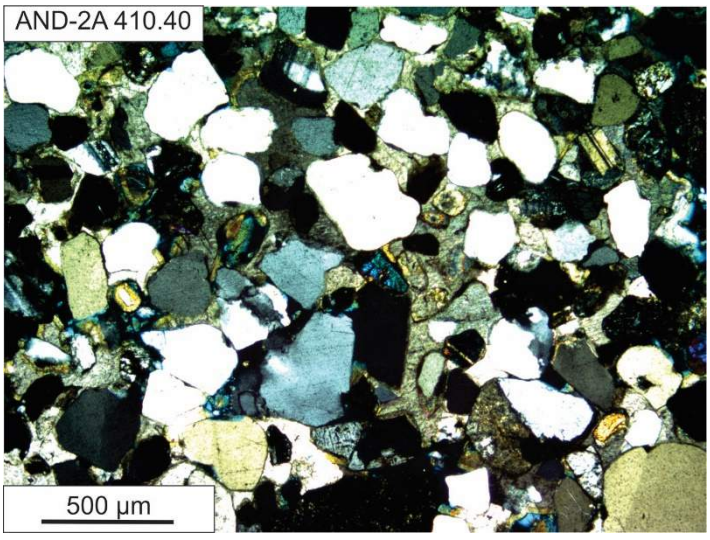
AND-2A 410.40
500 µm

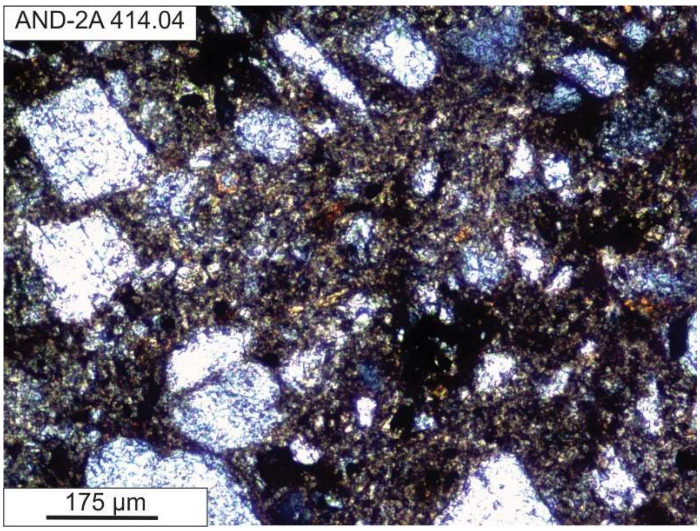
AND-2A 414.04
175 µm

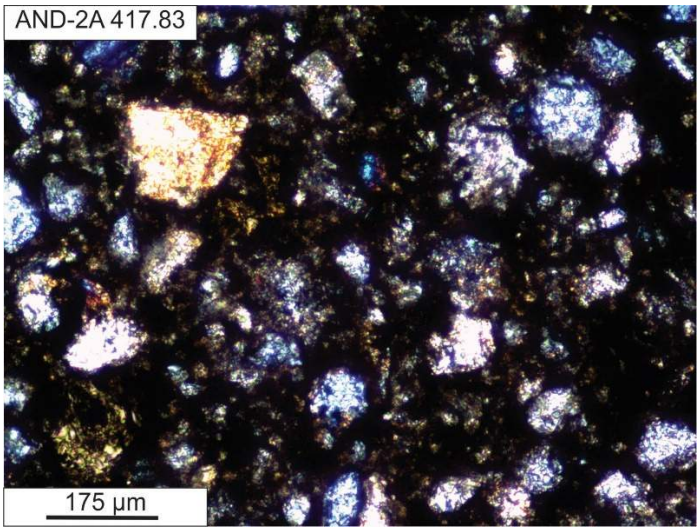
AND-2A 417.83
175 µm

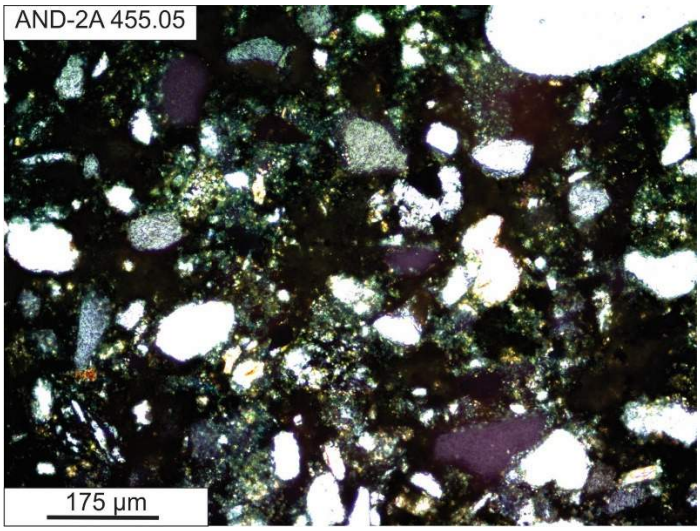
AND-2A 455.05
175 µm

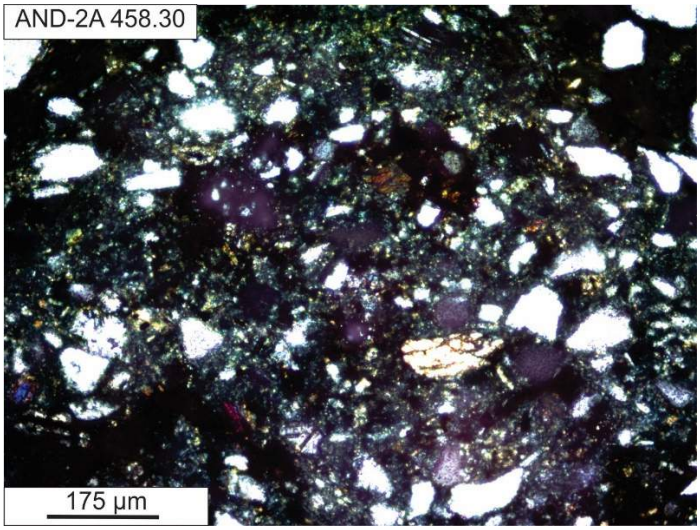
AND-2A 458.30
175 µm

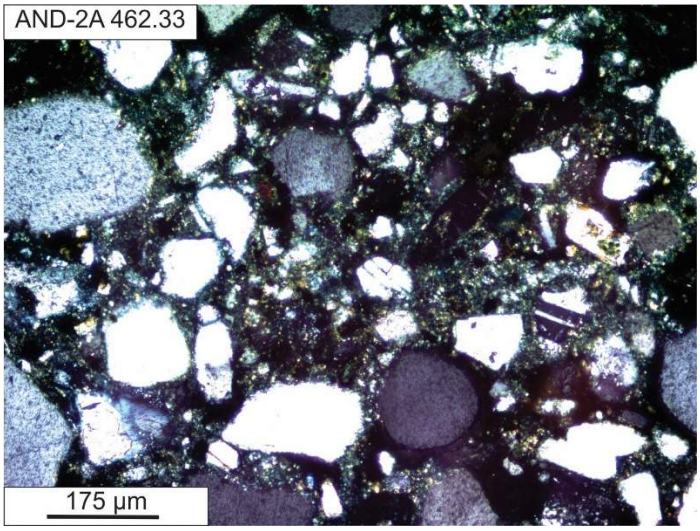
AND-2A 462.33
175 µm

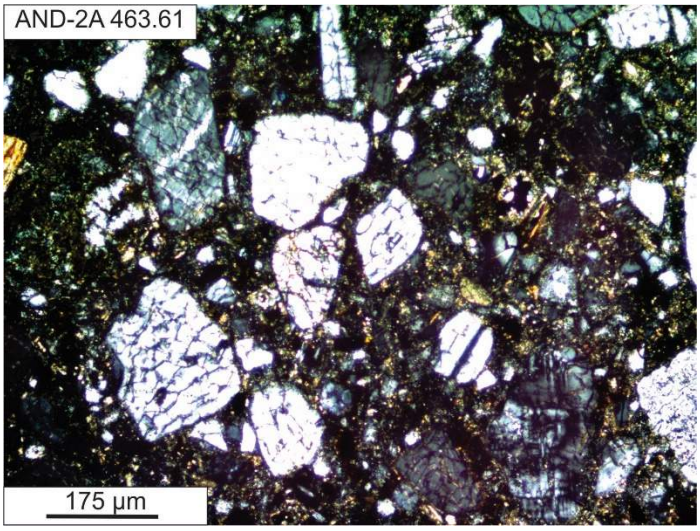
AND-2A 463.61
175 µm

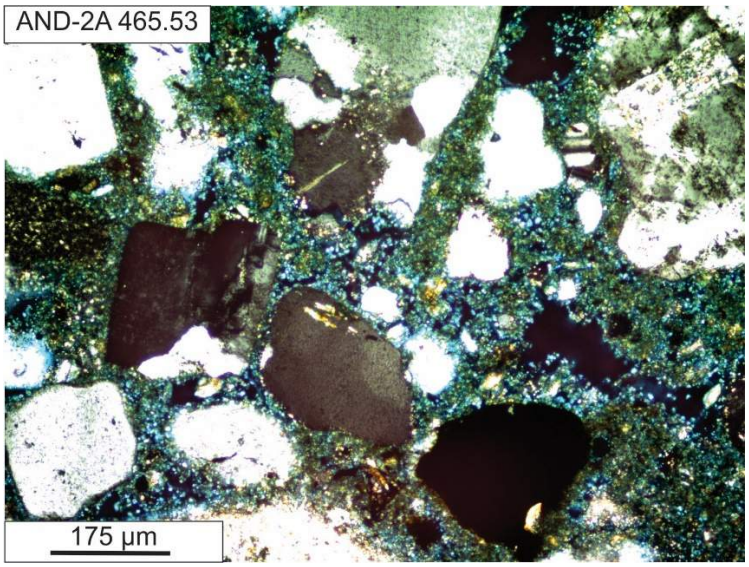
AND-2A 465.53
175 µm

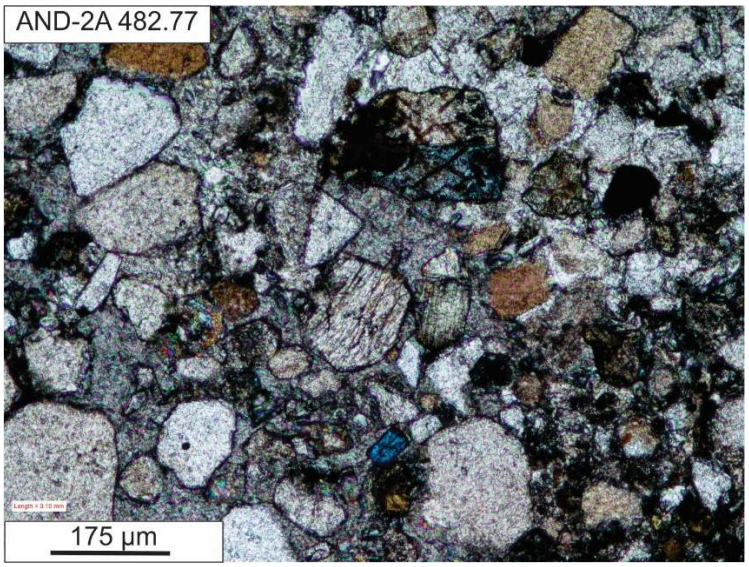
AND-2A 482.77
175 µm

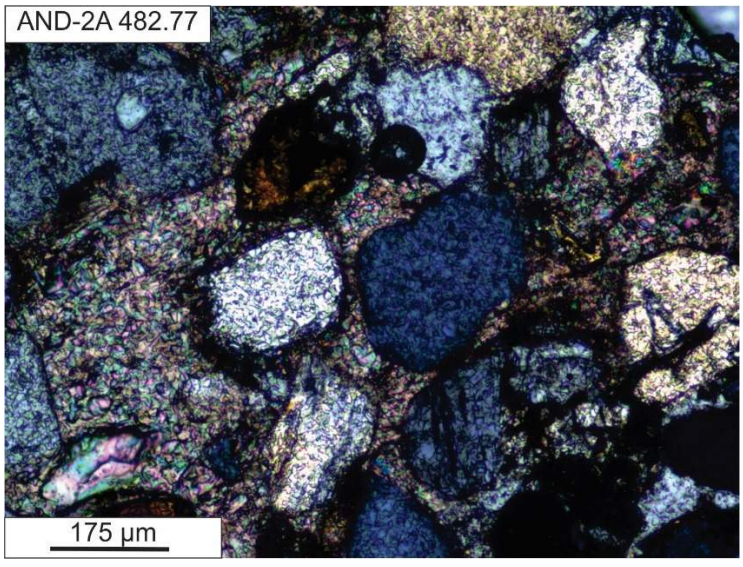
AND-2A 482.77
175 µm

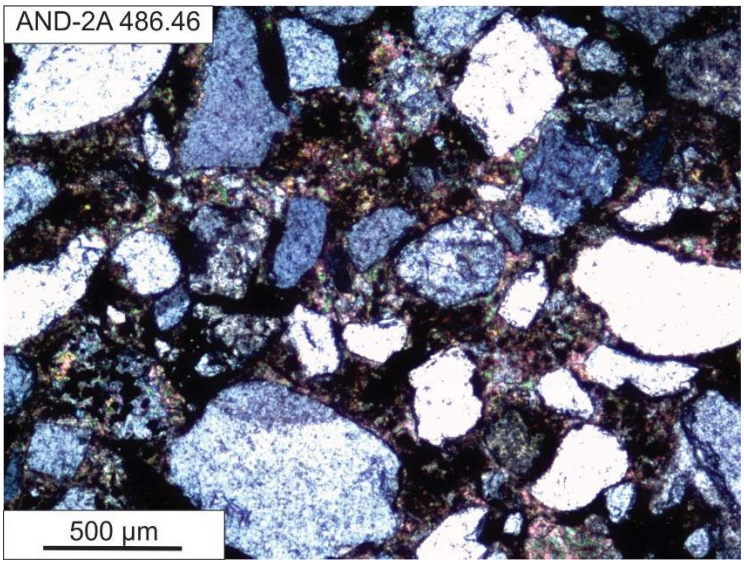
AND-2A 486.46
500 µm

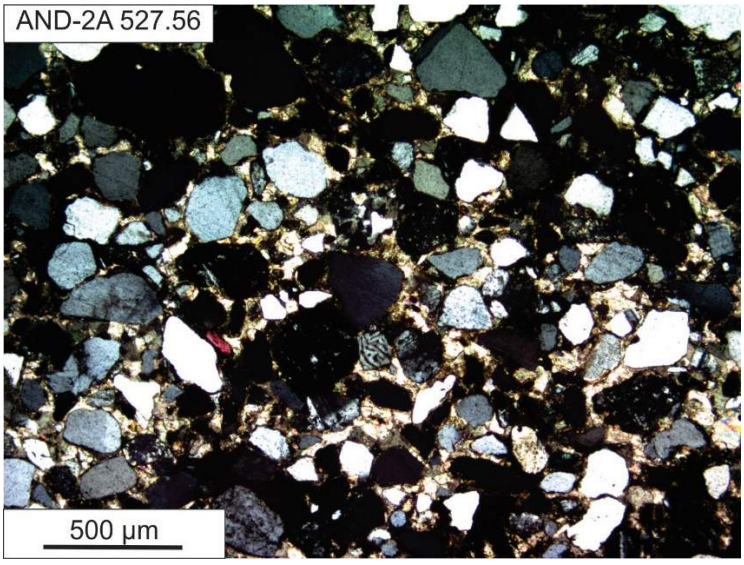
AND-2A 527.56
500 µm

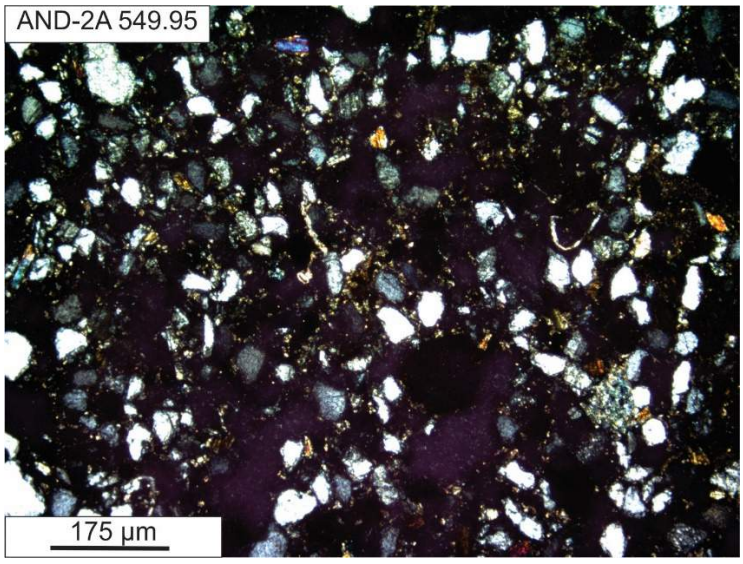
AND-2A 549.95
175 µm

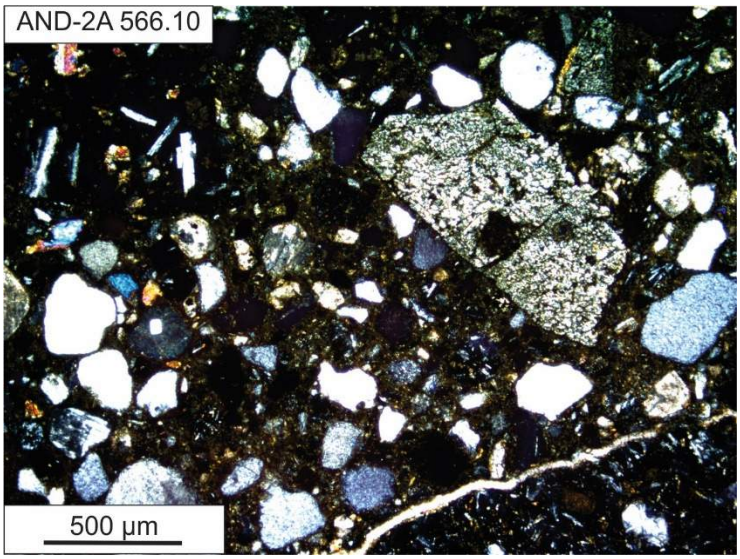
AND-2A 566.10
500 µm

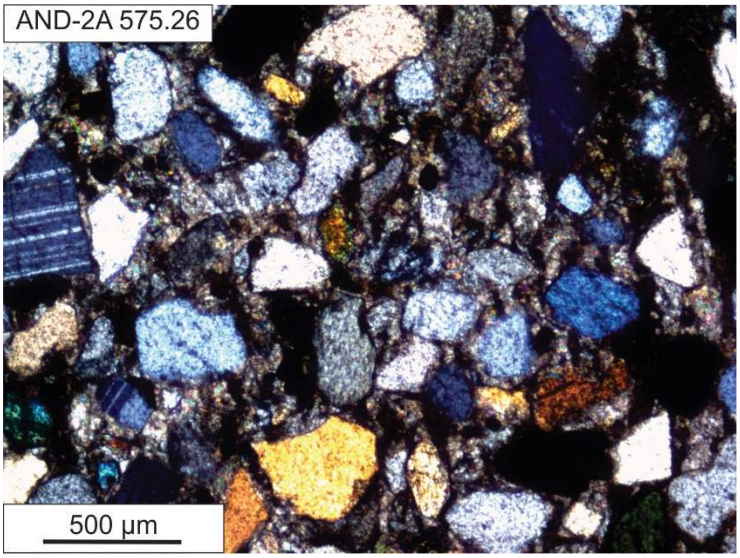
AND-2A 575.26
500 µm

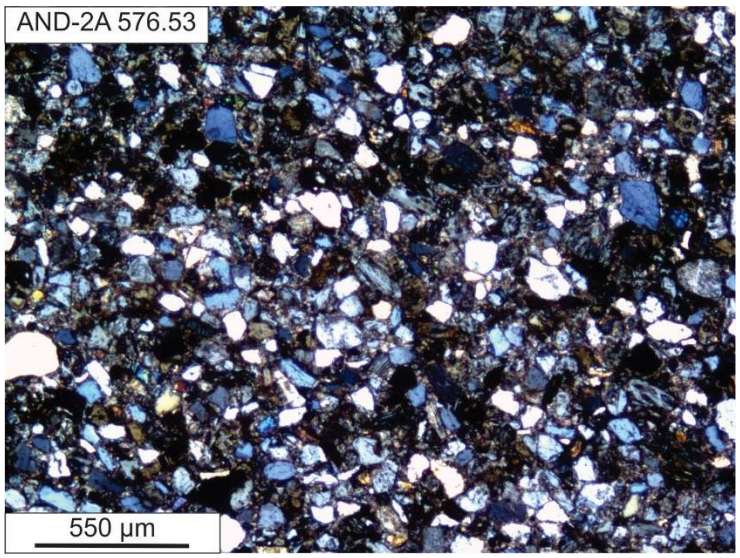
AND-2A 576.53
550 µm

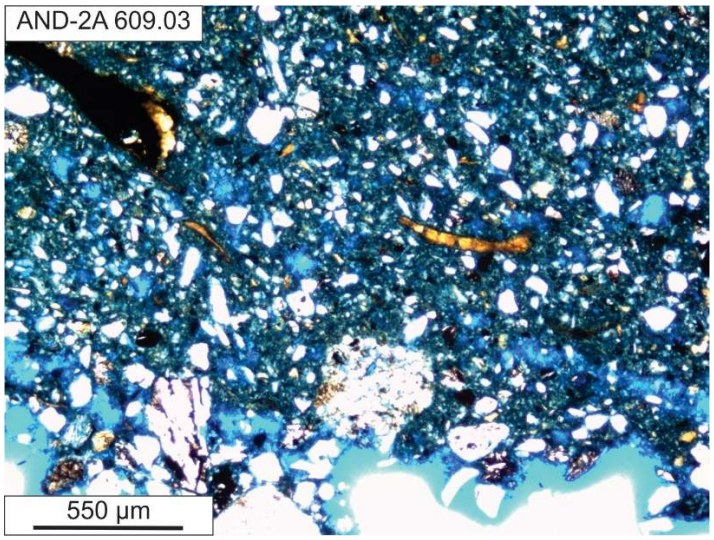
AND-2A 609.03
550 µm

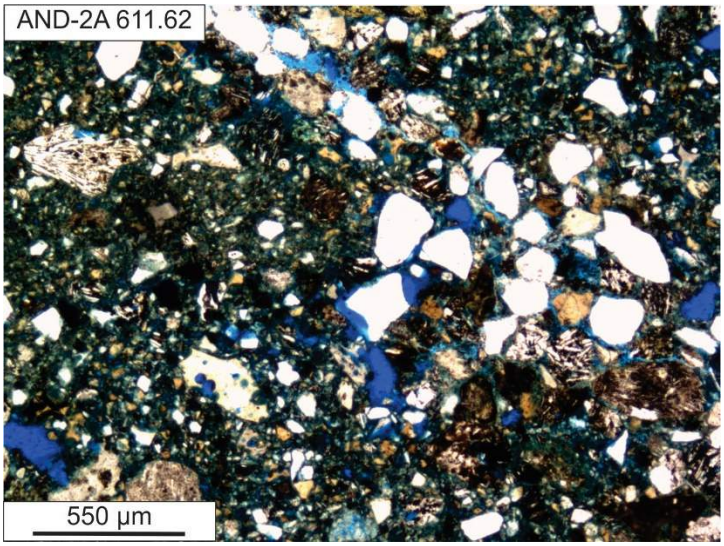
AND-2A 611.62
550 µm

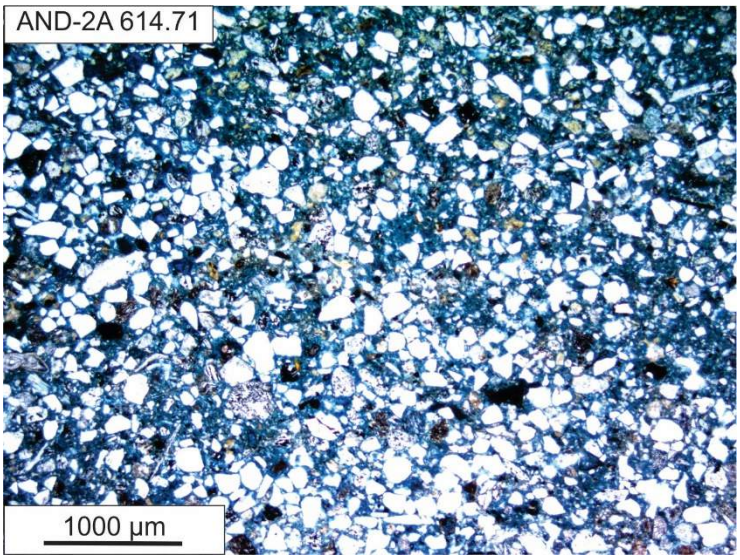
AND-2A 614.71
1000 µm

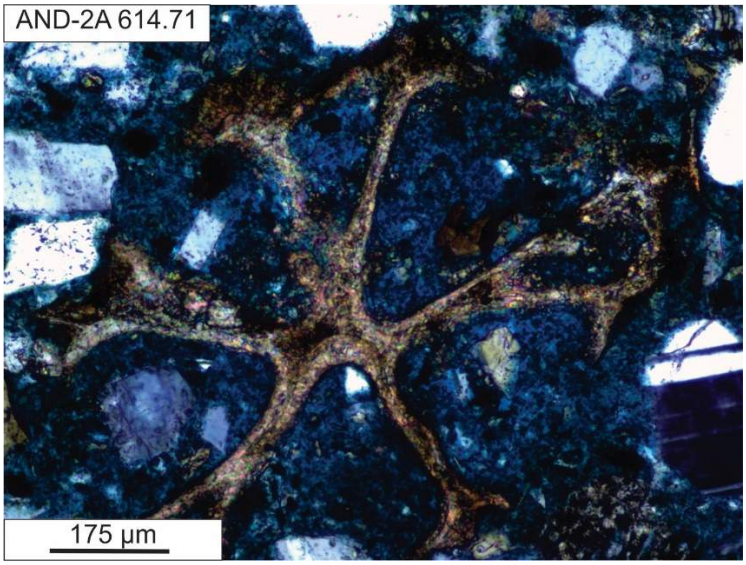
AND-2A 614.71
175 µm

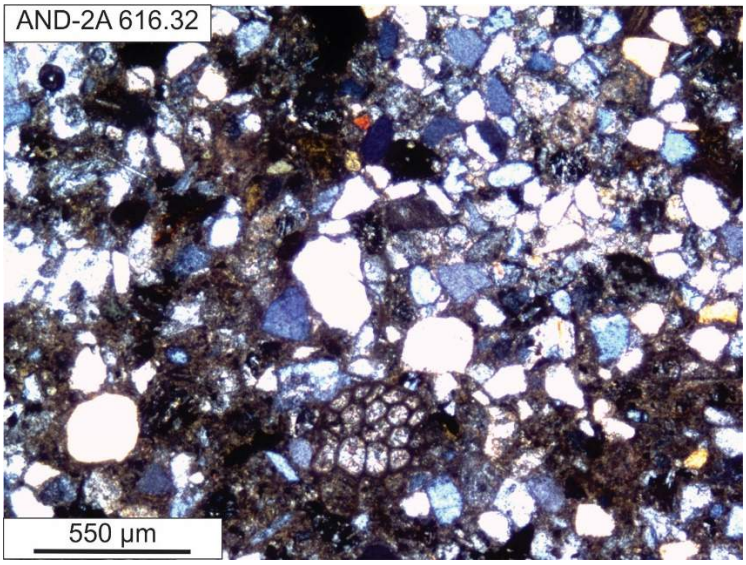
AND-2A 616.32
550 µm

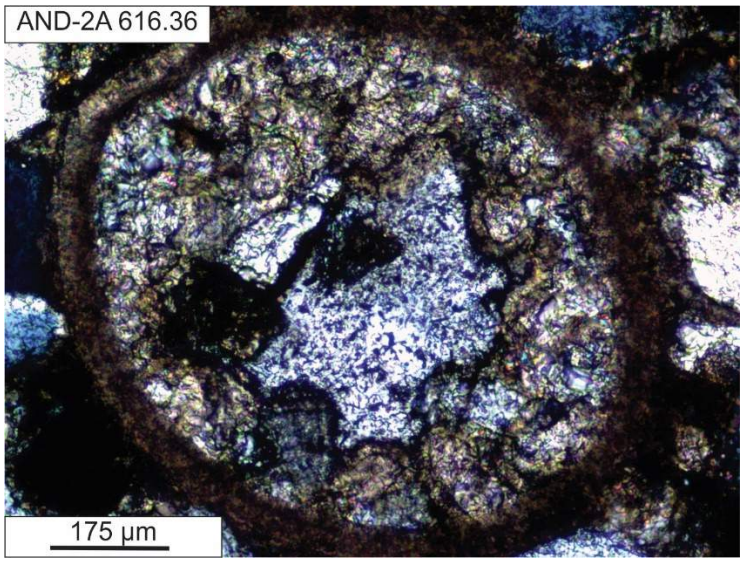
AND-2A 616.36
175 µm

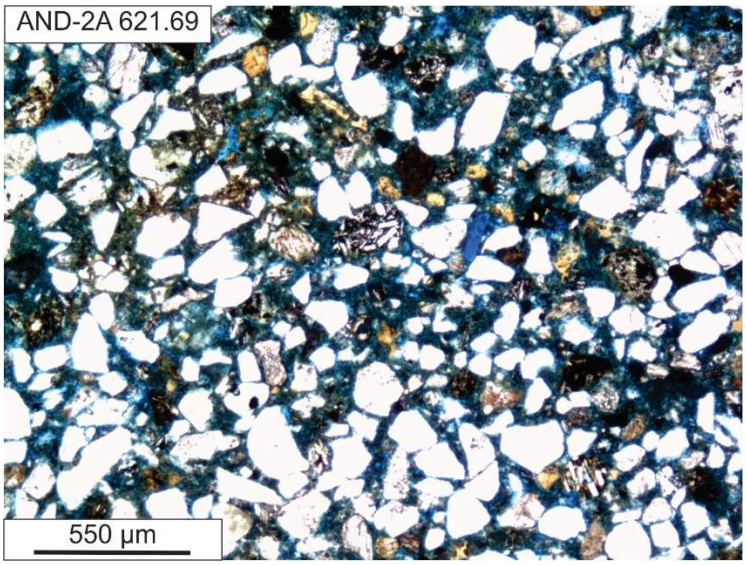
AND-2A 621.69
550 µm

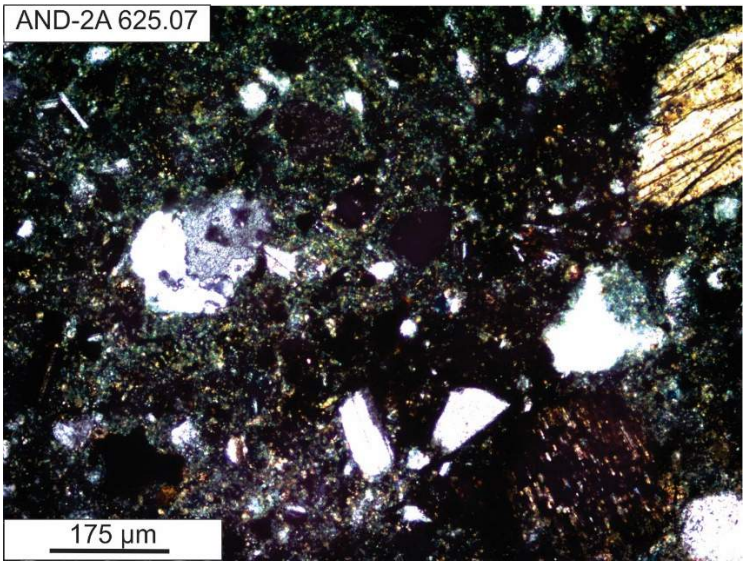
AND-2A 625.07
175 µm

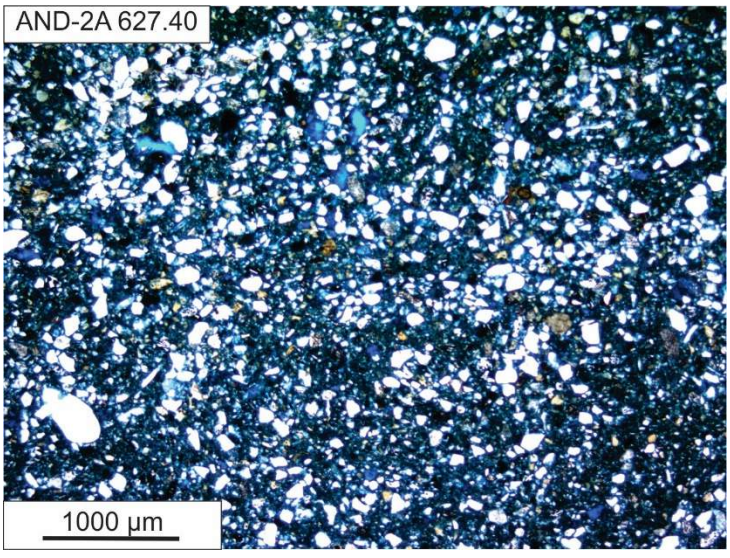
AND-2A 627.40
1000 µm

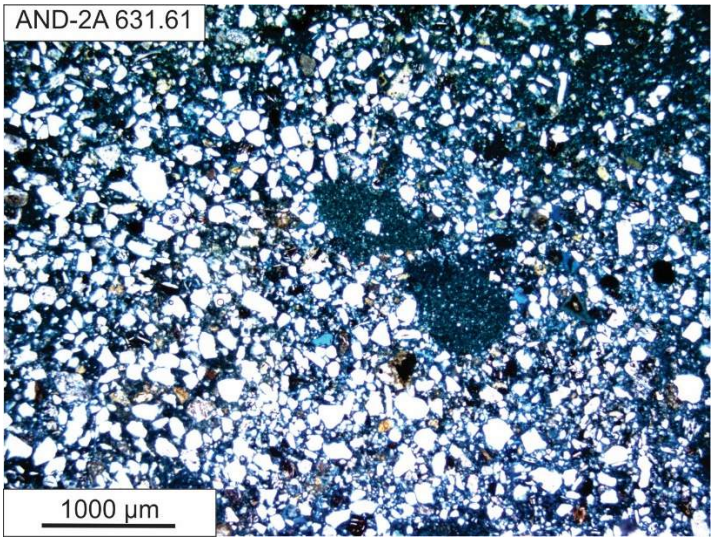
AND-2A 631.61
1000 µm

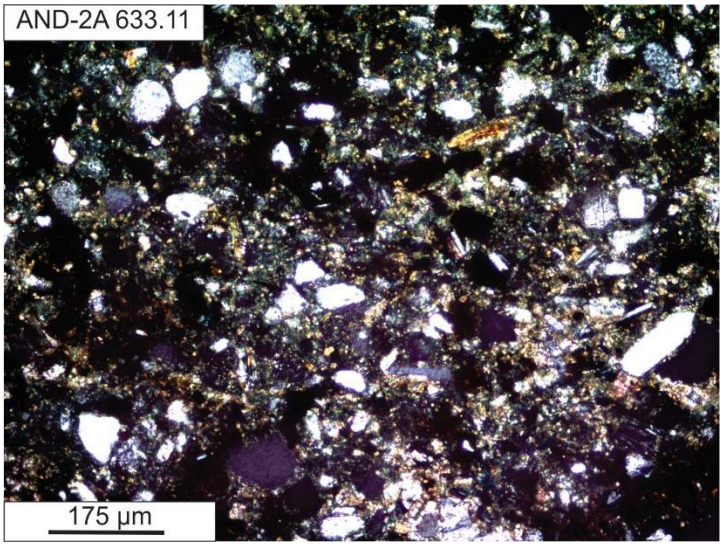
AND-2A 633.11
175 µm

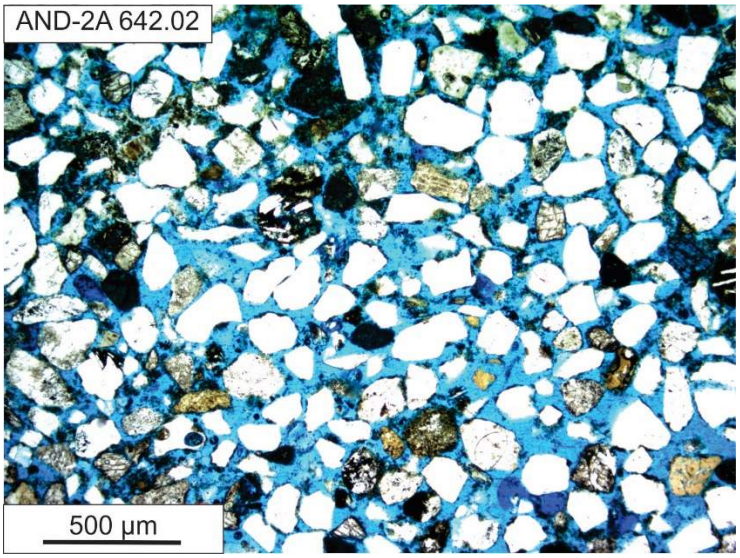
AND-2A 642.02
500 µm

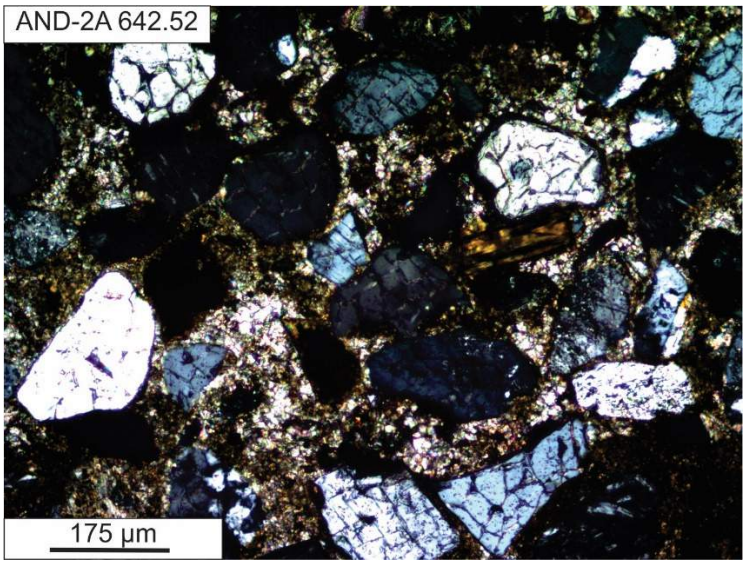
AND-2A 642.52
175 µm

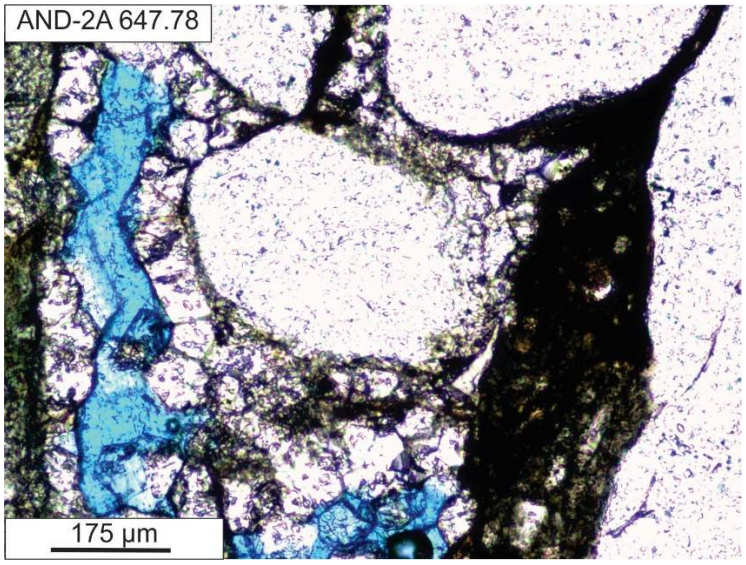
AND-2A 647.78
175 µm

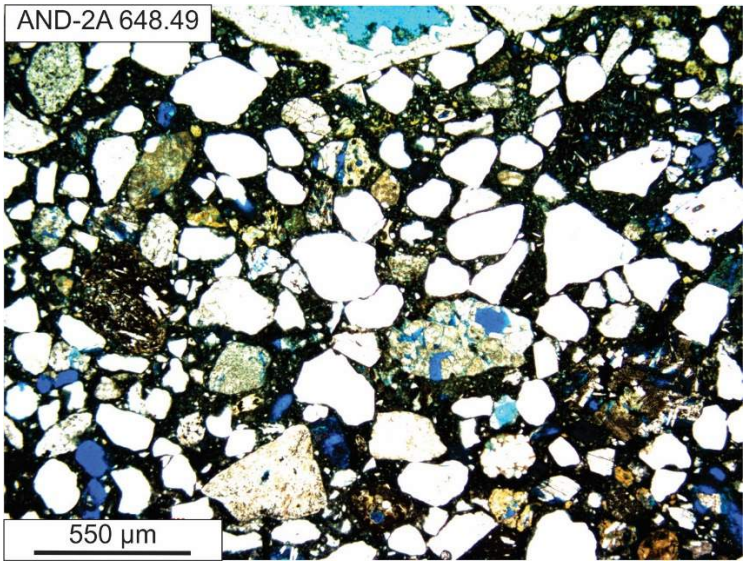
AND-2A 648.49
550 µm

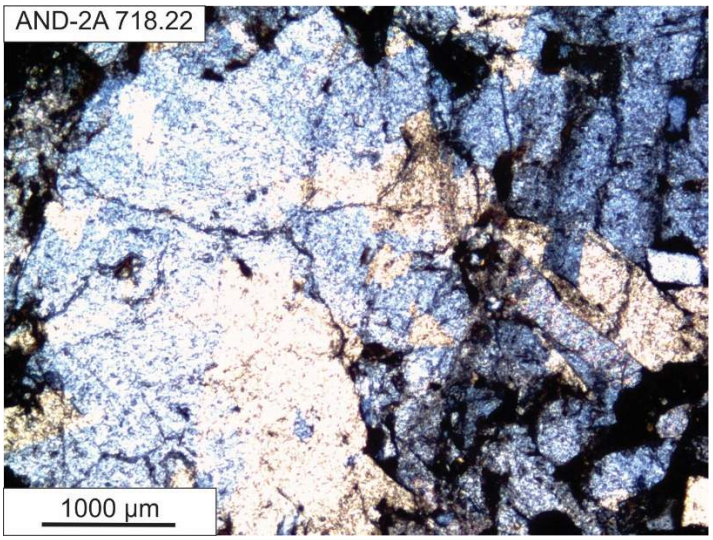
AND-2A 718.22
1000 µm

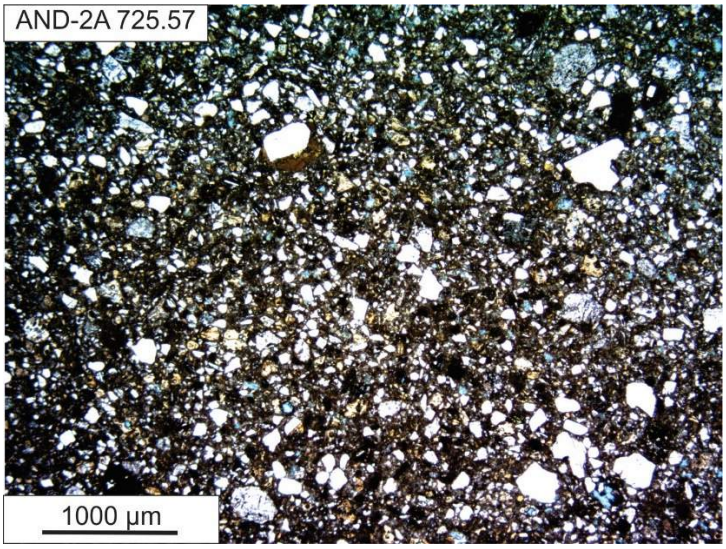
AND-2A 725.57
1000 µm

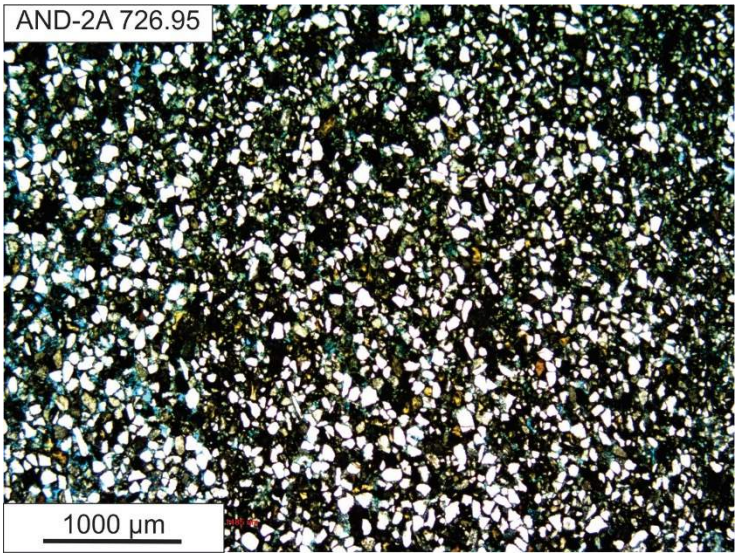
AND-2A 726.95
1000 µm

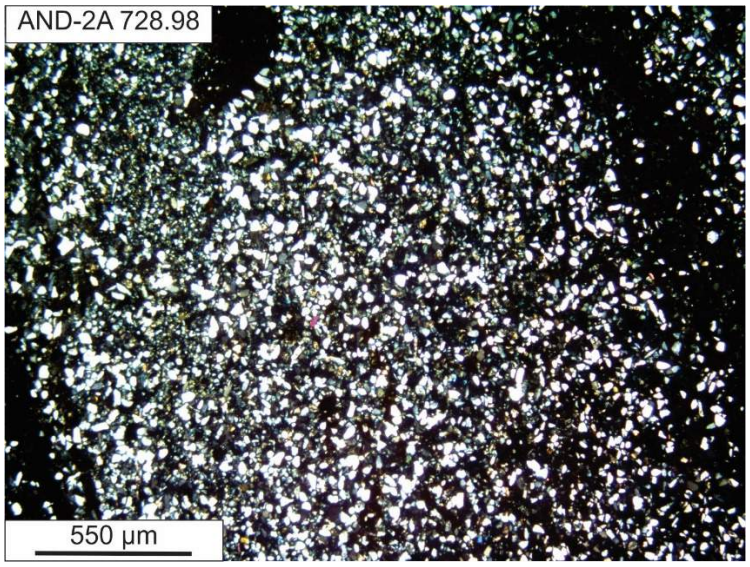
AND-2A 728.98
550 µm

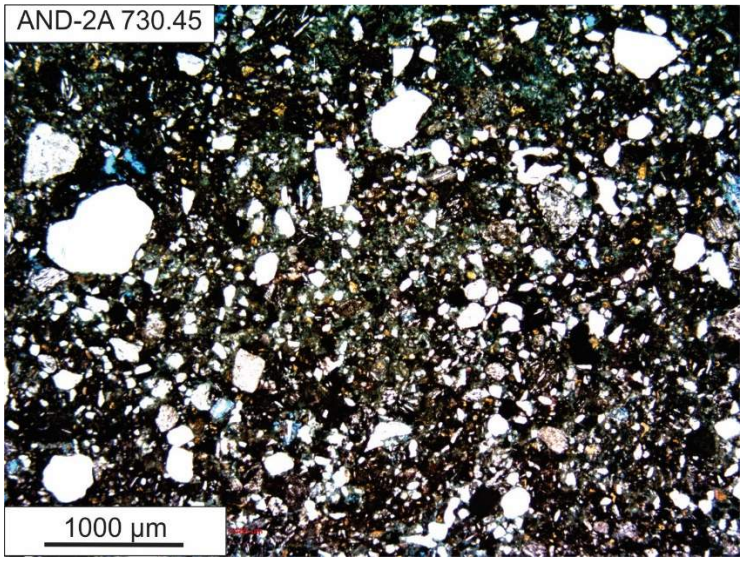
AND-2A 730.45
1000 µm

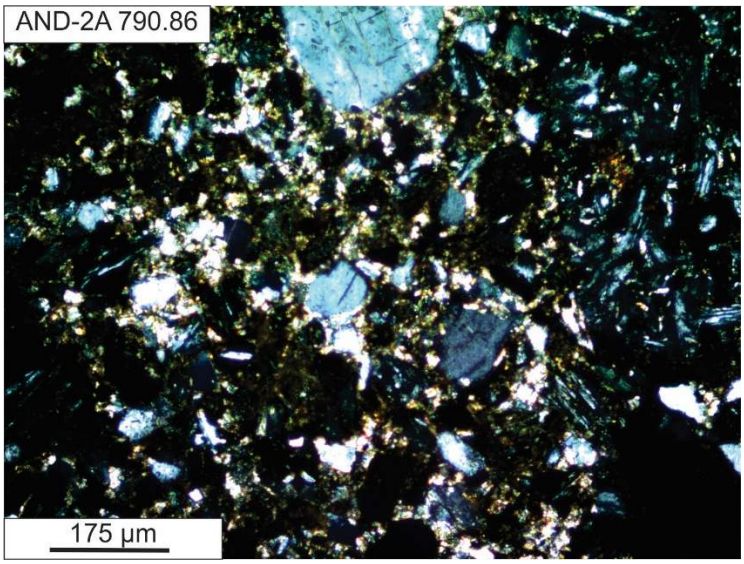
AND-2A 790.86
175 µm

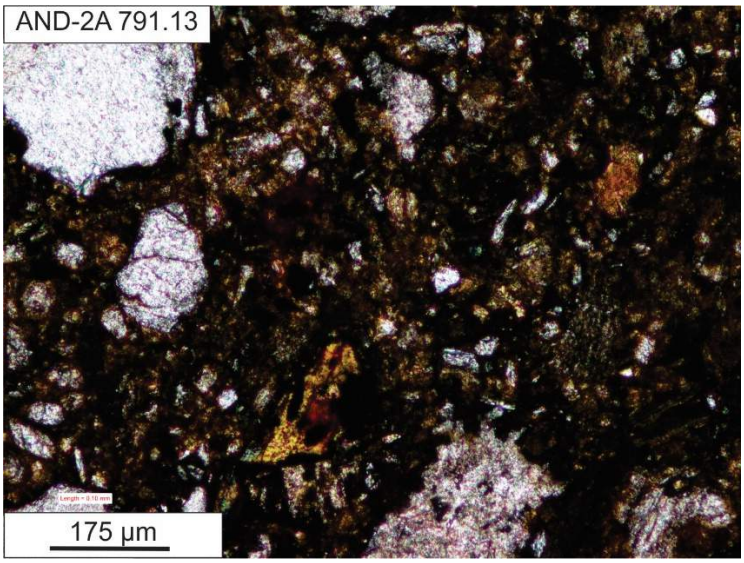
AND-2A 791.13
175 µm

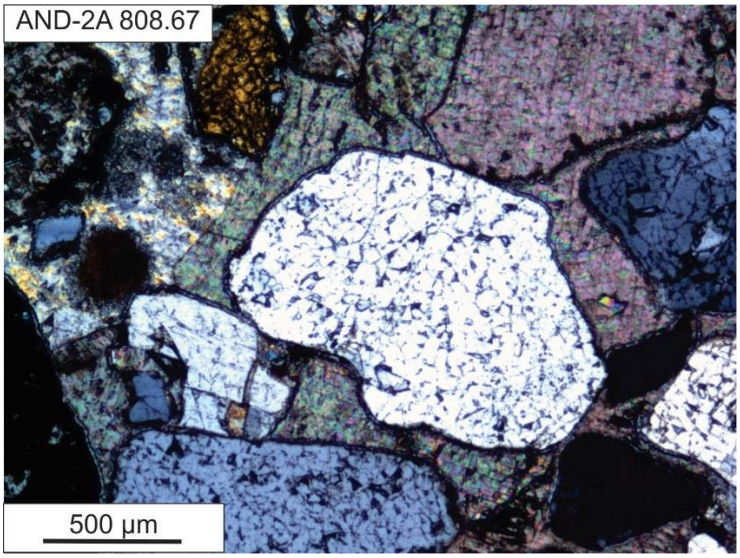
AND-2A 808.67
500 µm

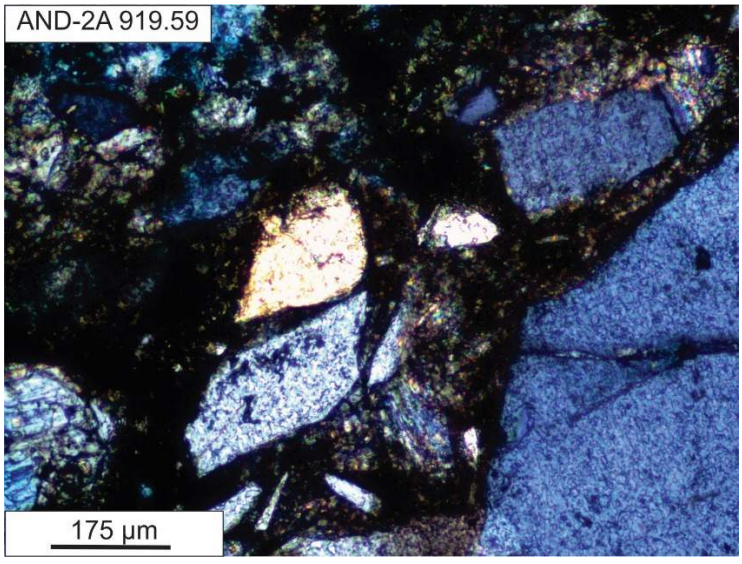
AND-2A 919.59
175 µm

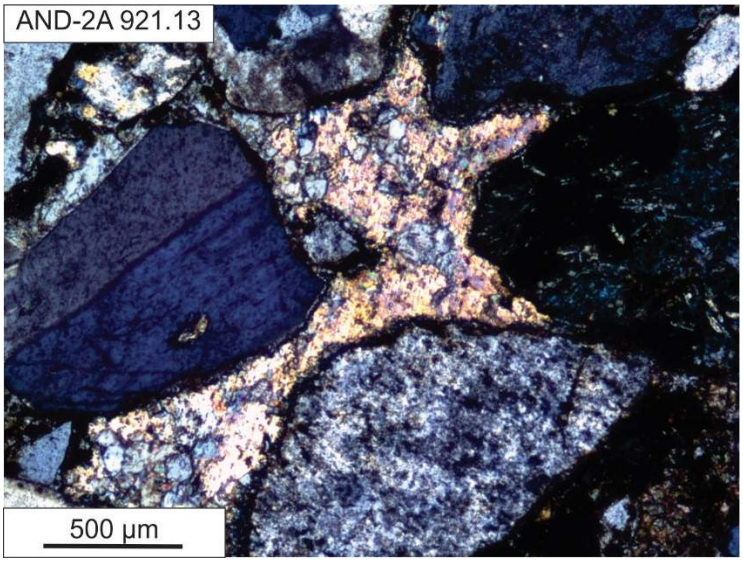
AND-2A 921.13
500 µm

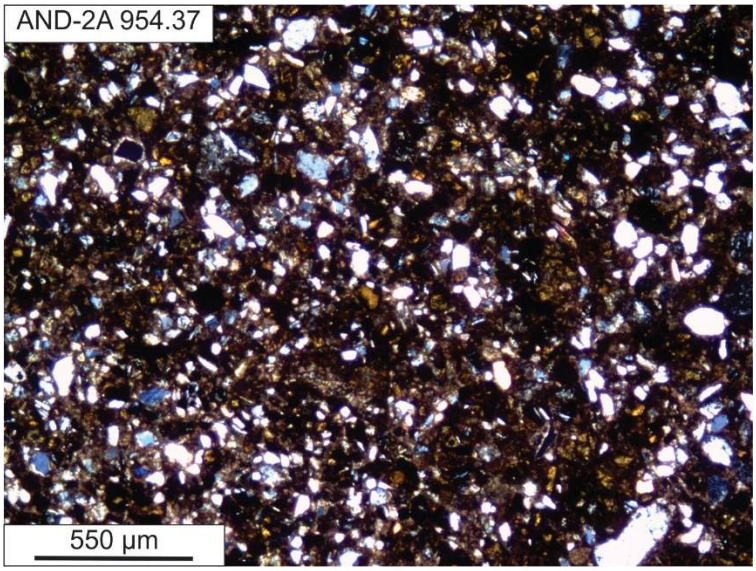
AND-2A 954.37
550 µm

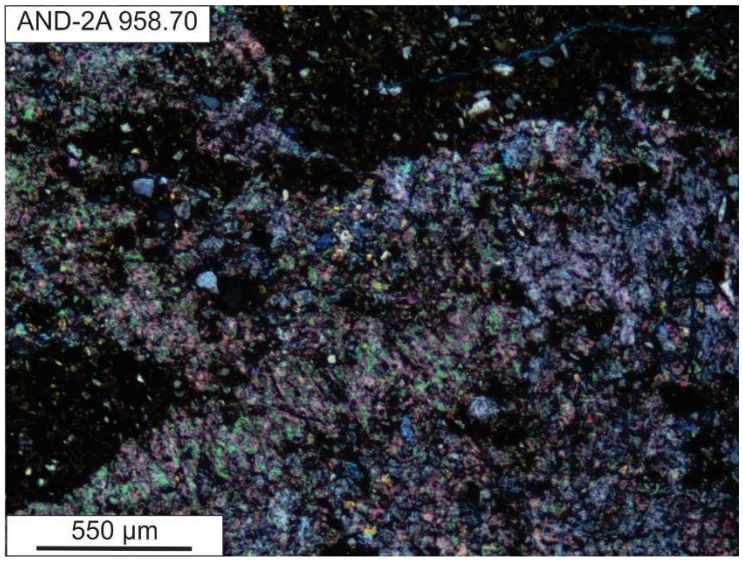
AND-2A 958.70
550 µm

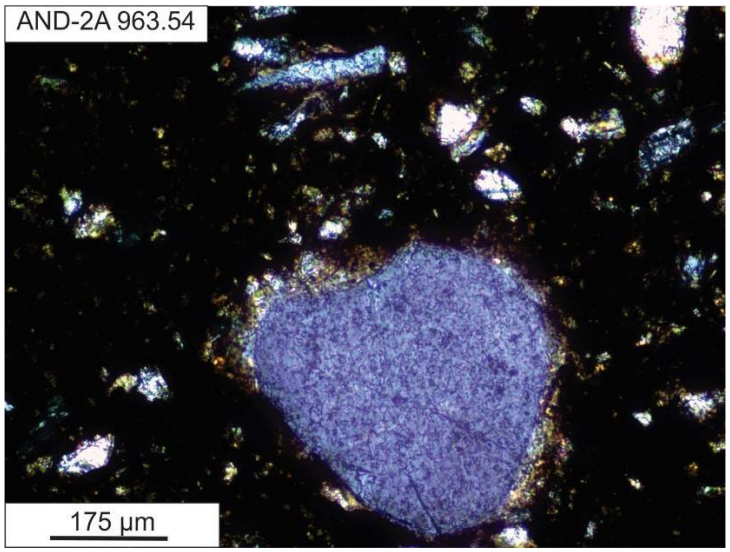
AND-2A 963.54
175 µm

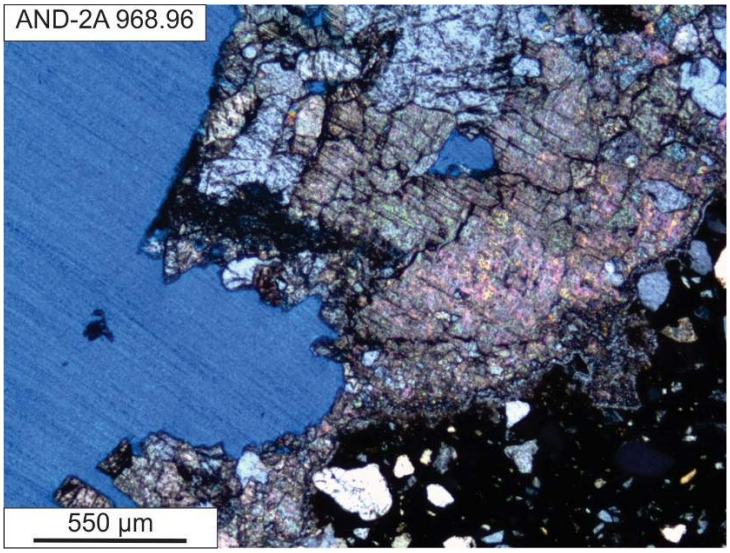
AND-2A 968.96
550 µm

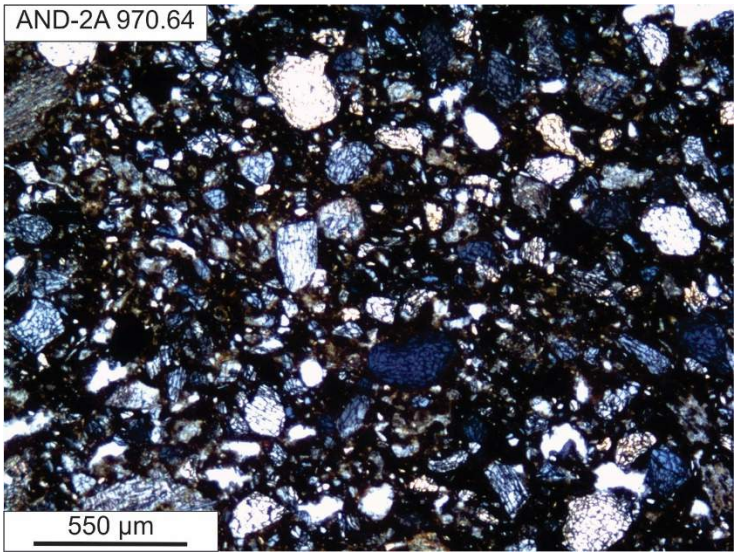
AND-2A 970.64
550 µm

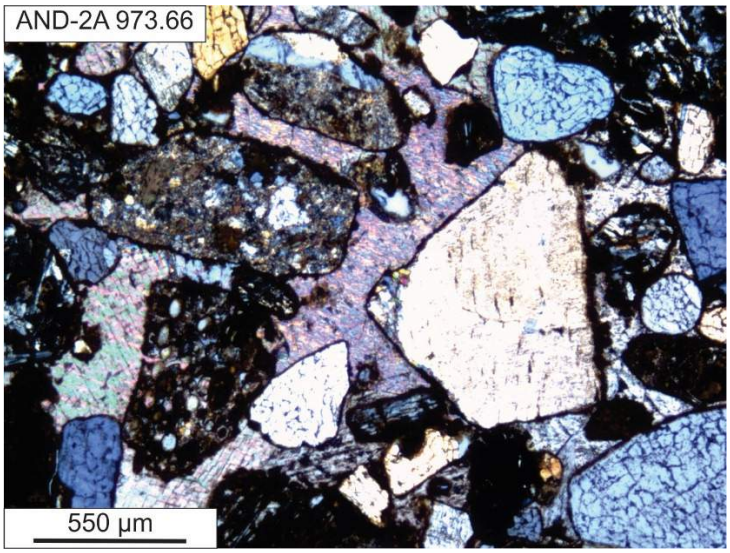
AND-2A 973.66
550 µm

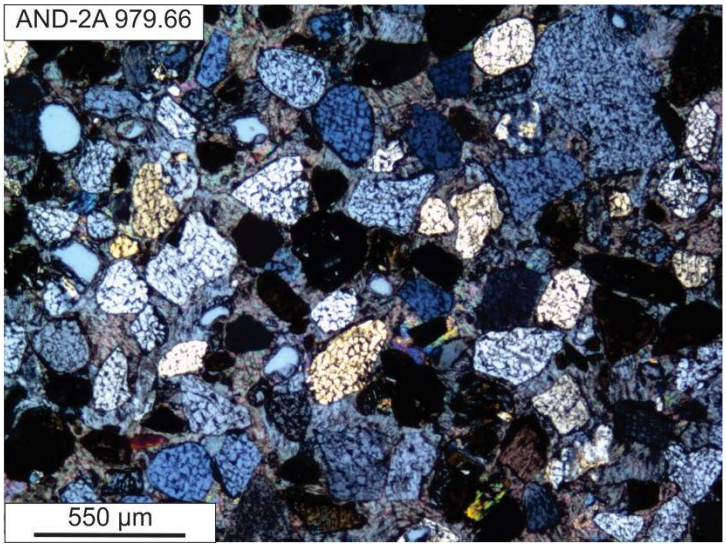
AND-2A 979.66
550 µm

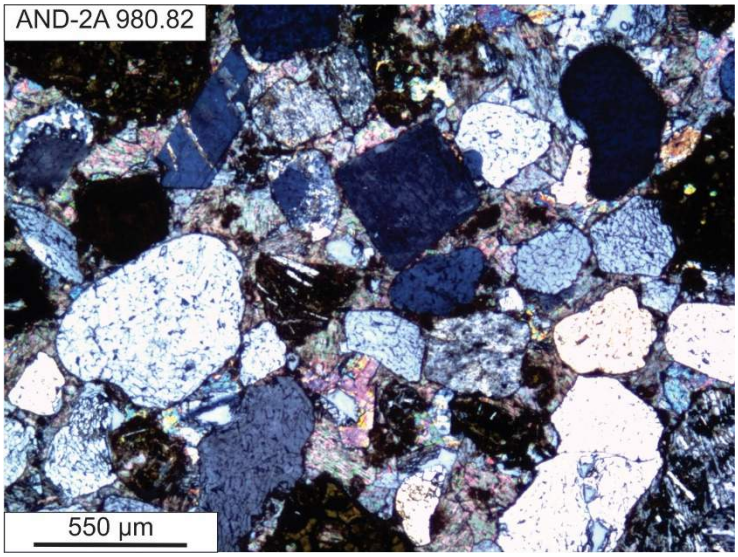
AND-2A 980.82
550 µm

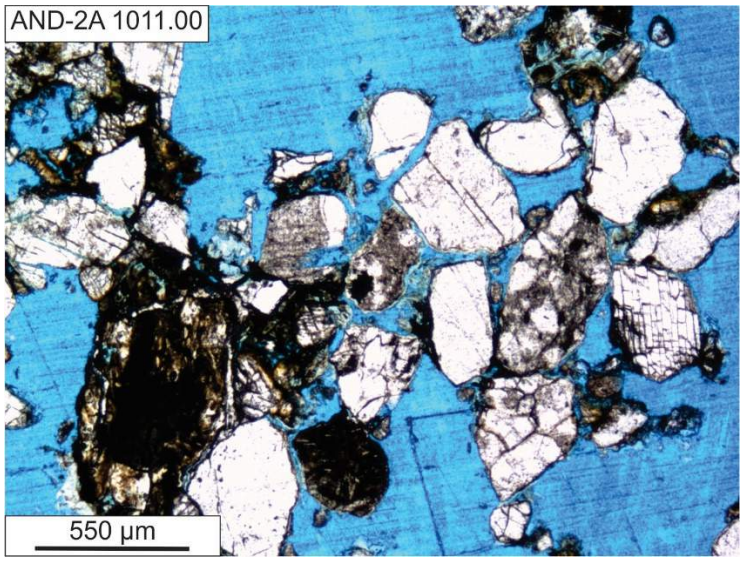
AND-2A 1011.00
550 µm

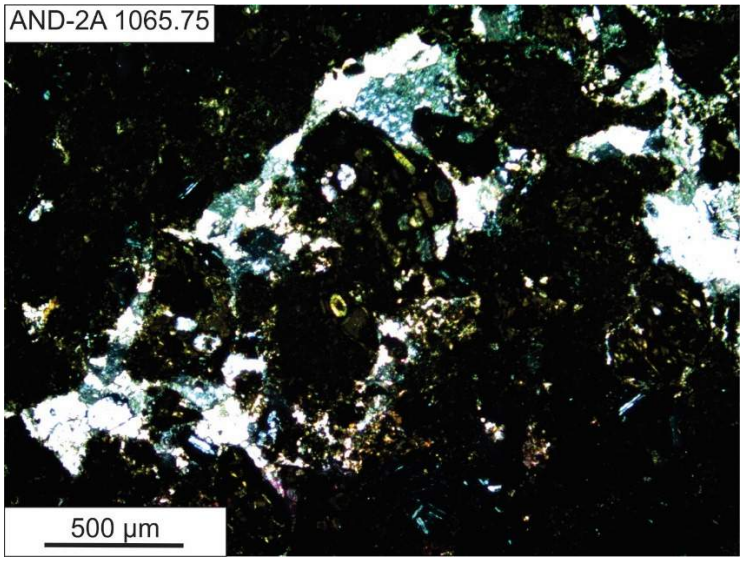
AND-2A 1065.75
500 µm

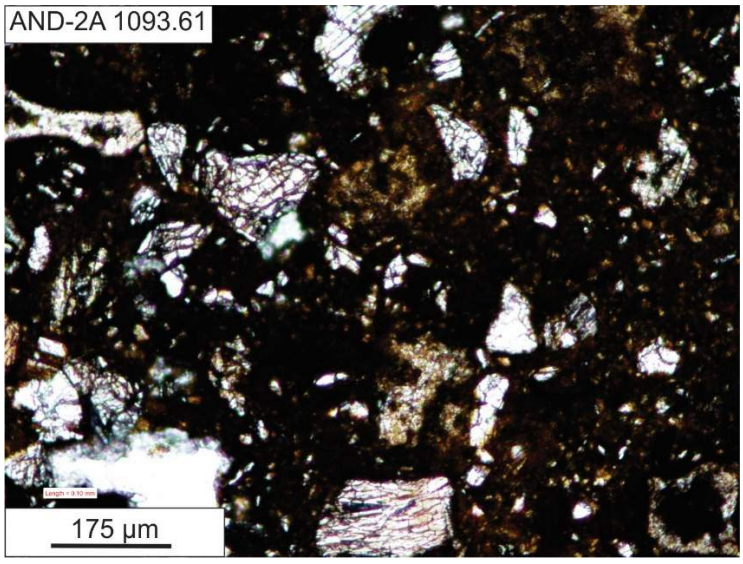
AND-2A 1093.61
175 µm